Imaging the neurodegenerative component of a demyelinating disorder : multiple sclerosis

Léorah Bosque-Freeman

UPMC
SORBONNE UNIVERSITÉS

UNIVERSITE PIERRE ET MARIE CURIE

ECOLE DOCTORALE CERVEAU COGNITION COMPORTEMENT

Imagerie de la dégénérescence neuronale dans une maladie démyélinisante: la sclérose en plaques

Présentée par Léorah Freeman

Thèse de Doctorat, Spécialité Neurosciences

Dirigée par M. le Pr Bruno Stankoff

Présentée et soutenue publiquement le 10 décembre 2015

Devant un jury composé de :

M. le Pr Gilles EDAN : Rapporteur

M. le Pr Jeroen GEURTS : Rapporteur

Mme le Pr Aurélie KAS : Examinateur

Mme le Dr Françoise DURAND-DUBIEF : Examinateur

M. le Dr Michel BOTTLAENDER : Examinateur

M. le Pr Bruno STANKOFF : Directeur de thèse

To my daughters, Maéva and Shoshanah, who bring sunshine to my rainiest days…

« Let all that you do be done in love » Corinthians 16:14

Acknowledgements

This dissertation would not have been possible without many people who have inspired, challenged, supported, and trusted me. To each of them, I would like to express my appreciation and deepest gratitude.

I am incredibly fortunate to have Pr Bruno Stankoff as my advisor. I would like to thank him for shaping my approach to neuroimaging research and for sharing with me his unique insights on MS pathophysiology. His guidance and patience, never condescending and always supportive, have allowed me to not only explore the world of research but to blossom as a scientist.

I don't think I would be where I am today if it were not for Pr Catherine Lubetzki. Her passion for the cause of MS and the compassion she shows her patients and students have inspired me tremendously. I can't thank her enough for her support throughout my career and for the opportunities she has opened for me.

I am very grateful to Pr Jerry Wolinsky, who has followed up with me since my first observership in his department and later welcomed me to his lab as a post-doctoral fellow. I am truly indebted to him for taking the time to share with me his clinical and research expertise and for encouraging my independence.

I would like to thank Dr Michel Bottlaender for teaching me about PET imaging and for his critical input.

My sincere thanks also go to Pr Gilles Edan, Pr Jeroen Geurts, Pr Aurélie Kas and Dr Françoise Durand-Dubief for accepting to serve on my thesis review committee. I look forward to your challenging questions, your critique of this work and your valuable insights on future endeavors.

I would like to thank my colleagues for their contribution to this work and for their words of encouragement, particularly Celine Louapre, Benedetta Bodini, Daniel Garcia-Lorenzo, Laure Bottin, Claire Leroy, and Benjamin Granger.

This work would not have been possible without the neurologists of the MS team, Dr Rana Assouad, Dr Caroline Papeix, and Dr Elisabeth Maillart, the nurses of the Centre d'Investigation Clinique, the PET staff at Service Hospitalier Frederic Jolliot, and our collaborators, Drs Ayman Tourbah and Frederic Dollé.

I am very grateful for the generosity of the agencies who have funded my work: Journées de Neurologie de Langues Française (JNLF), Institut National de la Santé et de la Recherche Médicale (INSERM), and the National Multiple Sclerosis Society (NMSS).

I would like to express my heartfelt appreciation to our MS patients who have humbled me and given me purpose.

Life would not have been as delightful without the many friends who have kept me centered. I love you all.

I would like to thank my loving and caring family. Thanks to my dad who truly understands and shares every little bit of excitement I have about what I do, to Danièle for being such a calming and loving presence in my life. Thanks to my sister Taliah, and my mom who always believed in me. Thanks to my in-laws John and Kathy for their constant love and encouragement.

To my husband Travis, thank you for your unfailing love and support, your interest in my work, your understanding of my calling for medicine and research, and above all for the many technical solutions you have provided that have made this work possible!

Table of Contents

Figures

Tables

Abbreviations

25-FW	25-foot walk
9-HPT	9-hole peg test
^{1}H-MRS	Proton Magnetic Resonance Spectroscopy
BBB	Blood Brain Barrier
BP	Binding potential
BZD	Benzodiazepine
CBF	Cerebral blood flow
CDMS	Clinically definite MS
CIS	Clinically isolated syndrome
CL	Cortical lesion
CNS	Central nervous system
CSI	Chemical Shift Imaging
CWP	Cluster-wise p-value
DGM	Deep grey matter
DIR	Double inversion recovery
DIS	Dissemination in space
DIT	Dissemination in time
DMT	Disease modifying therapy
DTI	Diffusion Tensor Imaging
EAE	Experimental autoimmune encephalomyelitis
ECTRIMS	European committee for treatment and research in multiple sclerosis
EDSS	Expanded disability status scale
FDA	Food and Drug Administration
FDG	Fluorodeoxyglucose
FLAIR	Fluid attenuated inversion recovery
fMRI	Functional MRI
FMZ	Flumazenil
FOV	Field of view

FSPGR	Fast spoiled gradient recalled echo
GA	Glatiramer acetate
GM	Grey matter
IFN	Interferon
MAGNIMS	Magnetic Resonance Imaging in MS
MMSE	Mini mental state examination
MRI	Magnetic resonance imaging
MS	Multiple sclerosis
MSFC	Multiple Sclerosis Functional Composite
MTI	Magnetization transfer imaging
MTR	Magnetization transfer ratio
NAA	N-acetyl aspartate
NAGM	Normal appearing grey matter
NAWM	Normal appearing white matter
NMO	Neuromyelitis optica
NO	Nitric Oxide
NODDI	Neurite density and orientation dispersion
PASAT	Paced auditory serial addition test
pCASL	Pseudo-continuous arterial spin labeling
PET	Positron emission tomography
PPMS	Primary progressive multiple sclerosis
PSIR	Phase sensitive inversion recovery
RIS	Radiologically isolated syndromes
RRMS	Relapsing remitting multiple sclerosis
SDMT	Symbol digit modalities test
SPMS	Secondary progressive multiple sclerosis
WM	White matter

Introduction

Multiple sclerosis (MS) is the most frequent demyelinating disease of the central nervous system (CNS), affecting about 2 million individuals worldwide. The disease remains a major public health issue as the leading cause of non-traumatic neurological disability among young adults. Significant progress has been made in the past decades to address the inflammatory component of the disease, which has lead to the emergence of more successful disease modifying therapies (DMT) and to better clinical outcomes for patients at least in the early phases of the disease. Yet our picture of MS remains fuzzy at best, and our reach in terms of therapy limited as none of the drugs currently available has been shown to successfully prevent disability progression.

The classical dichotomy between inflammation and neurodegeneration had to be challenged to further our understanding of progression in MS. While inflammatory and demyelinating lesions of the white matter (WM) remain the hallmark of the disease and the most characteristic marker for diagnosis, grey matter (GM) changes and in particular neuronal damage is now thought to play a major role in the neurological decline of MS patients. Recognizing that besides myelin, synapses, dendrites and neurons are early targets of the disease process could have profound therapeutic implications. While this has been suggested in post-mortem tissue samples, further evidence in patients at different stages of the disease is critically needed. Several have tried to measure neurodegeneration in vivo using brain volumetry or non-conventional magnetic resonance imaging (MRI). But these techniques for the most part lack specificity to the neuronal compartment. Thus the development of a new imaging technique able to specifically assess the neuronal component of GM damage in MS patients may have significant impact.

[^{11}C]Flumazenil (FMZ) is an antagonist of the central benzodiazepine (BZD) receptor, a component of the ubiquitous $GABA_A$ receptor complex present on neurons throughout the cortical and subcortical grey matter. [^{11}C]FMZ positron emission tomography (PET) could possibly detect and quantify neuronal damage in the grey matter, and provide great insights into the pathophysiology of neurological decline in MS. This has been the working hypothesis of the work presented here.

This manuscript will first attempt to present current concepts of WM and GM damage in MS from a histological, immunological and neuroimaging point of view, highlighting the shift from inflammation to neurodegeneration in our understanding of disability progression. We'll underscore the need for new imaging techniques specific of the neuronal compartment to fully capture the neurodegenerative process and its relevance over the course of the disease. In the second part of this work we will propose PET with [^{11}C]-FMZ as potential marker of neuronal damage in MS by presenting the detailed methods and results of a pilot study conducted in relapsing remitting (RRMS) and secondary progressive MS (SPMS). Finally we will discuss our findings in the context of current and sometimes-conflicting ideas and theories of neurodegeneration in MS. We'll aim to expand the scope of this work by presenting future avenues of research relevant to our topic.

Multiple Sclerosis: from Inflammation to Neurodegeneration

1. GENERAL CONSIDERATIONS

Since its first pictorial descriptions by Jean Cruveilhier in his *Anatomie Pathologique du corps humain* [1] and Robert Carswell in *Pathological Anatomy: Illustrations of the Elementary Forms of Disease* [2], followed by its identification and classification as a distinct entity by Jean Martin Charcot, we have come a long way in our ability to diagnose and document the features of *la sclérose en plaques*. Multiple Sclerosis is now recognized as one of the most common diseases of the central nervous system (CNS), and is a very active field of research.

1.1. Epidemiology

In a recent review of existing literature, Melcon et al. [3] estimated the median MS incidence at 5.2 (range 0.5-20.6) per 100.000 p-yrs and median prevalence at 112/100.000 pop. Incidence and prevalence were found highest in North America. While low in childhood, MS incidence peaks between 20 and 40 years of age with a mean age of onset of symptoms often found around 30 years [4].

What was thought as a predominantly male disease at the beginning of the 20th century is now known to affect women disproportionately. Sex ratios of about 2-2.5/1 have been frequently reported but could be as high as 4.1 in some US communities [5]. The sex prevalence of MS seems to undergo dynamic changes, with several recent examples of increasing sex ratios. In Denmark, Koch-Henriksen and colleagues reported that the incidence of MS in men had remained virtually the same whereas that of women had doubled since 1970 [6]. This phenomenon may indicate potential environmental changes, not just a better diagnosis of benign cases in women.

MS prevalence varies greatly between continents. As mentioned above, North America was found to have the highest incidence and prevalence in a recent study [3], followed by Europe. In contrast, South and East Asia, South America and North Africa had much lower rates. However the notion of a latitudinal gradient suggested by early epidemiologic studies is now being increasingly questioned as genetic and

environmental factors are thought to play a key role over geography in the prevalence and incidence of MS. Of particular interest, lower circulating levels of vitamin D have been associated with a higher risk of MS [7] [8]. It has also been shown that vitamin D levels are inversely associated with clinical relapses and MRI activity in MS patients [9]. Other environmental factors such as cigarette smoking [10] and Epstein-Barr virus infection [11] have been identified.

1.2. Diagnosis of Multiple Sclerosis

1.2.1. Clinical features

Initial presentation can greatly vary from patient to patient. Common presenting symptoms include: optic neuritis, brainstem or spinal cord manifestations or in less frequent instances hemispheric symptomatology. In up to one fourth of cases, symptoms at presentation may be multifocal [12]. When a patient presents with symptoms suggestive of WM tract damage, the exclusion of an alternate diagnosis is imperative before a diagnosis of MS can be made. Such diagnosis will then rely on the demonstration of "dissemination in space" (DIS), and "dissemination in time" (DIT) based on clinical grounds alone (clinically definite MS or CDMS) or a combination of clinical and radiological findings.

A "relapse" is defined as "patient-reported symptoms or objectively observed signs typical of acute inflammatory demyelinating event in the CNS [...] with duration of at least 24 hours, in the absence of fever or infection" [13]. Based on the McDonald criteria of the International Panel on Diagnosis of MS, initially published in 2001 [14], subsequently revised in 2005 [15] and 2010 [13], a diagnosis of MS can be reached on clinical findings alone if the patient presents with a history of 2 or more relapses and objective clinical evidence of 2 or more lesions. It should be expected for MRI findings to be consistent with a diagnosis of MS, though not mandatory in this case. In all other presentations (2 attacks with objective evidence of only one lesion, single relapse, progressive course), MRI will play a central role in demonstration of DIS and DIT.

1.2.2. Magnetic Resonance Imaging

MRI is currently the most useful paraclinical tool for the diagnosis of MS. MS white matter plaques, the pathological hallmark of the disease, can be detected with great sensitivity particularly on T2-weighted or Fluid attenuated inversion recovery (FLAIR) sequences. Their objective presence on MRI is considered an essential requirement for the diagnosis of MS. These lesions are often periventricular with a characteristic ovoid shape, but can also be seen in juxtacortical or infratentorial areas (Figure 1).

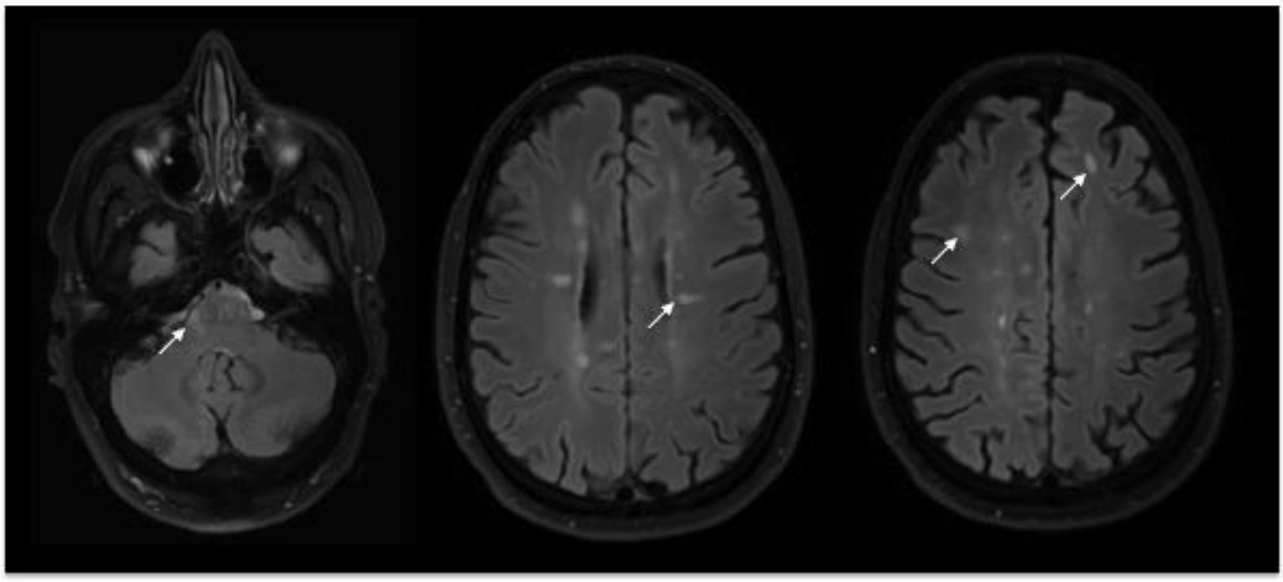

Figure 1: MS lesions visible as hyperintensities on FLAIR images. Left: Infratentorial lesion found in the pons (arrow). Middle: numerous periventricular lesions, some of which have classic ovoid shape (arrow). Right: subcortical lesions in frontal areas (arrows).

MRI lesions enhancing after injection of Gadolinium (Figure 2) reflect active inflammation and breakdown of the blood-brain barrier (BBB) and are thus considered more recent (≤3 weeks on average).

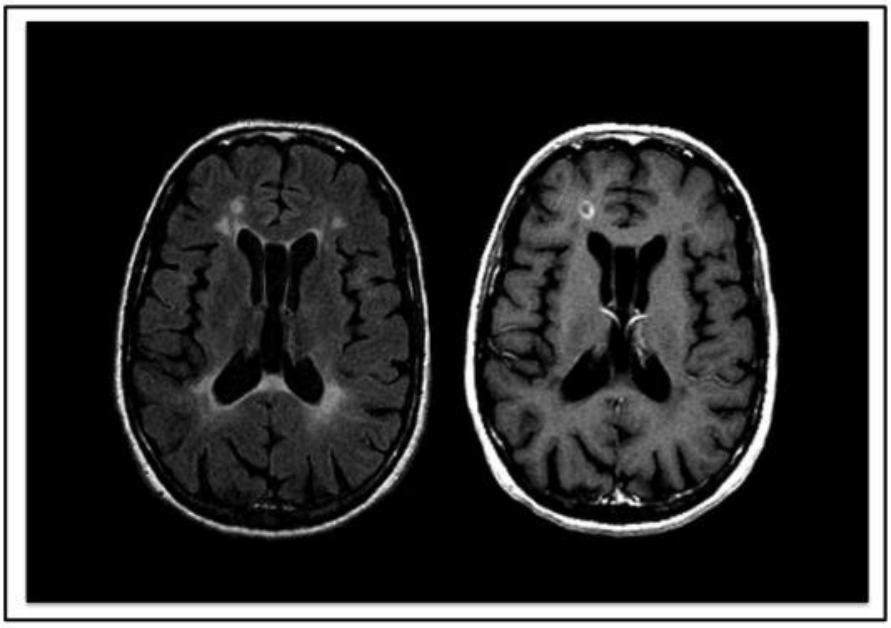

Figure 2: MRI of the brain post-gadolinium injection in one MS patient. Periventricular lesions are seen as hyperintense foci on Flair image (left). Recent area of inflammation enhances after gadolinium injection on T1-weighted scan (right)

Spinal cord lesions have been reported in up to 90% of MS patients [16] and asymptomatic lesions have been detected in up to one third of patients presenting with a demyelinating event suggestive of MS. Spinal cord MRI at time of diagnosis can thus be useful to demonstrate DIS of the disease process. Spinal cord lesions, however, much less frequently present with contrast enhancement and are therefore rarely useful for demonstration of DIT. It is currently not recommended to perform follow-up spinal MRI in CIS patients, as it seems to have limited value [17]. However, it is important to perform spinal MRI for differential diagnosis in patients presenting with symptoms suggestive of spinal cord demyelination [18]. Compressive myelopathy can easily be ruled out. Other disorders can present with spinal cord lesions and the topography and extent of the lesions should be critically analyzed. Particular consideration will need to be given to neuromyelitis optica (NMO). In MS, short-segment lesions (figure 3) are the rule, whereas NMO lesions are longitudinally expansive (more than three vertebral segments in length) on sagittal views. MS lesions are often located on the periphery of the cord on axial views. They contrast with NMO lesions, which are often central and expand axially within the spinal GM.

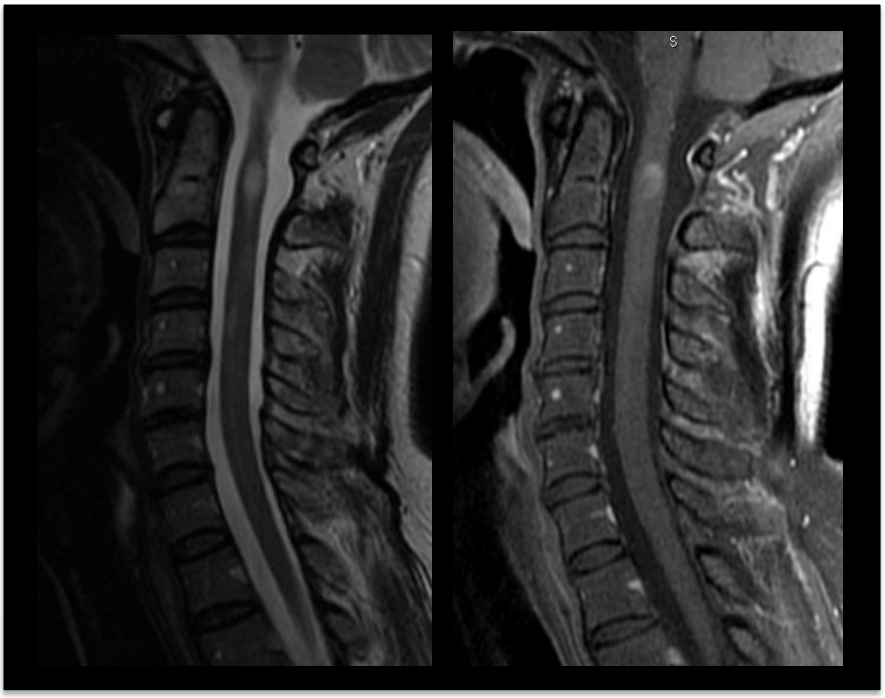

Figure 3: Active cervical cord lesion in MS on sagittal MRI. Lesion is visible as T2 hyperintensity (left) and enhances after Gadolinium injection on T1-weighted scan (right). MS lesions typically extend over <2 vertebral segments.

While earlier diagnostic criteria using MRI were based on lesion number [19], revised and simplified criteria by Swanton and colleagues now focus on lesion location (periventricular, juxtacortical, infratentorial, spinal cord) for demonstration of DIS [20]. Confirmation of DIT can be achieved on a single MRI with presence of enhancing and non-enhancing lesions, or otherwise by detection of additional lesions on follow-up scans. The revised McDonald criteria have the clear objective of allowing early diagnosis of MS in patients presenting with typical symptoms of CNS demyelination. Still, the risk of over-diagnosing MS remains real and as the Magnetic Resonance Imaging in MS (MAGNIMS) committee recently recommended: “MRI scans should be interpreted by experienced readers who are aware of the patient’s clinical and laboratory information” [17].

1.2.3. Summary of 2010 revision of McDonald criteria

Clinical Presentation	Additional Data Needed for MS Diagnosis
≥2 attacks[a]; objective clinical evidence of ≥2 lesions or objective clinical evidence of 1 lesion with reasonable historical evidence of a prior attack[b]	None[c]
≥2 attacks[a]; objective clinical evidence of 1 lesion	Dissemination in space, demonstrated by: ≥1 T2 lesion in at least 2 of 4 MS-typical regions of the CNS (periventricular, juxtacortical, infratentorial, or spinal cord)[d]; or Await a further clinical attack[a] implicating a different CNS site
1 attack[a]; objective clinical evidence of ≥2 lesions	Dissemination in time, demonstrated by: Simultaneous presence of asymptomatic gadolinium-enhancing and nonenhancing lesions at any time; or A new T2 and/or gadolinium-enhancing lesion(s) on follow-up MRI, irrespective of its timing with reference to a baseline scan; or Await a second clinical attack[a]
1 attack[a]; objective clinical evidence of 1 lesion (clinically isolated syndrome)	Dissemination in space and time, demonstrated by: For DIS: ≥1 T2 lesion in at least 2 of 4 MS-typical regions of the CNS (periventricular, juxtacortical, infratentorial, or spinal cord)[d]; or Await a second clinical attack[a] implicating a different CNS site; and For DIT: Simultaneous presence of asymptomatic gadolinium-enhancing and nonenhancing lesions at any time; or A new T2 and/or gadolinium-enhancing lesion(s) on follow-up MRI, irrespective of its timing with reference to a baseline scan; or Await a second clinical attack[a]
Insidious neurological progression suggestive of MS (PPMS)	1 year of disease progression (retrospectively or prospectively determined) plus 2 of 3 of the following criteria[d]: 1. Evidence for DIS in the brain based on ≥1 T2 lesions in the MS-characteristic (periventricular, juxtacortical, or infratentorial) regions 2. Evidence for DIS in the spinal cord based on ≥2 T2 lesions in the cord 3. Positive CSF (isoelectric focusing evidence of oligoclonal bands and/or elevated IgG index)

If the Criteria are fulfilled and there is no better explanation for the clinical presentation, the diagnosis is "MS"; if suspicious, but the Criteria are not completely met, the diagnosis is "possible MS"; if another diagnosis arises during the evaluation that better explains the clinical presentation, then the diagnosis is "not MS."

[a]An attack (relapse; exacerbation) is defined as patient-reported or objectively observed events typical of an acute inflammatory demyelinating event in the CNS, current or historical, with duration of at least 24 hours, in the absence of fever or infection. It should be documented by contemporaneous neurological examination, but some historical events with symptoms and evolution characteristic for MS, but for which no objective neurological findings are documented, can provide reasonable evidence of a prior demyelinating event. Reports of paroxysmal symptoms (historical or current) should, however, consist of multiple episodes occurring over not less than 24 hours. Before a definite diagnosis of MS can be made, at least 1 attack must be corroborated by findings on neurological examination, visual evoked potential response in patients reporting prior visual disturbance, or MRI consistent with demyelination in the area of the CNS implicated in the historical report of neurological symptoms.

[b]Clinical diagnosis based on objective clinical findings for 2 attacks is most secure. Reasonable historical evidence for 1 past attack, in the absence of documented objective neurological findings, can include historical events with symptoms and evolution characteristics for a prior inflammatory demyelinating event; at least 1 attack, however, must be supported by objective findings.

[c]No additional tests are required. However, it is desirable that any diagnosis of MS be made with access to imaging based on these Criteria. If imaging or other tests (for instance, CSF) are undertaken and are negative, extreme caution needs to be taken before making a diagnosis of MS, and alternative diagnoses must be considered. There must be no better explanation for the clinical presentation, and objective evidence must be present to support a diagnosis of MS.

[d]Gadolinium-enhancing lesions are not required; symptomatic lesions are excluded from consideration in subjects with brainstem or spinal cord syndromes.

MS = multiple sclerosis; CNS = central nervous system; MRI = magnetic resonance imaging; DIS = dissemination in space; DIT = dissemination in time; PPMS = primary progressive multiple sclerosis; CSF = cerebrospinal fluid; IgG = immunoglobulin G.

Table 1: 2010 revised McDonald criteria for diagnosis of MS (from Polman et al., Annals of Neurology, 2011) [13]

1.3. Evolution and prognosis

1.3.1. Clinical phenotypes

Clarity and consistency in defining clinical phenotypes is essential for demographic studies, clinical trials and management of therapy in clinical practice. Newly revised classification proposed by Lublin and colleagues [21] recommends that patient phenotype be assessed on clinical grounds with input from imaging studies when needed. According to the new consensus, 3 disease phenotypes can be defined: clinically isolated syndrome, relapsing-remitting disease, and progressive disease including primary progressive and secondary progressive.

Clinically Isolated Syndromes (CIS) refer to the initial clinical presentation of the disease in patients with symptoms typical of demyelination of the CNS WM tracts, but who fail to show evidence of dissemination in time of the disease process. Patients with CIS may "convert" to definite MS if they meet criteria for DIS and DIT on clinical or radiological grounds.

A majority of patients diagnosed with definite MS will follow a relapsing remitting (RR) disease course characterized by exacerbations (relapses) with periods of clinical stability in between. Patients may recover fully or partially from relapses (figure 3-top). On the opposite end of the spectrum, 15% experience a gradual worsening from onset with no initial exacerbations (primary progressive course, figure 3- bottom)

Patients with an initial RR form of the disease may subsequently experience progression independently of relapse activity. This phenomenon is called secondary progression (SP, figure 3-middle). It is important to note that progressive disease (SPMS or PPMS) does not progress in a uniform fashion and patients may experience periods of relative clinical stability.

Assessment of disease activity may provide insights into individual prognosis and guide patient management. Thus, current consensus recommendations have included disease activity as a modifier of basic phenotype courses mentioned above. Clinical activity is defined by relapses or radiological activity (presence of contrast-enhancing lesions, new or unequivocally enlarged T2 lesions).

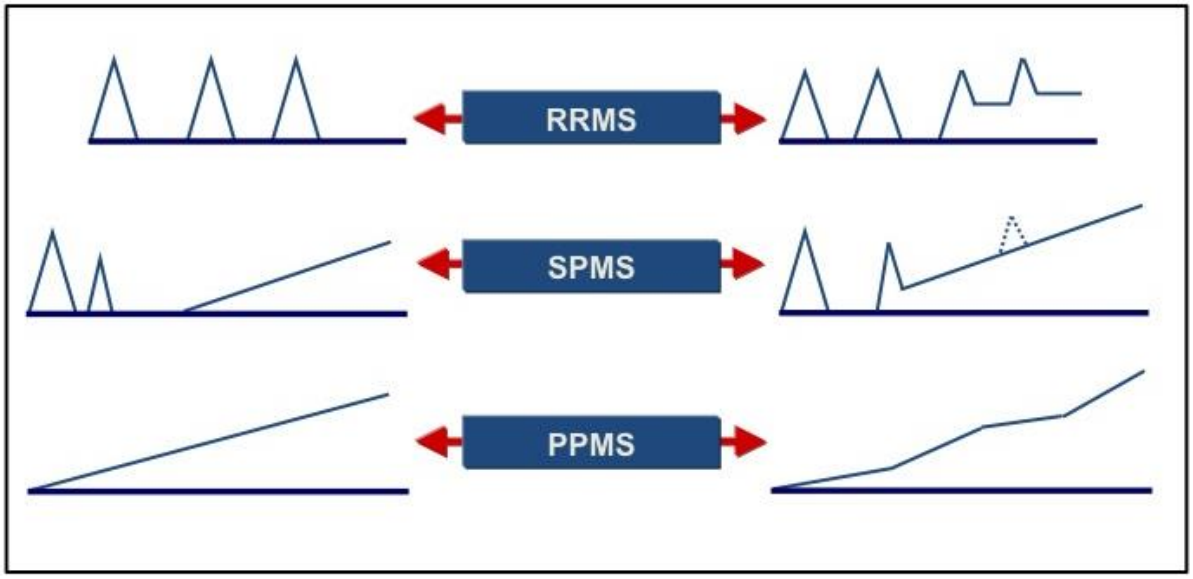

Figure 4: Clinical phenotypes of MS: Relapsing Remitting MS (RRMS, top) without (left) and with (right) accumulation of neurological deficits, Secondary progressive MS (SPMS, middle) without (left) or with (right) clinical exacerbations and primary progressive MS (PPMS, bottom) with linear course (left) or periods of relative stability (right).

With widespread availability of MRI, we have seen an increase in incidental abnormal findings. Radiologically isolated syndromes (RIS) are defined as MRI findings suggestive of MS in persons without typical MS symptoms and with normal neurological findings. This entity was recently introduced in the phenotypic description by Lublin et al. [21]. RIS individuals often have brain MRI performed for reasons such as headaches [22]. Okuda et al. [23] proposed a formal definition of RIS. The RIS Consortium recently presented the results of a retrospective study of 451 RIS subjects from 22 databases in 5 countries [24]. This study showed that 34% of RIS individuals would develop an initial clinical event within 5 years of RIS diagnosis. Age < 37 years, male sex, and spinal cord involvement appear to be the most important independent predictors of symptom onset. Prospective follow-up of RIS subjects should shed more light on this entity and help define the basis for treatment with disease modifying therapies (DMTs).

1.3.2. Prognosis and prediction

It is important to understand clinical phenotypes as a dynamic process. Patient with CIS may convert to RRMS, and patients with RRMS may subsequently follow a SP course. Brownlee et al. [25] followed 157 patients with CIS over 6 years: 71 (45%) had a second attack and thus developed clinically definite MS, 36 (23%) had MRI-only MS, and 50 (32%) didn't have MS according to 2010 McDonald criteria at the end of the follow-up period. Several independent risks factors for conversion to MS have been identified: young age [26], presence of cognitive impairment at onset [27], genetic factors such as HLA-DRB1 [28], and vitamin D deficiency [8]. One of the most significant predictors of conversion to MS from CIS is the presence of brain abnormalities on baseline MRI [29], with number, location and activity of the lesions all providing prognostic information.

While relapses may have unforgiving consequences in rare cases, the socio-economic impact of the disease is driven by the increasing and unrelenting disability progression that can follow the RR phase. Scalfari et al. recently provided a review of the London Ontario MS database [30], which evaluated 806 patients annually or semi-annually for 28 years (shortest follow-up=16 years). None of the patients received DMTs. At the end of the study period, 66.3% of patients had developed a SP course. The authors demonstrated that the rate of conversion to SPMS increases proportionally to disease duration. However they highlighted the fact that individual prognosis was highly variable. About 25% of patients will become progressive within 5 years of onset of the disease, while on the opposite end of the spectrum, 25% of patients will remain RR at 15 years. This natural history study confirmed previous findings suggesting that male sex [31] and older age of onset [32] were significant risk factors for conversion to SPMS. The role of early clinical activity in the probability and latency of secondary progression remains debated. Annual relapse rates are today the primary endpoint of many controlled clinical trials, and some have argued it could be used as a surrogate for disability progression [33]. Total relapse numbers were however found to have no or little significant effect on the risk of progression, the latency to onset of the SP phase or attainment of high disability levels [34] [35].

Beyond conversion to SP course, physical disability in the clinical setting or in research trials can be assessed using the Expanded Disease Severity Scale (EDSS, Annex A). This scale quantifies disability in eight functional systems (FS). These ratings are then used in conjunction with observations and information concerning gait and use of assistive devices to rate the EDSS from 0 (normal neurological examination) to 10 (death due to MS). In a recent publication [36], Tintore et al. performed multivariate analyses incorporating not only demographic and clinical data but also MRI and biological variables to determine the risk of attaining EDSS= 3.0 in individual patients. Their comprehensive work on a prospective cohort of 1015 patients with CIS highlights the importance of radiological and biological metrics to more accurately assess early risk of disability. They found that oligoclonal bands in the cerebro-spinal fluid (CSF), as well as the presence of over 10 lesions on baseline MRI were associated with a higher risk of accumulation of disability (up to EDSS= 3.0) with adjusted hazard ratios of 2.0 (95% CI 1.2–3.6) and 2.9 (95% CI 1.4– 6.0). In a presentation at the latest ECTRIMS meeting (Barcelona, 7-10 October 2015), the authors presented a more dynamic prediction model, which included not only baseline metrics but also data acquired at one year after CIS diagnosis. Again, MRI metrics such as new T2 lesions at 1 year were identified as relevant prognostic markers that modified baseline risk score at 12 months. The inclusion of dynamic variables improved risk prediction, with a reasonable C-statistic of 0.75. The model however was not designed to predict the risk of disability beyond EDSS=3.0 or the risk of entering a secondary progressive course.

Beyond the early stages of the disease, focal MS pathology appears less relevant to disease progression. Particularly, once a threshold of disability is reached, progression may not be influenced by relapses either before or after onset of the SP phase [37]. Leray and colleagues [38] proposed the concept of MS as a 2-stage disease. The early phase is defined from clinical onset to irreversible EDSS= 3.0 and is thought to be mainly dependent on focal damage to the WM. The second or late phase, from irreversible EDSS=3.0 to irreversible EDSS=6.0, is thought to be independent of focal inflammation and may instead be underpinned by diffuse inflammatory and neurodegenerative changes. In an observational study of 2054 patients referred to the Rennes MS clinic, the authors were able to show that disability progression in the first phase of MS does not influence progression during the second phase. Duration of the early phase was

found to be highly variable while the duration of the late phase was remarkably constant, as illustrated in figure 5. The dissociation between the 2 phases of MS, with different underlying mechanisms, is supported by MRI evidence. Calabrese et al. followed RRMS patients with at least 5 years of clinical history (mean>10 years) and showed that at this stage, variables such as T2 lesion volume did not influence the risk of entering the secondary progressive phase of the disease [39].

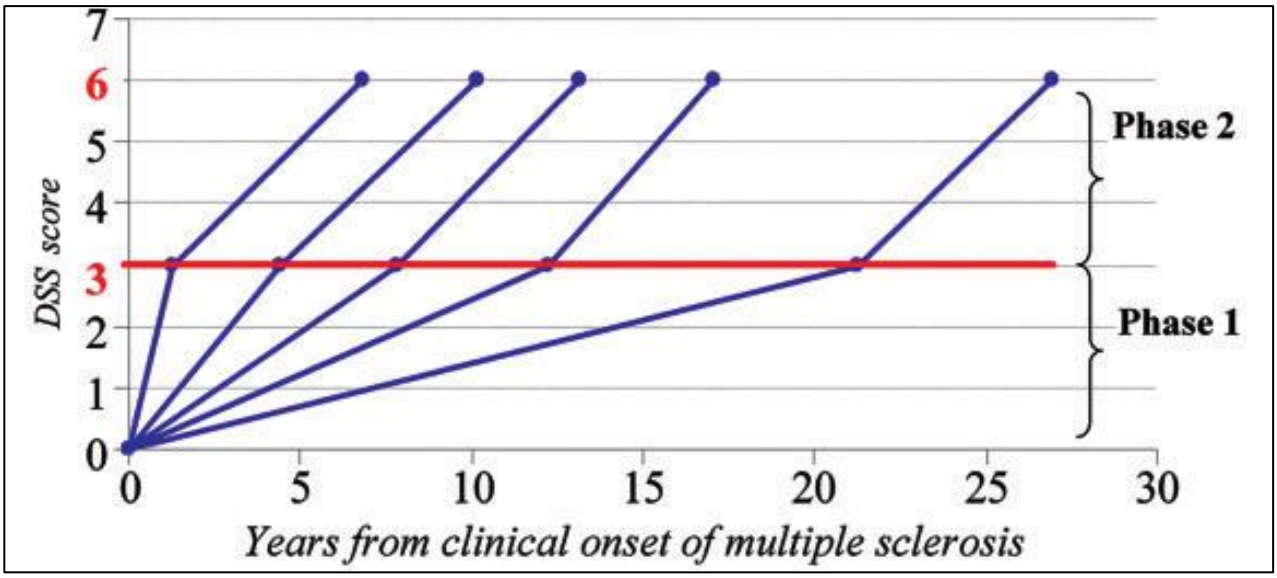

Figure 5: Duration of the 2 phases of MS (from Leray et al., Brain, 2010). Disability progression during Phase 2 (mean time from EDSS 3 to EDSS 6) in five subgroups defined according to the duration of Phase 1 (mean time from MS clinical onset to EDSS 3) in 718 MS patients who have reached both EDSS 3 and EDSS 6.

Patient prognostication is a complex and dynamic task in MS, as different clinical, radiological and biological factors can influence outcome depending on the disease stage. This reality reflects the variety of pathological mechanisms thought to underpin disability progression in MS, which will be discussed in a later section

1.3.3. Disease-modifying therapies available in 2015

The last 20 years have seen the emergence and systematic use of DMT in MS. There are currently 13 FDA-approved therapies with many more emerging drugs under trial or consideration. Available DMTs primarily target the inflammatory process of the disease and their mechanisms of action are illustrated in figure 4.

This major development in the MS therapeutic arsenal has almost exclusively benefitted patients with RRMS. All currently approved therapies have been shown to prevent, with varying degrees of efficacy, exacerbations and new brain T2 and Gadolinium enhancing lesions in RRMS. When studied in CIS, first line injectable immunomodulators such as glatiramer acetate (GA) or interferons (IFN) also reduced the risk of conversion into clinically definite MS [40].

The notion of "*sustained disability progression",* as used in RRMS clinical trial outcomes is defined as a worsening of EDSS performance that persists for 3 to 6 months. As noted by Lublin et al. [21], worsening in RRMS can occur in the context of multiple attacks, poor recovery after severe exacerbation or true onset of a progressive phase. Kalincik et al., recently suggested that disability outcomes of clinical trials based on 3-6 months "confirmed disability progression" overestimate the accumulation of permanent disability by 30% [41]. Consequently reported effects on "sustained disability progression" may not reflect actual efficacy on the accrual of disability occuring independently of relapse activity. In fact, when tested in SP or PPMS, none of the currently available therapies have demonstrated any effect in slowing progression or reversing disability, leaving about half of the MS patient population with a sense of neglect and frustration.

It has become clear that the pathological processes driving the progressive phase of the disease differ from that of the RR phase. To develop future therapies able to slow, prevent or even reverse progression, we will need to understand the specificity of this disease process, especially the early phenomena contributing to the accumulation of disability. We will need to develop reliable biomarkers that can substitute for clinical endpoints to speed up drug development. Such biomarkers may also allow early identification of patients at risk of progression.

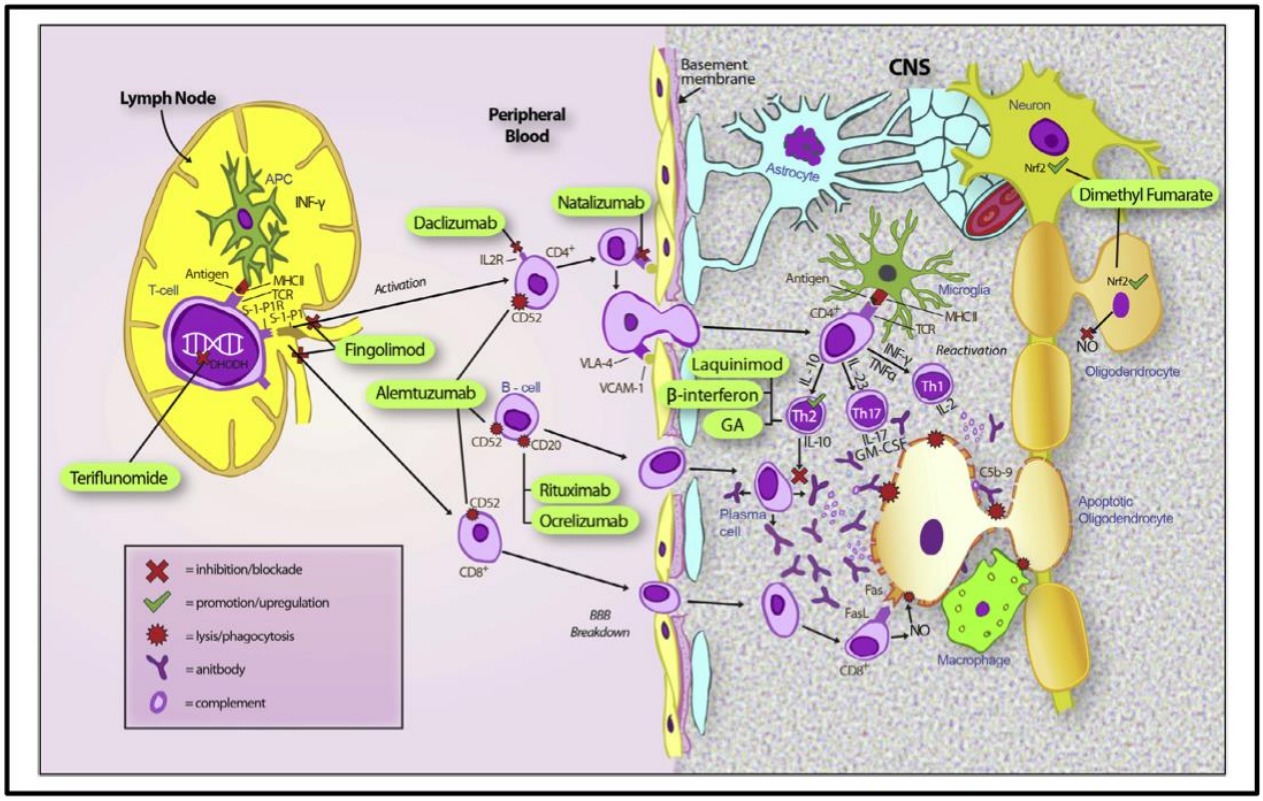

Figure 6: Illustration of mechanisms of action of currently available or in-trial MS therapies. APC = antigen presenting cell, BBB = blood–brain barrier, C5b-9 = complement complex 5b-9, CNS = central nervous system, FasL = Fas ligand, GA = glatiramer acetate, IFN = interferon, MHC I = major histocompatibility complex I, NO = nitrous oxide, Nrf2 = nuclear factor (erythrocyte derived) related factor 2, S-1-P1 = sphingosine-1-phosphate 1, TCR = T cell receptor, VCAM-1 = vascular cell adhesion molecule 1, VLA-4 = very late antigen 4. From Broadley et al., Journal of Clinical Neuroscience, 2014 [42].

2. MECHANISMS OF DISABILITY PROGRESSION

2.1. White matter damage

2.1.1. Focal demyelination and inflammation

The pathological hallmark of the disease is the formation of WM plaques of demyelination. Clinical relapses are considered the physical expression of these WM lesions. In the early stages of the disease, active WM tissue demyelination within plaques is associated with significant inflammation, BBB damage and microglial activation. Inflammatory infiltrates composed of clonally activated CD8+ T-lymphocytes and to a lesser degree CD4+ T-lymphocytes and B-cells are characteristically detected around post-capillary venules or scattered throughout the brain parechyma. Data suggest that the extent of T- and B-cell infiltration correlates with the degree of demyelination in focal active lesions [43]. Remyelination can occur in MS lesions. This process is particularly stable and extensive in animal models of the disease, but more limited in a majority of MS patients. A study of 168 WM lesions showed that only 22% were completely remyelinated as "shadow plaques", 73% partially remyelinated and 5% completely demyelinated [44].

Axonal transection, also a prominent feature of acute and active lesions, appears related to local inflammatory changes [45] [46]. Several factors may contribute to axonal transection during acute inflammatory injury of the WM. Activated T-cells may initiate a pro-inflammatory cascade resulting in the production of interferon gamma, which will subsequently activate macrophages to produce nitric oxide (NO). NO is a potent mitochondrial inhibitor and will disrupt ATP synthesis. Excitotoxicity due to increased release of glutamate by microglial cells or macrophages during the inflammatory process may further hinder mitochondrial function. Glutamate release leads to overstimulation of glutamate receptors on the post-synaptic membrane of neurons and loss of calcium homeostasis. Increased intracellular calcium concentrations activate enzymes involved in cytoskeleton disruption, DNA damage and mitochondrial dysfunction, leading to acute loss of axonal integrity [47].

Focal damage to the WM can be particularly well appreciated using MRI. T2-weighted sequences can detect WM plaques with great sensitivity. Beyond the diagnostic process, MRI can help detect subclinical disease activity by the presence of contrast-enhancing lesions or presence of new/enlarging lesions on subsequent scans. These markers of disease activity are particularly useful to the clinician to evaluate response to therapies which currently target the inflammatory process of the disease. Treatment non responders, or suboptimal responders, in whom a change of therapy should be considered, can thus be identified [17]. However, as we have seen earlier, MRI studies fail to show significant correlations between focal WM demyelination and inflammation and severity of progression, especially once the patient reaches a certain threshold of disability [48] [49] [39] [38].

To this day, conventional MRI cannot differentiate WM lesions that are fully or partly remyelinated from fully demyelinated ones, though this may be of importance in our understanding of the impact of WM lesions. Indeed, experimental studies have established that remyelination may promote short-term neuronal function recovery and help prevent subsequent axonal degeneration, possibly via trophic effects of axon-myelin interactions [50]. At the patient population level, studies of post-mortem tissue have shown diversity in the amount of remyelination between MS cases independently of the disease stage [51]. A patient may thus exhibit extensive or low remyelinating capacity. This was further confirmed by PET study of MS patients using radiotracer [^{11}C]PIB, a thioflavine derivative sensitive to changes in myelin content in tissue (figure 7) [52]. We recently longitudinal follow-up of MS patients with [^{11}C]PIB PET to support the notion of a patient-specific "remyelination profile". We demonstrated that patients' dynamic remyelination potential was strongly associated with clinical scores (Bodini et al., manuscript in revision), bringing novel insights on the role of WM lesions in MS pathophysiology.

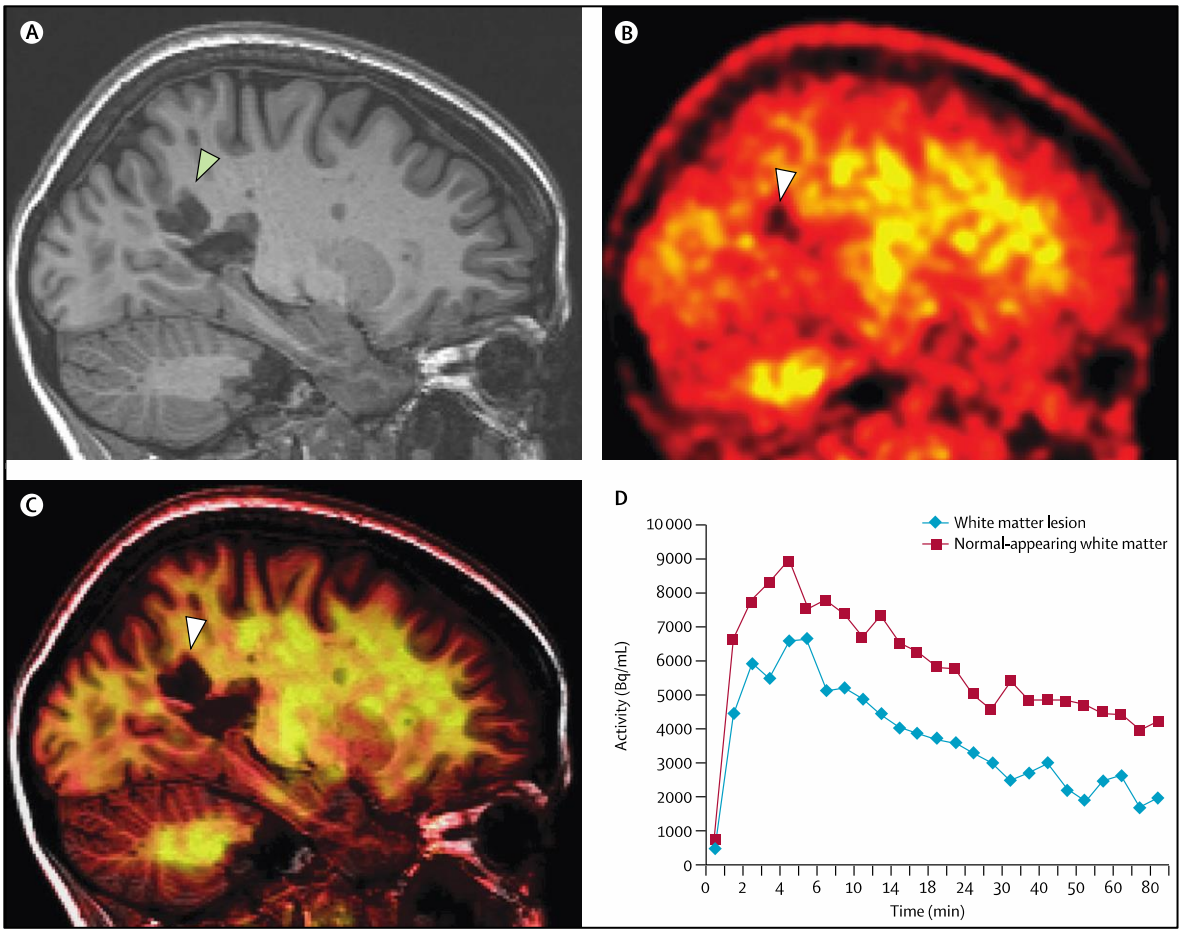

Figure 7: [11C]PIB in MS. The uptake of [11C]PIB is lower in MS lesions compared with normal-appearing white matter in patients with MS, suggesting the presence of demyelination. (A) T1-weighted image and (B) corresponding map of [11C]PIB PET binding in a patient with MS, showing lower [11C]PIB uptake in the GM in general compared with WM and lower uptake in a MS lesion (arrow head) compared to normal-appearing WM. (C) Coregistration of images shown in (A) and (B). (D) Time–activity curve of the normal-appearing WM (red) and the lesion seen in (A) (blue). PIB=thioflavine-T derivative 2-(40-methylaminophenyl)-6-hydroxybenzothiazole.

2.1.2. Diffuse white matter damage

In the progressive phase of the disease, inflammation becomes much less pronounced within plaques. Overall the percentage of an individual's lesions that are active declines as the disease evolves [53]. Lesions are either inactive or slowly expanding at the edges. Similarly, BBB leakage is much less evident [54]. This results in a decrease in frequency

of contrast-enhanced lesions and new/expanding T2 lesions on MRI, which become poor markers of evolution at this stage.

A characteristic feature of progressive MS is diffuse pathology of brain tissue, outside of focal lesions. Abnormalities have been described in the so-called "normal-appearing WM" (NAWM), ie WM tissue that appears normal both on macroscopic examination and MRI [55]. Pathologically, almost 75% of macroscopically normal white matter samples have been found histologically abnormal [56]. Areas of "dirty-appearing WM" (DAWM) have also been characterized on MRI as having an intensity higher than that of the NAWM, but lower than focal lesions. DAWM can be found in direct proximity of focal lesions or in locations not related to WM lesions and may represent a separate pathologic entity [57].

Pathology of the normal appearing white matter (NAWM) has been well described by post-mortem studies and has been found to differ significantly from that of early focal WM plaques. Kutzelnigg et al. analyzed 52 post-mortem MS brains at different stages of the disease and provided a clear picture of the diffuse pathology affecting the WM [58] (figure 8). The authors reported a global reduction in myelin staining in the NAWM due to decreased fiber density as well as diffuse axonal injury, which is most significant in the progressive MS cases compared to RRMS or acute MS. Axonal pathology is evident by the presence of axonal swellings, axonal end-bulbs and degenerating axons throughout the WM. It may be of importance to note that axonal degeneration is increased around MS lesions and in tracts emerging from plaques. Inflammation is also diffuse at the later stages of the disease and consists of perivascular cuffs of mononuclear cells and diffuse tissue infiltration by T-lymphocytes. Scattered microglial activation is another significant component of NAWM pathology and is profound at the later stages of the disease. Activated microglia, while present diffusely in the NAWM, tend to aggregate in the periplaque of slowly expanding, also called smoldering, lesions where it is associated with ongoing axonal injury [53]. Microglial cells are the resident macrophages of the CNS and can be activated following tissue injury [59]. They can then adopt diverse phenotypes, either protective or driving the degenerative process of the disease. Studies in animal models of MS have suggested that blood-borne monocytes, morphologically indistinguishable from resident microglia, may also infiltrate the brain parenchyma and play an important role in potentiating axonal degeneration [60].

Finally, meningeal inflammation, present at all stages of the disease, may influence the extent/topography of diffuse white matter damage.

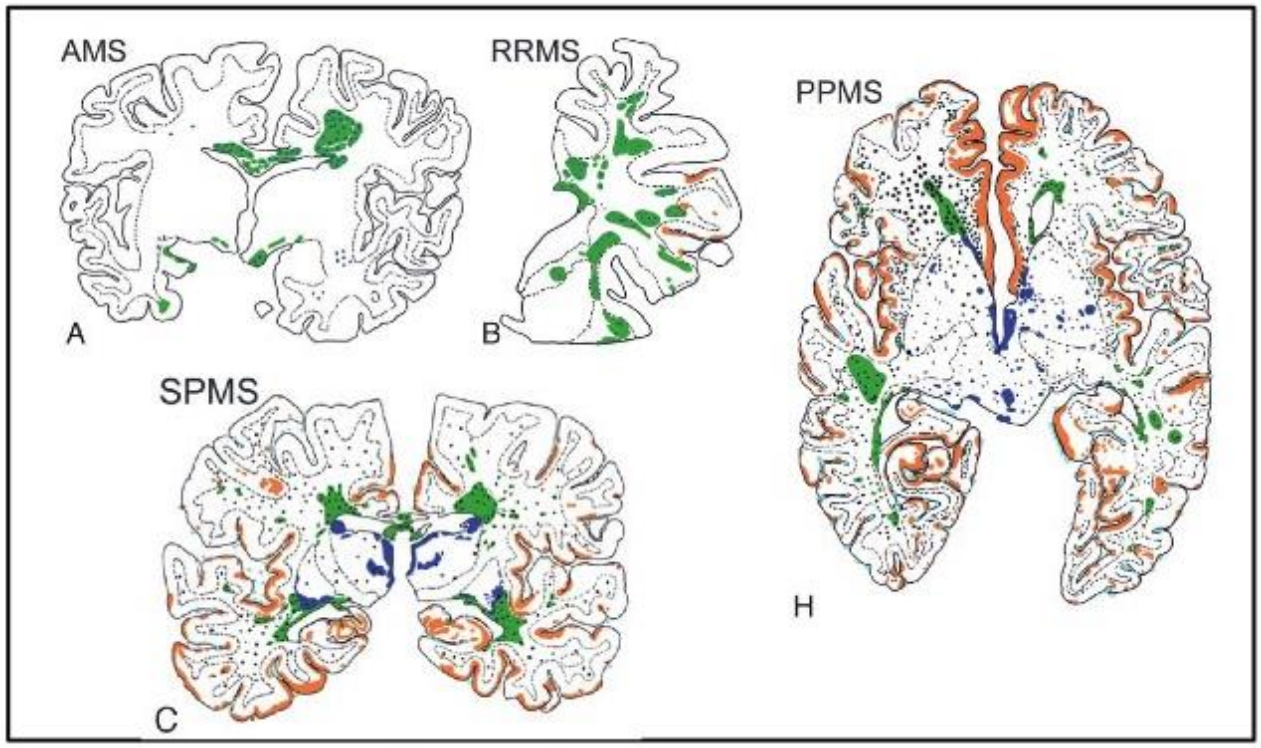

Figure 8: Pathology at different stages of the disease, acute MS (AMS), RRMS, PPMS and SPMS. White matter plaques (green) dominate the disease process in AMS and RRMS, while diffuse WM inflammatory infiltration (blue dots) and GM pathology (orange) are prevalent in PPMS and SPMS. From Kutzelnigg et al., Brain, 2005.

Few post-mortem studies have specifically focused on the DAWM as a separate entity from the NAWM. Moore et al. described a loss of myelin phospholipids that appeared intermediate between NAWM levels and that of focal plaques [61]. Seewann et al. reported in a larger number of subjects significant reduction of myelin density, extensive axonal loss and chronic gliosis [57]. Interestingly these changes appeared chronic in nature as no evidence of acute axonal damage, remyelination or BBB leakage were found.

Several mechanisms may have a role in the extensive axonal damage reported outside of MS lesions. The findings observed in the DAWM support a secondary neuro-degenerative process as a result of distant inflammatory lesional damage (wallerian

degeneration) [57]. Chronic demyelination in these areas may also imply loss of myelin trophic support, as suggested by evidence of axonal degeneration associated with genetic ablation of myelinating oligodendrocytes in animal models [50]. Loss of myelin staining in the NAWM however appears related to loss of fiber rather than primary demyelination. Recent studies in animal models have suggested that oligodendroglia may support axonal integrity through myelin-independent mechanisms. Impairment of these mechanisms may induce axonal damage without considerable demyelination. In particular, transport of lactate mediated by MCT-1 appears crucial to maintain axon function and survival [62]. Such axo-oligodendrocyte coupling may be particularly relevant when axons are energy-deprived [63].

By definition, NAWM is difficult to characterize using conventional MRI techniques such as T1- or T2-weighted sequences. MRI studies have used non-conventional imaging methods to assess the chonology of diffuse WM changes and the impact these changes can have on disease and disability progression. These advanced techniques include diffusion tensor imaging (DTI), magnetization transfer imaging (MTI) or Proton Magnetic Resonance Spectroscopy (^{1}H-MRS). Quantitative MRI studies have shown that diffuse WM changes are present from the early stages of the disease [64] and increase significantly over time. MRI studies have supported post-mortem evidence of NAWM damage occuring independently from focal damage [58] [65]. DAWM quantitative MRI measures, as reported by Vrenken et al., are intermediate between values of the NAWM and that of focal lesions [66].

MTI is a technique that is sensitive to microstructural changes in MS and its main metric, magnetization transfer ratio (MTR) is affected by myelin content and possibly axonal loss in post-mortem tissue [67]. Liu et al. found not only a significant decrease in MTR in the NAWM of MS patients compared to controls, but the authors were able to detect a clearly greater disease effect close to the ventricles [68]. It had already been shown that MS lesions are also more likely to occur around the ventricles [69]. Several factors could account for this pattern. Diffusion of CSF-mediated factors related to levels of meningeal inflammation has been suggested. CSF from MS patients has been shown to impair oligodendrocyte progenitor cells [70] as well as neuro-axonal function [71]. Decreased oxygen availability could also account for these findings as periventricular white matter is particularly prone to hypoperfusion in MS [72].

Metabolic neuro-axonal function can be assessed in the MS WM by evaluating N-acetyl-aspartate levels using Proton Magnetic Resonance Spectroscopy (^{1}H-MRS). The extent of NAA reduction within the NAWM at the early stages of the disease was found to correlate with subsequent cognitive deficits [73]. These results echo similar findings using MTI [74] and support the concept of a disconnection syndrome as an underlying mechanism of cognitive disability in MS.

PET imaging, using new tracers able to detect activated microglia and macrophages in vivo, has the potential to better our understanding of the role of diffuse microglial infiltration in disability progression. The translocator protein receptor (TSPO), a protein complex expressed by the outer mitochondrial membrane, is upregulated in activated microglial cells and macrophages, while maintaining low levels of expression in the brain parenchyma. These properties have encouraged the use of TSPO as a target for PET tracers. Compounds such as [^{11}C]PK11195, [^{11}C]PBR28 [75] or [^{18}F]DPA714 [76] all bind specifically to the TSPO complex, with different levels of affinity. Studies conducted using [^{11}C]PK11195 have found a significant increase in tracer uptake in widespread areas of periventricular and subcortical WM [77] suggesting diffuse infiltration by activated microglia at the SPMS stage of the disease. This technique was also able to detect the active inflammatory rim of chronic smoldering plaques. Giannetti et al. demonstrated the clinical significance of widespread microglial activation, showing that this phenomenon was detectable using PET with [^{11}C]PK11195 in the NAWM of patients with CIS and more pronounced in those who later developed CDMS (figure 9) [78].

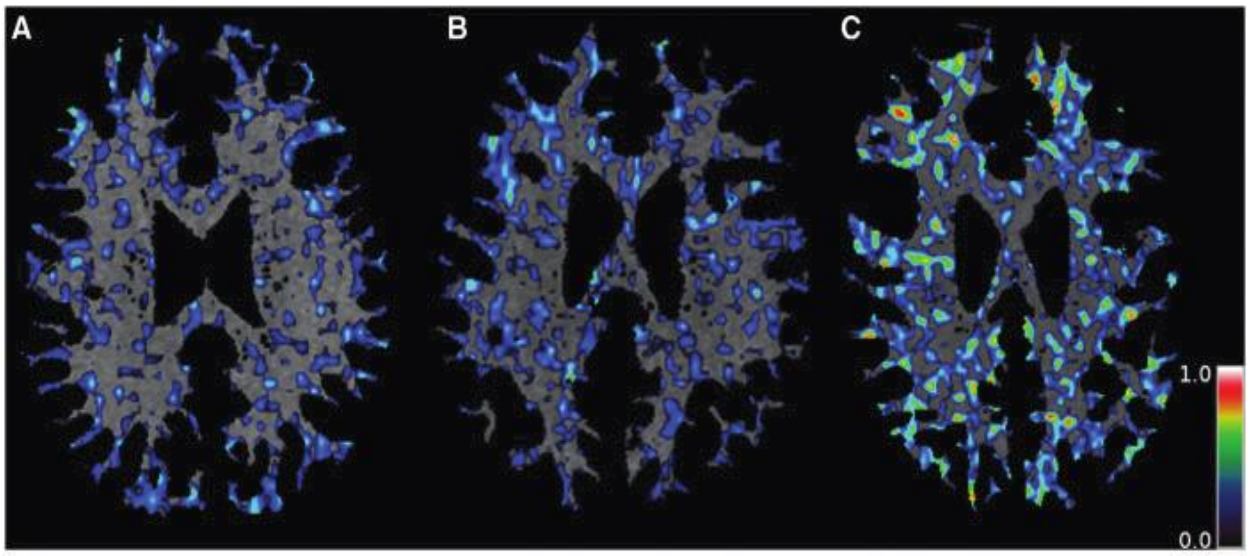

Figure 9: Normal appearing white matter on PK11195-PET images co-registered with MRI in three study subjects. The first subject is a healthy control (A) with PK11195 binding potential (BP_{ND}) in NAWM of 0.028; the second is a CIS subject without T_2 MRI lesions (B), an EDSS score of 3.5 and PK11195 BP_{ND} in NAWM of 0.037; the third is a CIS subject with T_2 MRI lesions (C), EDSS = 2.0 and PK11195 BP_{ND} in NAWM of 0.136. The color scale bar represents the BP_{ND} of PK11195. From Giannetti et al., Brain, 2015 [78].

2.2. Grey matter involvement

As studies have been limited in their ability to correlate neurological disability to focal WM pathology, the focus shifted not only to diffuse WM abnormalities but also to the possibility of associated GM damage. GM involvment in MS has perplexed scientists for many decades. Dawson's question "Is then, the process that attacks the cortex different in its nature and origin from that which affects the rest of the central nervous system?" still resonates, though histopathological and neuroimaging studies have provided great insight into the nature, extent and chronology of GM pathology in MS.

2.2.1. *Grey matter demyelination*

Unlike WM lesions, demyelination of cortical neurons is not visible macroscopically in post-mortem samples. In their seminal study, Brownell and Hughes (1962) [79] showed that about 22% of all brain lesions were located at least partly in the cerbral cortex and an additional 4% in the deep grey matter (DGM) structures. Improvement of immunocytochemical staining of myelin proteins has allowed more reliable investigation of GM demyelination, which has proven even more extensive than initially suspected. Recent pathological studies reported that the extent of GM demyelination often exceeds that of the WM in progressive patients [80], reaching up to 68% in extreme cases [58]. Grey matter demyelination is particularly extensive in the spinal cord, cerebellum, cingulate gyrus [80], thalamus [81] and hippocampus [82], regions that are of particular relevance to MS symptomatology, both physical and cognitive. Some have suggested that GM demyelination could, by impacting neuronal gene expression, reduce function in affected areas [82].

Lesions found in the MS grey matter differ strikingly from their WM counterparts. Lymphocyte infiltration, complement deposition, and BBB disruption, all typical pathological hallmarks of WM lesions, are not usually found in cortical lesions (CLs). Different types of CLs (figure 10) have been described according to their location and extent and include: leukocortical, intracortical and subpial [83] [84]. Leukocortical lesions consist of WM lesions which extend into the GM. Intracortical lesions project along vessels within the cortical ribbon. Subpial lesions are bandlike plaques which extend from the pial surface into the cortical layer 3 or 4 and can involve several gyri. In DGM structures, lesions are more often mixed GM/WM lesions (about 60%) [81], whereas subpial lesions are more frequent at the cortical level.

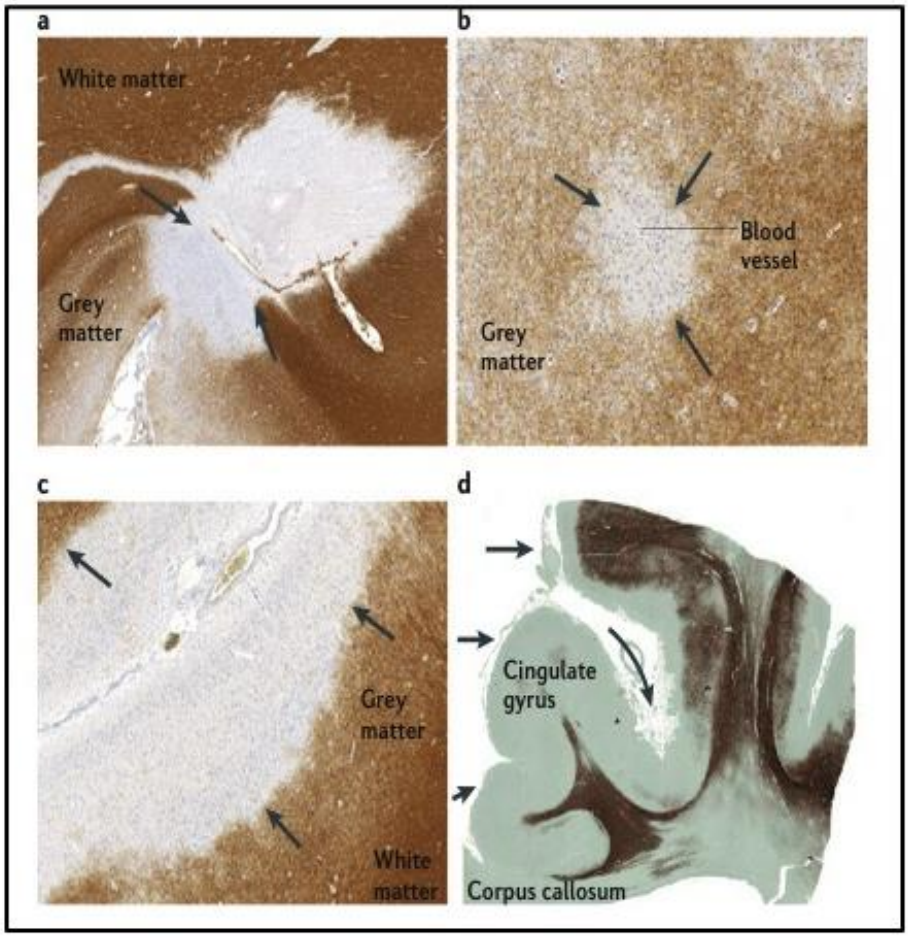

Figure 10: Different types of cortical lesions in MS: leukocortical (a), intracortical (b) and subpial (c). (d) highlights the extensive nature of subpial demyelinating lesions which can extend over several gyri. From Calabrese et al., Nature Reviews Neuroscience, 2015 [85].

At the earliest stages of the disease, leukocortical lesions were found to be the most frequent and inflammatory in nature [86], with predominantly perivascular CD3+ and CD8+ T-cell infiltrates and less commonly B-cell infiltrates. These differ from cortical lesions found at the latter stages of the disease, which are more frequently subpial and less inflammatory. Whether inflammation is a prerequisite to GM demyelination still remains unsettled.

It has been hypothesized that GM demyelination, and in particular subpial lesions, could be due to a myelinotoxic factor diffusing from the meninges. Subpial cortical lesions are often topographically related to mononuclear inflammatory infiltrates of the meninges in both early and late-stage MS [58] [86]. The presence of these meningeal B-

cell follicles has been associated with more extensive cortical damage and a more severe disease course [87].

The development of new MRI techniques sensitive to GM demyelination has allowed us to appreciate the clinical relevance of these lesions from the early stages of the disease. Sequences such as double-inversion recovery (DIR) or phase-sensitive inversion recovery have improved the detection of such lesions, and can be implemented on clinical grade scanners (figure 11). Although MRI techniques have become more sensitive to cortical demyelination, many cortical lesions remain undetected using MRI, especially with sequences available for routine practice. At 1.5T, only 18% of cortical lesions are detected when compared to histopathology [88] Higher field strength or combination of sequences can improve detection [89] [90] [91] [92]. Jonkman and colleagues recently reported that T2-weighted sequences at ultra-high field (7T) allowed prospective detection of 28% of cortical lesions [93]. Visualization of band-like subpial lesions still remains challenging [94] and availability of such techniques is currently limited. It is thus only the "tip of the iceberg" that can be seen and quantified using new MRI techniques [95]. But this "tip of the iceberg" still holds clinical significance. MRI measures of cortical demyelination have shown that GM lesions play an important role in physical and cognitive deficits (table 2). Cerebellar cortical lesion load also correlates with cerebellar function.

The potential contribution of CLs to the diagnostic process was recently suggested by Filippi et al. [96]. The authors found that the presence of at least one CL on baseline DIR MRI improved the identification of patients with CIS at risk of converting to CDMS. The applicability of new criteria of DIS which would include the presence of CLs remains to be further explored, especially considering the high false positive detection of CLs [88] [93] despite established consensus scoring recommendations [97].

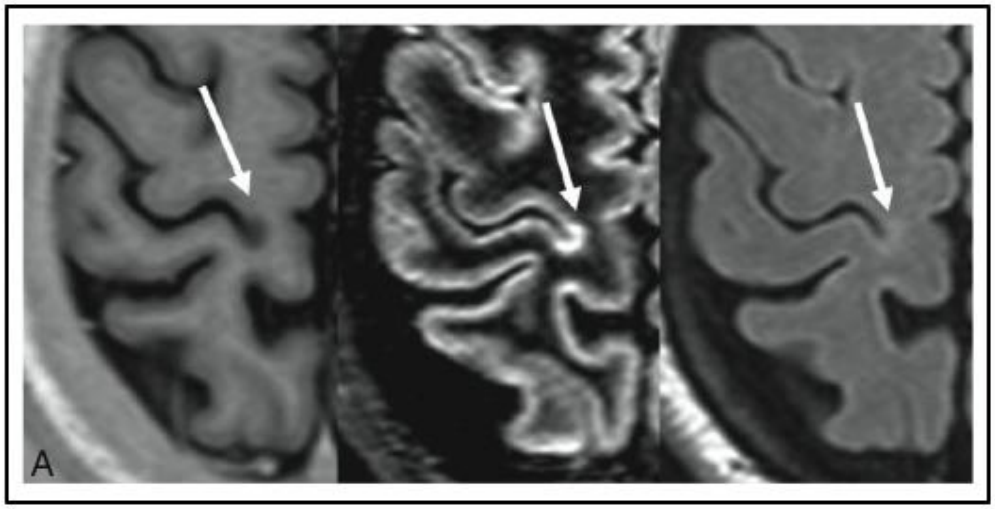

Figure 11: Improved detection of intra-cortical lesions (white arrow) using phase sensitive inversion recovery (PSIR, left) in combination with double inversion recovery (DIR, middle), compared to conventional fluid attenuated inversion recovery (FLAIR, right). Images kindly shared by Dr Flavia Nelson, Associate Professor of Neurology at the University of Texas, Medical School at Houston.

Study	Patients	Technique	Findings
Harrison et al., 2015 [98]	30 RRMS/ 6 SPMS	7T, MPRAGE and MPFlair	- CL volume correlates with EDSS more robustly than WM lesions. - CLs also associated with cognitive performance
Favaretto et al., 2015 [99]	10 CIS/ 24 RRMS/ 6 SPMS	3T, DIR and PSIR	- Cerebellar CL number correlates with cerebellar clinical scores
Harrison et al., 2015 [100]	28 RRMS/ 6 SPMS	7T, MPRAGE and MPFlair	- Thalamic lesion burden correlates with EDSS scores
Calabrese et al., 2013 [39]	334 RRMS	1.5T, DIR	- CLs one of three best predictors of conversion to SPMS at 5 years
Papadopoulou et al., 2013 [101]	65 CIS - RRMS/ 26 SPMS - PPMS	1.5T, DIR	- CL volume correlates with cognitive outcome measures but does not independently predict cognitive status
Calabrese et al., 2013 [102]	95 RRMS/ 45 "benign" MS	1.5T, DIR	- Low CL burden associated with benign disease course
Nelson et al., 2011 [103]	39 RRMS and SPMS	3T, DIR, PSIR	- Strong association between CLs and cognitive impairment
Mike et al., 2011 [104]	20 RRMS, 6 SPMS	3T, 3D Flair and 3D-IRSPGR	- CL metrics correlate with EDSS scores and cognitive measures (SDMT and CVLT-II)

Table 2: Selection of neuroimaging studies performed within the last 5 years that have assessed the clinical relevance of cortical lesions using MRI.

2.2.2. *Neurodegeneration*

As we have seen previously, degenerative changes in axons within acute WM lesions or NAWM have been well documented. Postmortem studies have also provided evidence of early and evolutive neuronal pathology in the MS grey matter. Peterson and colleagues reported neuritic changes within cortical lesions described as axonal transections, dendritic transections and apoptotic loss of neurons [83]. Axonal loss in GM structures is associated with on-going inflammatory activity [83] [81]. Yet, axonal damage in active GM lesions remains much less extensive than in acute active WM lesions. Neuronal death on the other hand was seen in chronic lesions without significant inflammation, suggesting that this phenomenon was not directly linked to the immune insult but might be a consequence of chronic injury. Wegner et al. quantified neuronal damage in the MS neocortex. The authors found a 10% reduction in mean neuronal density in leukocortical lesions compared to normally myelinated cortex, with decrease in neuronal size and significant changes in neuronal shape [105] [106]. Synaptic loss was significant in lesional cortex and occurred in greater proportion than neuronal soma reduction (-50% synaptophysin signal), suggesting that loss of dendritic arborization is an important feature in MS [105]. Pathologic changes in neuronal morphology, as well as reduced neuron size and axonal loss were also detected in normal-appearing cortex compared to controls [105] [107]. Klaver et al. reported a 25.4% loss of NeuN-positive neurons, reduced axon density (-31.4%) and 11.4% smaller neurons in type III cortical lesions (figure 12), while axonal density and neuronal size were also significantly reduced in the NAGM (-33.0% and -13.1% respectively) [108].

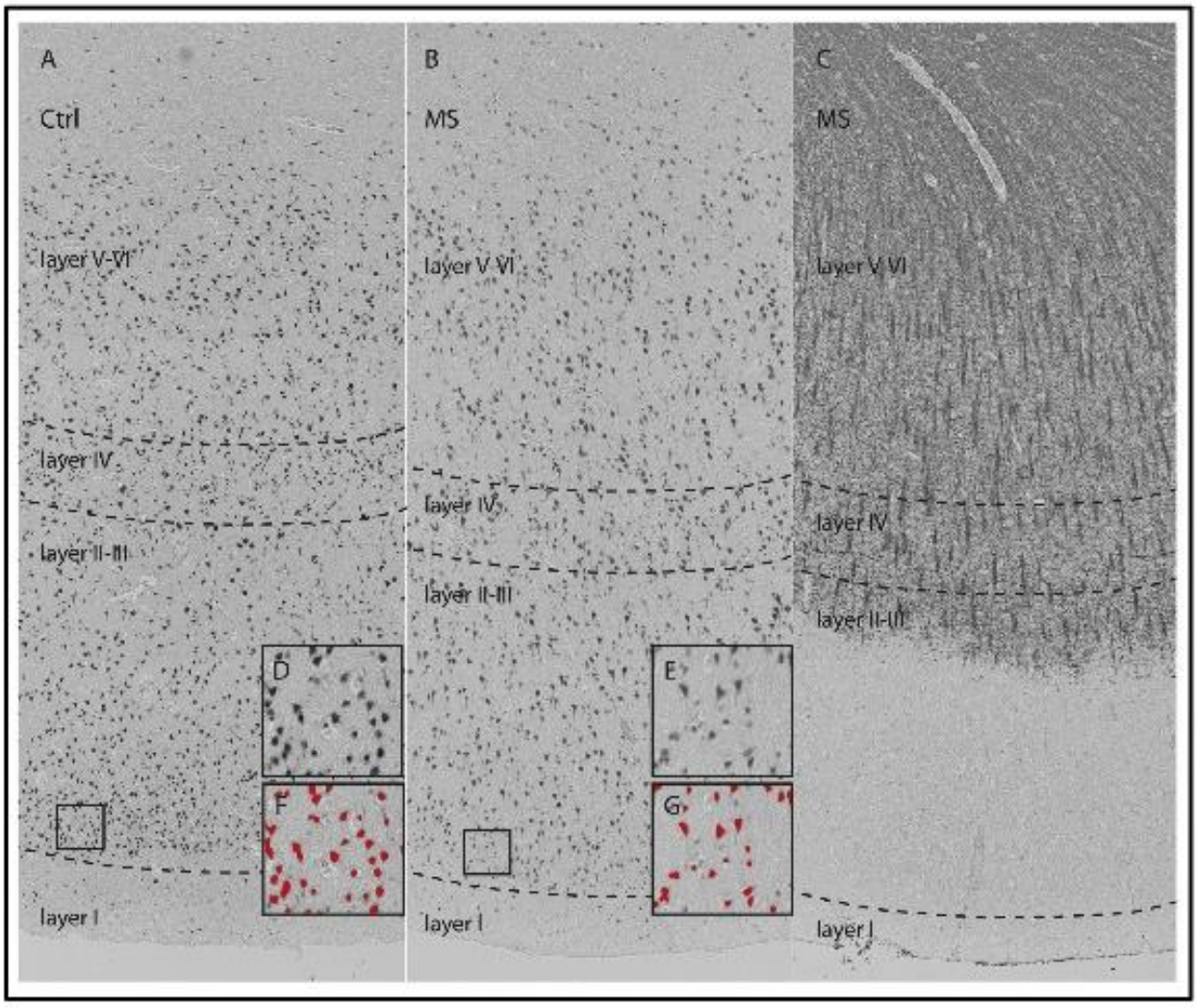

Figure 12: Neuronal loss in Type III cerebral cortical lesions in MS. Control (Ctrl) (A) and MS (B) sections immunostained for NeuN demonstrating overall neuronal loss in MS cortex. (C) Antimyelin PLP immunostained section from a patient with MS (B) showing subpial demyelination (original magnification: 100x). High-magnification pictures from cortical layer II (D, E), with matching pictures demonstrating the quality of segmentation scripts (F, G) (digital zoom from original magnification: 100x). From Klaver et al., J Neuropathol Exp Neurol, 2015 [108].

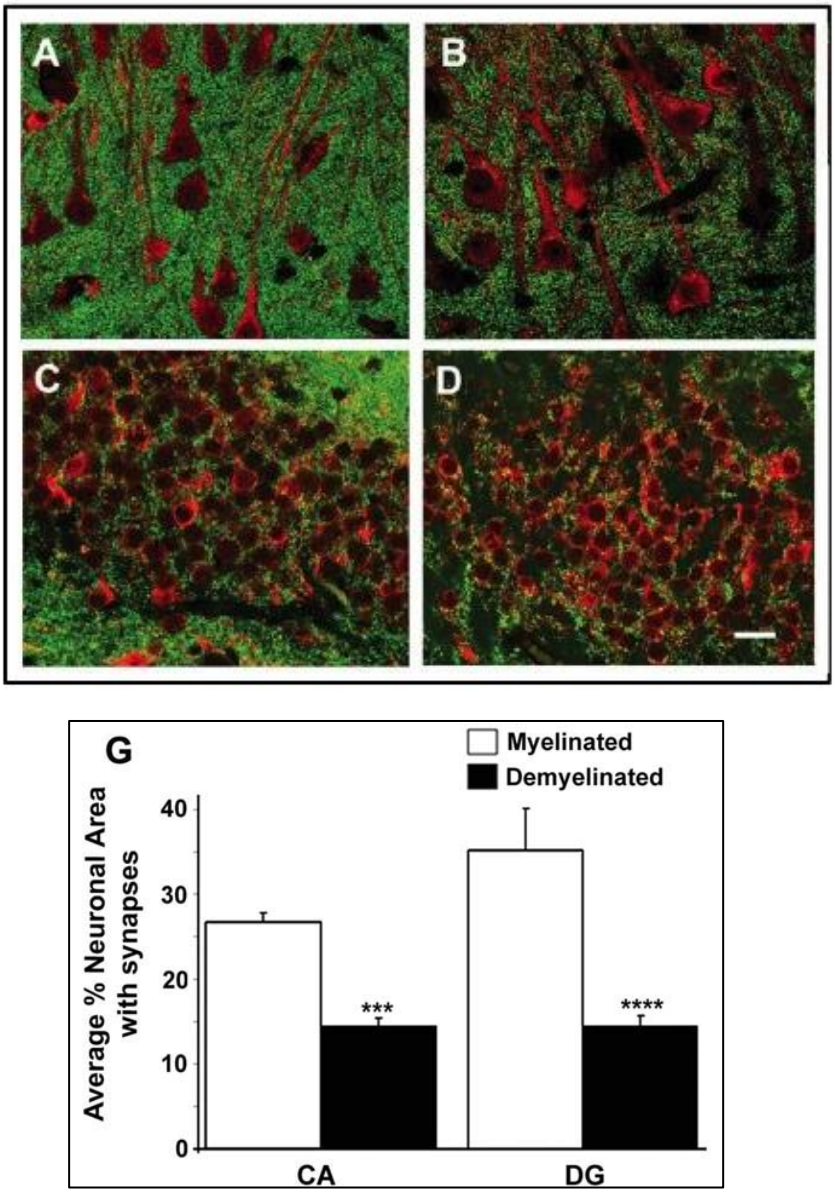

Figure 13: Synaptic loss in demyelinated hippocampus. Confocal images of multiple sclerosis (MS) hippocampus immunostained with antibodies specific to MAP2 (red) and synaptophysin (green) show punctuate presynaptic terminals (green) surrounding neurons in CA1 (A, B) and dentate gyrus (C, D) regions in MS myelinated (A, C) and MS demyelinated (B, D) hippocampus. Compared to myelinated MS hippocampi, pre- synaptic terminals were significantly decreased (G) in demyelinated MS hippocampi. From Dutta et al., Annals of Neurology, 2011 [109].

The neurodegenerative changes seen in the MS cortex are more subtle than those described in DGM structures, particularly the thalamus. Cifelli and colleagues reported

a 23% reduction in mean neuronal density corresponding to a 35% loss of total neuronal numbers in the MS thalamus compared to controls [110]. Unlike neocortical structures, neuronal density was decreased in both demyelinated and non-demyelinated DGM compared to control DGM, though the loss of neurons may be more pronounced in demyelinated areas [81]. Neuronal atrophy and morphologic changes were also detected in the MS DGM regardless of myelination status and may precede or accompany neuronal loss. In the hippocampus, neuronal counts were decreased by up to 30% depending on location [111]. Also in the hippocampus, Dutta et al. reported substantial reduction in synaptic density (figure 13) [109]. They found decreased expression of neuronal proteins involved in axonal transport, synaptic plasticity, and neuronal survival in demyelinated hippocampi as well as altered expression of neuronal miRNA [109] [82]. These findings may explain, at least partly, some of the cognitive deficits observed in MS patients.

The mechanisms underlying neuronal pathology remain to be fully established. Of particular interest is the interplay between WM and GM pathology. At least at the late stage of the disease, which is more frequently explored by post-mortem studies, focal WM damage fails to correlate with neuronal changes in the GM [112] [113]. However recent neuroimaging studies demonstrated that focal WM pathology, at least in relevant locations, might impact MRI-driven GM atrophy measures at earlier stages of the disease [114] [115] [116]. It can also be suggested that loss of myelin and reduction in axonal density observed diffusely in the NAWM plays a role in the neurodegenerative process by promoting retrograde or trans-synaptic degeneration (figure 14). In support of this hypothesis, anatomical connection has been shown to influence the progression of neurodegeneration. Recent studies have provided evidence of neuronal dysfunction in connected GM neurons and correlated loss of integrity of WM tracts to histopathological measures of neurodegeneration in corresponding GM structures [112]. This was further supported by reports of tract-specific associations between cortical thinning patterns and MRI-derived metrics of NAWM integrity [117]. These findings suggest a link between diffuse damage of the WM and neurodegenerative processes in connected GM. Many however argue that WM pathology cannot satisfactorily explain the full extent of diffuse GM damage observed in MS, including pathological changes observed therein

[85]. Despite a clear degree of relationship, neuronal damage may also occur independently from WM pathology.

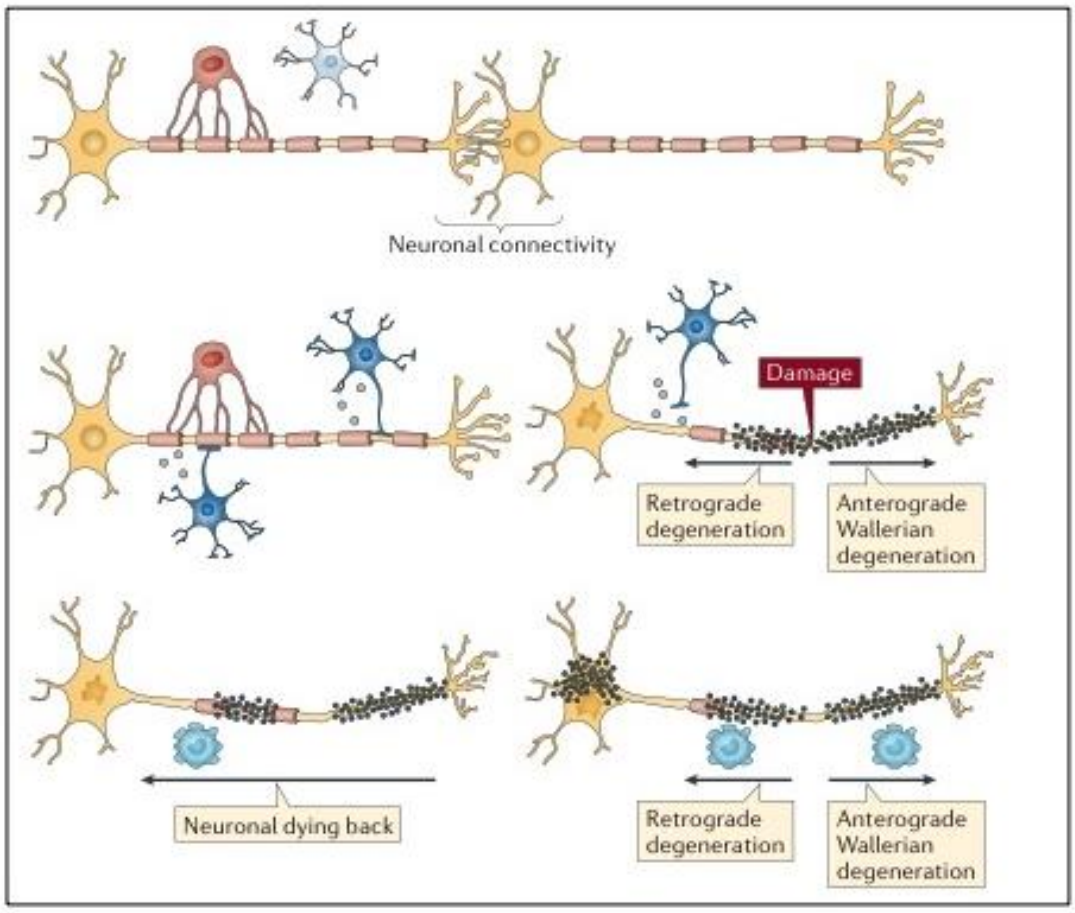

Figure 14: Undisturbed neuronal connectivity (upper panel) can be impaired by retrograde degeneration (middle panel) propagating backwards in cortical neurons whose axons have been damages by WM lesions or along WM tracts. The WM tract damage can lead to microglial inflammation (middle panel) and retrograde neuronal cell death (lower panel), as well as anterograde Wallerian degeneration below the damage. From Calabrese, Nature Reviews Neuroscience, 2015 [85].

Neurodegenerative processes appear particularly prominent in certain types of GM demyelinated lesions. Local inflammation, microglial activation, or loss of trophic support from surrounding glia can all contribute to neurodegeneration within demyelinated lesions. However, neuronal changes in non-demyelinated areas have been reported both in the neocortex and in subcortical GM structures [105] [107] [108],

suggesting that focal GM demyelination and neurodegeneration are at least partly distinct phenomena in progressive MS.

A number of studies have drawn attention to the inflammatory process occuring in the meningeal compartment. Meningeal inflammation is widespread and can be exacerbated by the presence of B-cell follicles in the meningeal space (figure 15) in a proportion of patients with progressive MS [87] [118]. These lymphoid structures appear to spatially coincide with subpial demyelinating lesions and were associated with quantitative increase in microglial activation within the GM [118]. SPMS cases with B-cell follicles presented a more severe disease course, with younger age at onset, younger age at irreversible disability and earlier death, emphasizing the clinical significance of these findings [87]. Magliozzi et al. later demonstrated significant neuronal loss with a gradient away from the pial surface and more severe cortical thinning in SPMS patients characterized by B-cell follicle-like structures in the meninges [113]. The link between meningeal inflammation and GM damage is further corroborated by studies pointing to a specific role exerted by both meningeal T cells and activated microglia in diffuse axonal loss in the spinal cord [119]. These findings strengthen the hypothesis that meningeal inflammation is implicated in neurodegeneration in MS and contributes to clinical severity and progression.

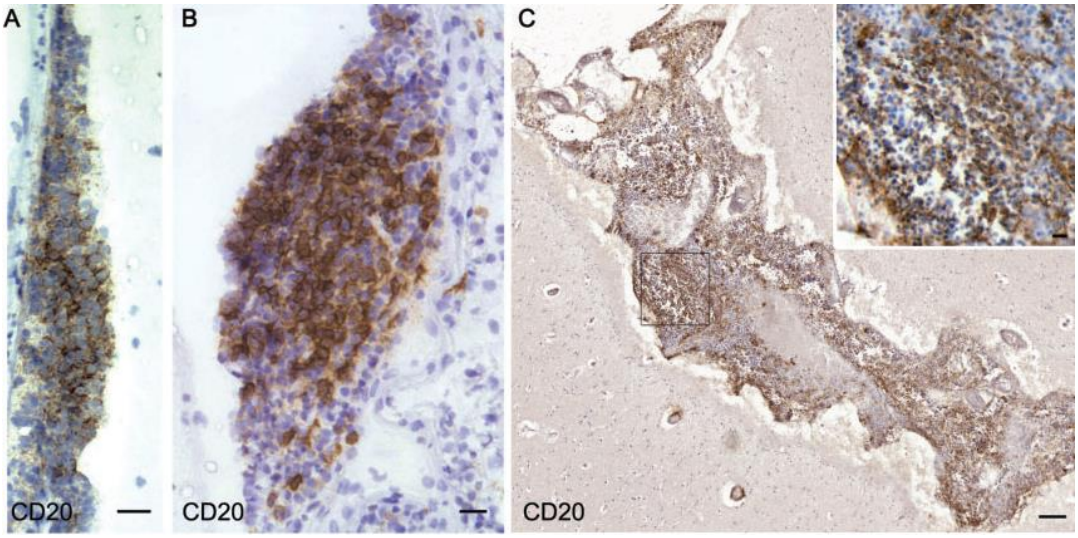

Figure 15: B-cell follicle-like structures in meningeal space of SPMS patient. (A, B) follicle of modest size. (C) Extensive infiltrate filling entire sulcus. From Howell et al. Brain, 2011 [118].

Both inflammatory cells present in the meninges and activated microglia in the GM can induce the production of oxygen and nitric oxide (NO) species by enzymes including nicotinamide adenine dinucleotide phosphate oxidase [120]. This oxidative burst can lead to or further amplify mitochondrial dysfunction and energy failure which are increasingly being recognized as major pathways of neurodegeneration in MS [121] [122]. Neurons in MS GM exhibit decreased respiratory chain function and mitochondrial gene expression [123]. Furthermore, multiple clonally expanded deletion of neuronal mitochondrial DNA are found diffusely and irrespectively of lesions in the MS cortex [124]. Respiratory deficiency creates a mismatch between energy demand and ATP supply which is thought to drive neuronal dysfunction or degeneration via excessive stimulation of calcium-dependent degradative pathways [125].

Sodium channel redistribution along denuded axons can aggravate this imbalance by significantly increasing energy demand in a context of supply deficit, leading to a state of “virtual hypoxia” [126]. Demyelinated axons are unable to maintain ionic balance between intracellular and extracellular space. Sodium channel influx triggers calcium cellular entry by reversing activity of Na^{+}/Ca^{2+} exchangers, resulting in elevated intra-axonal calcium levels. Increased Ca^{2+} concentration can be further exacerbated by injury-induced release of calcium from neuronal intracellular stores. Multiple degradation pathways are subsequently activated resulting in mitochondrial damage, activation of NO synthase, proteases and lipases which will contribute to neuronal injury [127].

Iron stored within oligodendrocytes and myelin sheaths may be liberated following demyelination. In its extracellular form, iron generates reactive oxygen species and contributes actively to oxidative damage. Iron is absorbed by microglia and macrophages where it accumulates until these cells degenerate and cause a second oxidative burst upon liberation of their iron content in the extracellular space [128]. Iron may also accumulate in axonal processes and contribute along with extracellular iron to axonal and neuronal degeneration [129]. As iron physiologically accumulates in an age-dependent fashion with a plateau around age 40-50 , an amplification of neuro-degenerative processes may be observed with age.

Additional factors have been thought to contribute to the imbalance between energy supply and demand and to downstream neurodegeneration. Decrease in cerebral blood

flow, thought to be mediated via release of vasoconstrictive peptides such as Endothelin-1 (ET-1) by activated astrocytes [130], has been reported in MS patients evaluated by MRI from the early stages of the disease [131] [72] [132]. Cerebral hypoperfusion might play a role in certain lesion formation [133], axonal and neuronal damage and consequently in disability progression [134] [135]. Toxic exogenous factors such as free radicals and cyanates from smoking may further exacerbate mitochondrial dysfunction and oxidative stress-related mechanisms [136].

Glutamate excitotoxicity may also play a role in GM neuronal degeneration beyond acute inflammatory attacks. MS-related modifications of glutamate levels in specific GM regions have been reported using MR spectroscopy [137], though these findings were not confirmed by others [138].

In conclusion, many well-conducted studies of post-mortem tissue have shown that GM damage dominates the pathological process as MS progresses. These studies have demonstrated the clinical significance of the degenerative process occuring in the MS GM and underscored the need to understand its causes. Strong focus on the very early stages of the disease is necessary to determine the primary insult affecting the MS grey matter and longitudinal follow-up will shed light on the relationship between demyelination, inflammation and neurodegeneration at different stages of the disease. Such approach may not be feasible using post-mortem or biopsy tissue samples. Development of pathology-specific imaging techniques, in particular techniques able to assess specifically the neuronal compartment, are necessary to further our understanding of GM pathology in MS. They will also prove uniquely useful to monitor individual patients in the clinical setting or in the context of clinical trials focused on neuroprotective therapy.

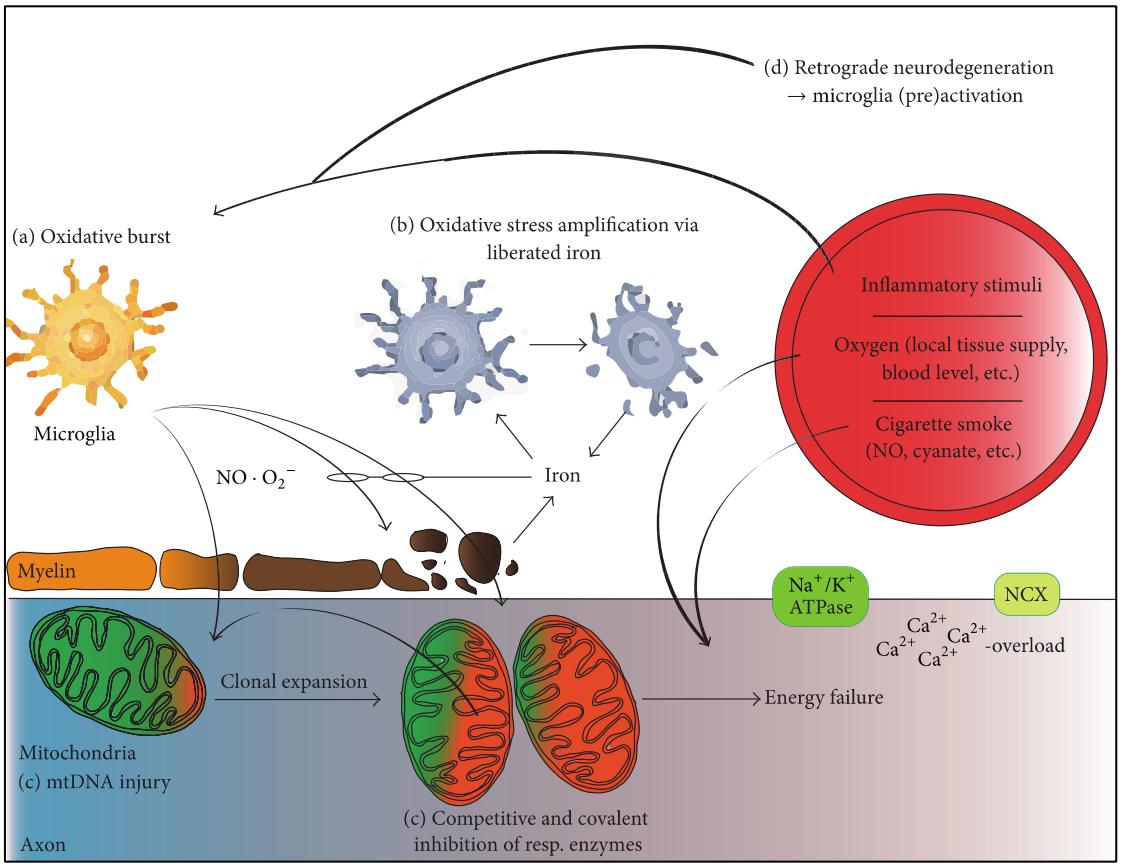

Figure 16: Oxidative stress-related mechanisms of tissue injury in multiple sclerosis. (a) Microglia is activated by unknown trigger pathology, the breakdown of the blood-brain barrier, and local and systemic inflammatory stimuli. Microglia releases nitric monoxide and superoxide molecules into the extracellular space. Additional amplification mechanisms involve microglia preactivation via axonal degeneration (d). (b) Iron is physiologically stored within the myelin sheets and liberated into the extracellular space upon demyelination. Extracellular iron amplifies oxidative stress inducing the production of highly reactive hydroxyl radicals. Iron is absorbed by microglia, which show histological signs of cell death under the high iron load and thus may release iron and initiate a second wave of oxidative stress. (c) Mitochondrial DNA (mtDNA) is vulnerable to free radical-mediated damage resulting in mtDNA deletions, which are found in neurons and axons of patients with multiple sclerosis. Mitochondria carrying such mutations are amplified by the clonal expansion in neurons. The mitochondrial respiratory chain is inhibited by covalent modifications caused by free radicals both competitively and irreversibly. A combination of these factors leads to energy failure via decreased ATP production. Exogenous factors, such as free radicals and cyanate delivered by smoking, inhibit mitochondrial function in experimental conditions. From Haider, Oxidative Medicine and Cellular Longevity, 2015 [128]

Imaging Neurodegeneration in the MS Grey matter

In vivo imaging techniques, in particular MRI, have had a major impact in MS. Detection of MS lesions on conventional acquisitions, such as T2- or T1-weighted sequences, has enabled earlier diagnosis of the disease and follow-up of subclinical inflammatory activity. As the role of neurodegeneration in MS pathogenesis and disability progression is clearly established, new treatments that could slow, halt or reverse this process are now being proposed. Unfortunately classic MRI measures of disease activity do not inform on the neurodegenerative process and we are witnessing a shift in imaging targets, from inflammation and demyelination to neurodegeneration [139] [140].

1. GREY MATTER ATROPHY

The cortex represents 65% of brain parenchymal tissue and GM largely drives the atrophic process occuring in MS. GM volume can be measured on conventional MRI sequences with freely available tools among which the most commonly used are FSL (http://fsl.fmrib.ox.ac.uk/fsl/fslwiki/), FreeSurfer (http://freesurfer.net) and SPM (http://www.fil.ion.ucl.ac.uk/spm/). This has tremendously helped the field in understanding the occurrence and chronology of GM tissue loss, as total and regional GM volumes, as well as cortical thickness can be assessed (Figure 17). MS lesions tend to be recognized as GM by the different softwares used in research, a misclassification that may affect GM volume estimation and obscure disease-mediated volume changes. This is why a procedure, called "lesion inpainting" is generally applied before GM segmentation. This procedure replaces lesional voxels with values approximating NAWM intensity [141]. It has been shown to significanly improve accuracy of GM volume and cortical thickness estimation.

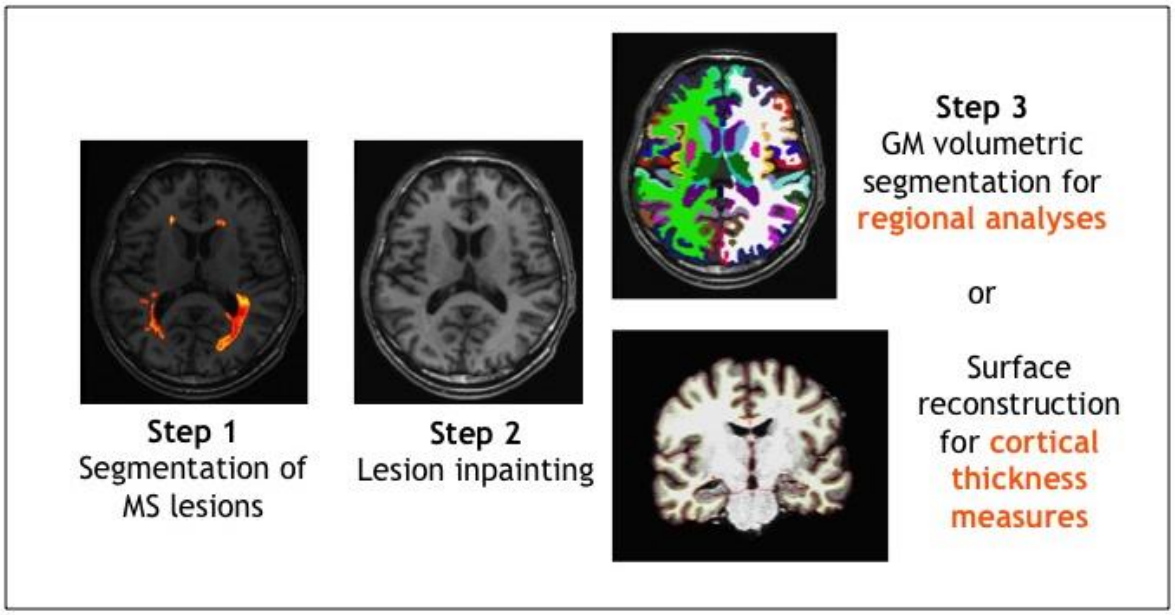

Figure 17: Example of FreeSurfer for GM volume and cortical thickness estimation. After a first step of WM lesion segmentation, a procedure of lesion inpainting is used to limit misclassification of WM lesions as GM. Then the volumetric pipeline can be used for estimation of global or regional GM volumes and region-of-interest (ROI) analyses. The surface reconstruction pipeline allows estimation of cortical thickness.

At the group level, GM atrophy can be seen from the first clinical event as loss of GM volume or cortical thinning [142] [143] [144]. Topographically, GM atrophy is most evident in the DGM structures such as the thalami, hippocampi, and in the cerebellum [145] [146] at the early stages of the disease. It later extends to neocortical structures and becomes widespread as MS progresses, clearly dominating the disease process in the later stages.

Interestingly, GM atrophy doesn't follow the same dynamic pattern of accrual as WM atrophy. In a longitudinal study over 4 years, Fisher and colleagues demonstrated that GM atrophy increases with disease stage from CIS to SPMS while WM tissue loss remained constant [147]. Rocca et al. also reported that GM and WM damage followed different trajectories in the first 2 years after CIS [143], suggesting that these 2 events may be at least partly independent.

In CIS patients, GM volume loss can predict conversion to CDMS, and shorter time to second attack [144] [148]. GM volume has emerged as a clinically relevant measure with

strong relation to disability progression. Many studies have shown that GM volume correlates with measures of physical and cognitive disability in cross-sectional as well as longitudinal cohorts [147] [149] [150] [151] [152]. GM atrophy has been shown to be more useful than WM atrophy in prediction models of future disability and is therefore regarded as a valuable outcome measure in clinical drug trials [153].

Unfortunately this measure is inherently non-specific and could be explained by the different processes taking place within the GM such as demyelination, glial pathology or neuronal damage. Postmortem studies have tried shedding light on the issue. Wegner and colleagues have shown that cortical thinning can occur within or outside lesions and is not related to the extent of cortical focal demyelination [105]. Recently, Popescu et al. confirmed that in non-lesional neocortex, cortical volume was not related to myelin density [107]. This was later supported by another study using different sampling techniques [154]. These observations suggest that demyelination is not the primary substrate of volumetric loss and cortical thinning. In contrast, significant correlations were found with neuronal density, neuronal size and axonal density indicating that, at the later stages of the disease, MRI-measured GM atrophy is driven by the neurodegenerative process.

There are several limitations however to the use of GM atrophy as a sensitive marker of neuronal damage in MS. First, measures of GM atrophy or cortical thinning do not reflect the entire spectrum of neurodegenerative changes occuring within the MS GM. Several studies have shown significant alterations in synaptic density or dendritic arborization in animal models of the disease [155], as well as in the MS neocortex [83] [105]. These changes are also particularly significant in the hippocampus. Dutta and colleagues reported decreased hippocampal neuronal gene expression, in particular KIF1A, which is involved in anterograde transport of synaptic vesicles to the presynaptic terminal. They found evidence of synaptic pruning even in the absence of significant neuronal loss and postulated that such changes could underlie the cognitive disturbances experienced by MS patients [109] [156]. Michailidou et al. recently confirmed the extent of synaptic pathology of the MS hippocampus [157], while Novkovic et al. related memory deficits to impairment of synaptic plasticity in experimental autoimmune encephalomyelitis (EAE), a common animal model of MS [158]. These findings clearly support the clinical significance of subtle changes in

synaptic density or dendritic arborization occurring in the GM. The changes remain nonetheless undetected by GM atrophy measures [107].

Another potential issue is that volumetric measurements may be influenced by water content, extracellular matrix, and inflammatory infiltration. Several studies reported robust changes in brain volumes between dehydrated and rehydrated states [159] [160]. A volume change of about 0.36% during the dehydration-rehydration interval is well above previously reported scan-rescan reproducibility errors and close to a recently proposed pathological "cut-off" for volume loss of 0.4% [161]. Furthermore, it can be a complicated task to distinguish true atrophy from "pseudoatrophy", a significant loss of brain volume, which may occur after initiation of anti-inflammatory therapy, and a phenomenon that is not yet fully understood [162].

2. QUANTITATIVE MRI

2.1. Diffusion Tensor Imaging

Diffusion denotes the random motion of molecules, also called Brownian motion. Water is the most convenient molecular species to study with diffusion MRI, though other metabolites may also be studied. Water molecules move in the brain and interact with many tissue components such as cellular or subcellular membranes or organelles. The distribution of motion of water molecules thus provides clues to the structure and organization of brain tissue. Molecular motion may not be the same in all directions, a phenomenon called anisotropy. Diffusion-weighted MRI only characterizes a single parameter, the diffusion coefficient D. Diffusion tensor imaging (DTI) is used to map and characterize the three-dimensional diffusion of water as a function of spatial location (figure 18). The diffusion tensor describes the magnitude, the degree of anisotropy, and the orientation of diffusion anisotropy. Consequently, the diffusion tensor is thought to be a sensitive marker for characterizing both normal and abnormal tissue microstructure [163]. It has been proposed recently as a way to assess GM integrity. The interpretation of diffusion tensor is complex. Common DTI metrics used

in MS are fractional anisotropy (FA), which reflect the prevalence of diffusivity along one direction, or Mean Diffusivity (MD) a measure of global water diffusion.

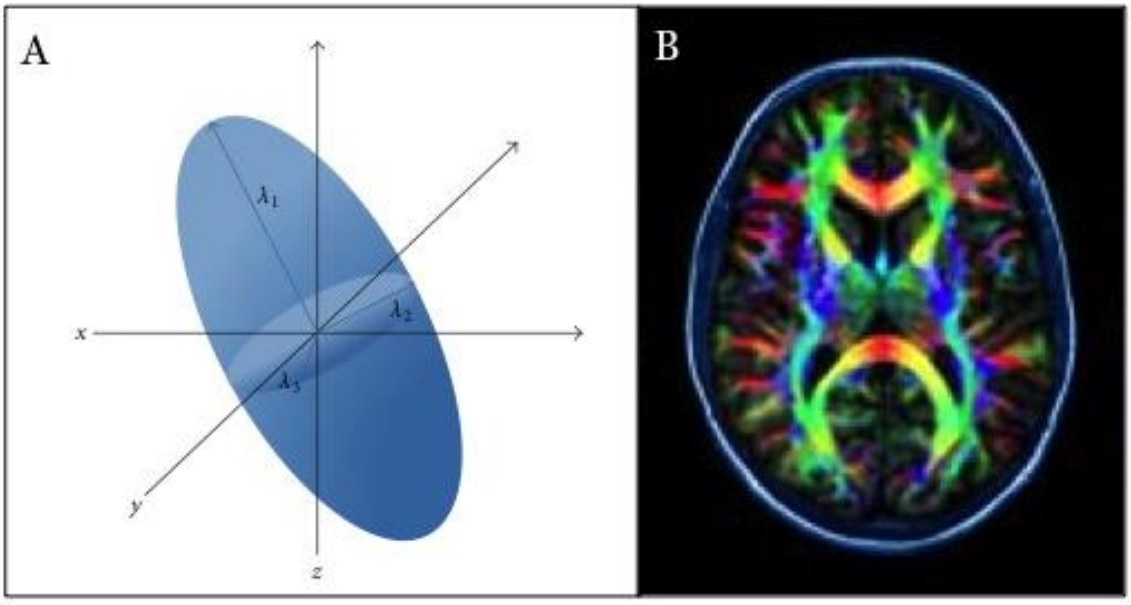

Figure 18: Diffusion Tensor Imaging. (A) Representation of an elliptical tensor with 3 main axes. The longest axis is the primary eigenvector (λ_1) and reflects the diffusion parallel to fibers ("axial" diffusivity). The other two axes are the second (λ_2) and third (λ_3) eigenvectors, whose average provides a measure of "radial" or perpendicular diffusivity. (B) DTI color map allows visualization of direction information about diffusion by color-coding direction information from the eigenvectors.

Progressive and widespread DTI alterations have been demonstrated in the MS GM, though these changes have shown conflicting directionality depending on the study. MD consistently increases across studies, while FA has been found to either decrease or increase. The discrepancy has been explained by possible differences in GM inflammation [164]. Increased FA and MD values have been reported in deep grey matter structures [165] or cortical NAGM and lesions [166] in RRMS and CIS. Decreased FA values were also found in similar structures and populations of MS patients [167] [168] [169]. Nonetheless, from a clinical point of view, DTI metrics are attractive. There is mounting evidence that DTI-detectable changes of the GM are more severe in disabling forms of MS [170]. Several authors reported significant correlations

between GM FA or MD and measures of clinical disability such as EDSS or the MS functional composite score (MSFC) [168] [166]. In a study by Yaldizli and colleagues, cognitive disability evaluated by the symbol digit modalities test (SDMT) correlated with DTI measures in non-lesional cortical GM, though the correlation didn't remain in a multivariate model including other MRI-derived metrics [167]. Using long-term follow-up, Rovaris et al. were able to demonstrate that GM DTI features could independently contribute to the identification of PPMS patients at risk of progression [171].

DTI findings reported by MS studies are often attributed to axonal degeneration and fiber transection [165] or microglial activation [166]. Local inflammation levels can also confound DTI measurements. Given the paucity of postmortem studies combining DTI and pathological analyses [172], current interpretation of DTI findings is far from definitive. Some have proposed measurements of "axial" diffusivity (the principal eigenvalue of the diffusion tensor) and "radial" diffusivity (the average of the second and third eigenvalues), which have been interpreted as axonal degeneration and demyelination respectively [173], though this claim was later found speculative at best [174]. More recently, different modeling techniques of diffusion-weighted MRI data have been proposed to try to better capture the relative contribution of neuronal damage, demyelination and inflammation to GM pathology [175] [176]. Their relevance and applicability in MS remain to be established.

For the reasons cited above, DTI appears to be a sensitive yet non-specific marker of GM damage in MS. This observation along with the difficulties associated with image noise, echo planar imaging (EPI)-induced distortions and partial volume averaging in large voxels, challenge the application of DTI measurements for diagnostic or prognostic purposes at the individual level in MS.

2.2. Magnetization Transfer Imaging (MTI)

MTI is a MRI technique that generates contrast based on the phenomenon of magnetization exchange between the unbound protons in free water and the protons bound to macromolecules. Changes in magnetization transfer ratio (MTR, which reflects

the exchange rate of magnetisation transfer between the two proton pools) have been detected in both MS WM [177] [66] [178] [179] and GM [180] [181] [182].

Using voxel-based techniques, it was shown that GM MTR reduction affects predominantly the DGM structures in the early stages of the disease, and the cortex during the progressive phase [182]. Filippi et al. reported that GM MTR was an independent variable associated with cognitive deterioration over a 13-year follow-up period [181]. This was further confirmed in PPMS patients [183]. Crespy et al. suggested that analysis of GM MTR maps could provide insights into individual GM pathology [180].

Though sensitive to microstructural changes in the MS GM, MTI metrics are not thought to reflect changes within the neuronal compartment. Histopathological studies have instead suggested that MTR is sensitive to demyelination in the WM [67], as well as in the GM [184] [185]. Yaldizli et al. later reported that MTR measures were indeed significantly lower in DIR-visible cortical lesions compared to non-lesional cortex [167]. Derashkhan and colleagues have proposed surface-based analyses of MTR cortical changes as a plausible method to quantify subpial demyelination, which remains hard to detect using DIR [186].

2.3. Proton Magnetic Resonance Spectroscopy

Proton Magnetic Resonance Spectroscopy (^{1}H-MRS) allows quantification of different metabolites in brain tissues (figure 19). It can be used to measure levels of N-acetyl Aspartate (NAA), a metabolite long recognized as an indicator of neuronal and axonal function. Based on immunohistochemical findings NAA is present in most neuronal cell populations, but the intracellular concentration appears to vary greatly between neuronal groups [187]. After synthesis by mitochondria, NAA is exported to the neuronal cytoplasm, where it remains present in high concentration [188]. Its function has yet to be fully established.

NAA levels can be measured using ^{1}H-MRS either within small volumes (single voxel ^{1}H-MRS, figure 14) or across larger areas (Chemical Shift Imaging, CSI). Hunter's angle,

drawn from the myoinositol peak to NAA peak is a visual way to assess normality of the NAA spectrum. It normally averages 45° from the x-axis. NAA or other metabolite concentrations are usually expressed as a ratio (relative quantification) rather than as absolute concentrations. In relative quantification, one metabolite peak is used as the concentration standard. A classic example is the ratio NAA/ Creatine. One of the limitations of such quantification method is that changes in the ratio can reflect changes in the concentration of the numerator, the denominator, or both and are usually more difficult to interpret than absolute concentrations.

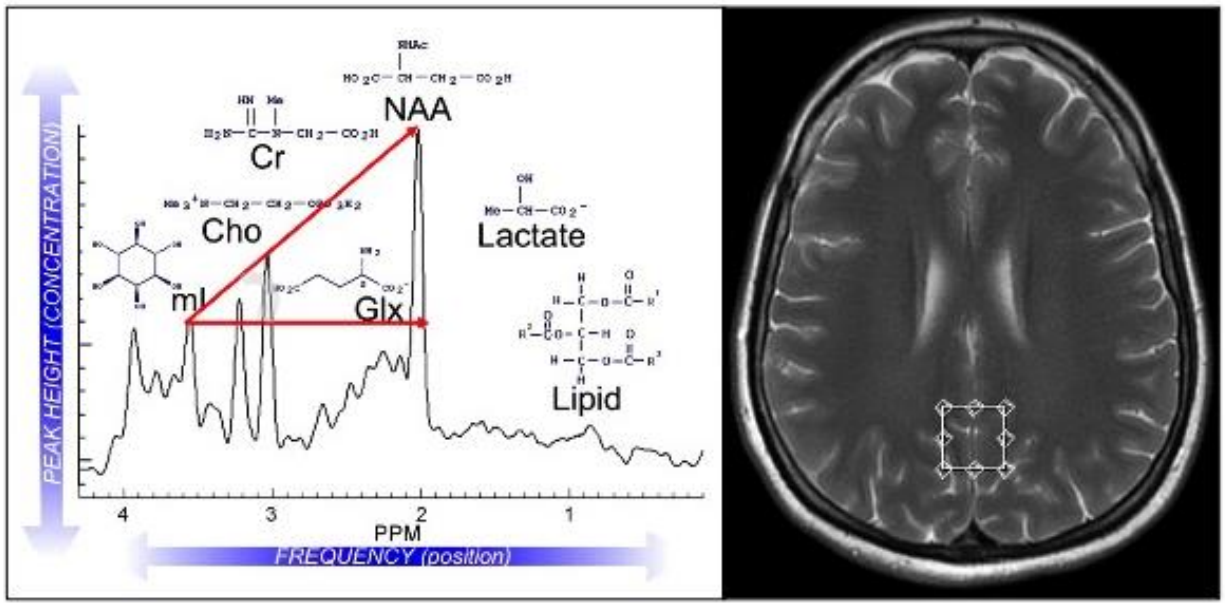

Figure 19: ^{1}H-MRS. Left: representative proton MRS spectrum of normal human brain with major peaks of interest depicted. Hunter's angle is represented in red. From Moffett et al. Progress in Neurobiology, 2007 [187]. Right: single voxel acquisition on posterior cingulate gyrus. From Pokryszko-Dragan et al., Journal of the Neurological Sciences, 2014 [189].

NAA levels have been found to be reduced by 10-20% on average in the thalamus of RRMS patients compared to controls [110] [190]. Geurts and colleagues also reported significant decrease in thalamic NAA in PPMS patients [191]. Lower NAA/Cr values were found in the posterior cingulate gyrus of RRMS patients when compared to controls in one study [189]. Though other groups were unable to detect similar metabolic changes in the cortical grey matter [191] [192] [193] [73].

A reduction in NAA levels can occur in case of neuronal loss or damage but can also reflect reversible metabolic dysfunction affecting the mitochondria. Histopathological studies have demonstrated robust correlations between NAA levels and axonal pathology [194]. Although MRS provides unique and specific metabolic information regarding neuronal function and viability, several factors have limited its utility. Among these limitations, the necessary sampling over large voxels, poor spatial resolution, and susceptibility artifacts in regions close to bone may explain why MRS has not been more widely used to assess GM and in particular cortical damage in MS, although this technique has been available for many years.

3. POSITRON EMISSION TOMOGRAPHY

3.1. Principles of PET imaging

A PET scanner is an imaging system that provides analytical tomographic measurements of the tissue concentration of compounds labeled with a positron emitting radionuclide (figure 20). Only minimal or "tracer doses" of neuroreceptor radiotracers need to be injected to estimate receptor parameters. After injection, the study subject is placed within the field of view (FOV) of the scanner where several detectors can register incident gamma rays. The radionuclide decays and emits positrons, which then annihilate with an electron to produce two 511 keV gamma rays. The gamma rays are emitted in opposite directions at approximately 180 degrees from each other and can be detected by the scanner's detectors. The annihilation event is usually very close to the site of positron emission because the emitted positrons rapidly lose their energy in tissue. The distance the positrons travel before annihilation is small, typically less than 2 mm. The detectors are connected with fast timing circuits that look for two simultaneous or "coincident" events on opposite sides of the head. Detection of the two coincident gamma rays defines a line, which intersects the position of the annihilation event. These "coincidence events" can be stored in arrays corresponding to projections through the patient. The raw data collected by the PET scanner is then

mathematically reconstructed to produce tomographic images of tissue radioactivity concentration. Coregistration of MRI and PET data enables the interpretation of functional data with localizing high-resolution structural information.

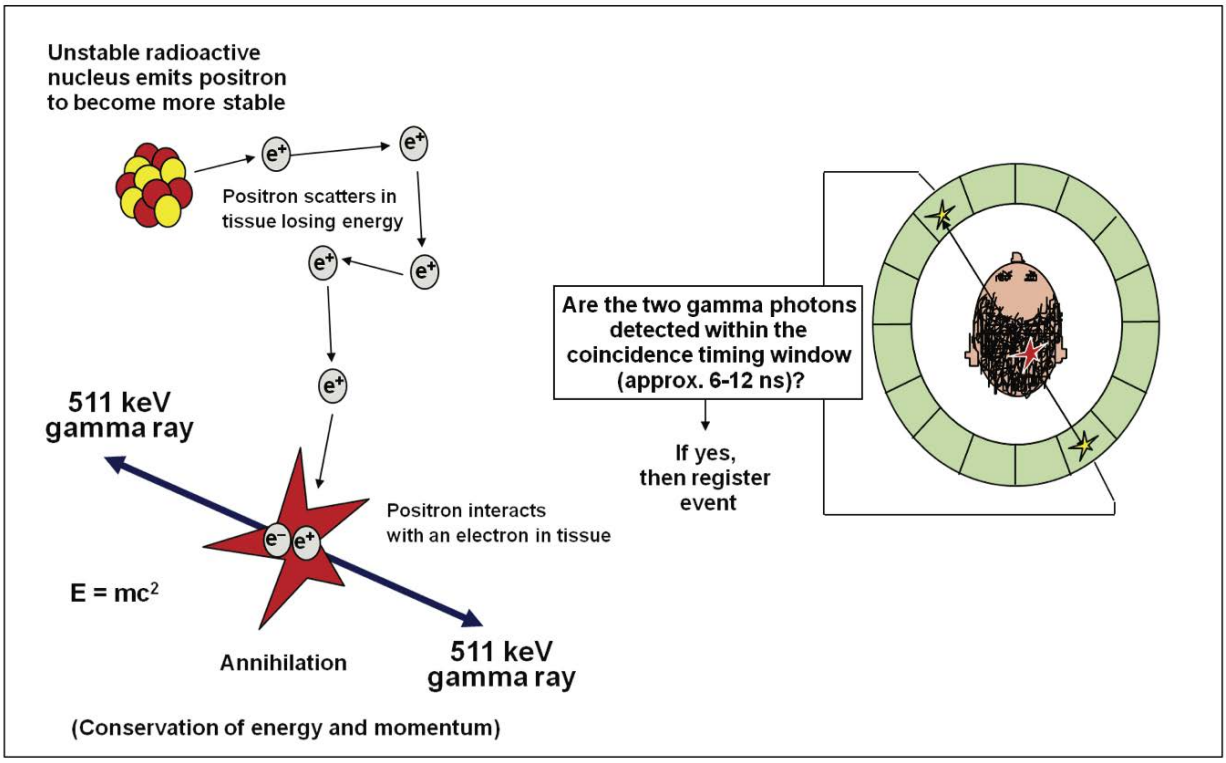

Figure 20: Principles of PET imaging. From Dr Mirwais Wardak, Brain Imaging with Positron Emission Tomography: Quantification and Biomedical Applications in Alzheimer's Disease and Brain Tumors, UCLA, 2013.

3.2. [^{18}F]-fluorodeoxyglucose (FDG) PET and neuronal metabolism

Glucose is the brain's main substrate for energy supply. Experimental studies have shown that glucose consumption closely reflects neuronal function in the healthy brain [195]. PET with [^{18}F]FDG can estimate the metabolic rate of glucose (CMRglc) because the tracer is taken up by brain tissue and phosphorylated like glucose. Typical resting state CMRglc values are in the range of 40 to 60 μmol glucose/100 g/min in the GM and around 15 μmol glucose/100 g/min in WM [196]. In diseases impairing neuronal function, significant reduction in CMRglc may be seen.

In MS, global reduction in brain CMRglc has been reported by Pozzilli et al. [197]. Bakshi et al. quantified a 9% reduction in brain glucose metabolism in MS patients compared to controls, with dramatic absolute reduction in the superior mesial frontal cortex, superior dorsolateral frontal cortex, mesial occipital cortex, lateral occipital cortex, deep inferior parietal white matter, and pons [198]. Longitudinal follow-up of 10 MS patients showed that brain glucose metabolism decreases over time with the most pronounced reductions of CMRglc detected in frontal and parietal cortices [199]. Reduction in regional or global CMRglc correlates with measures of cognitive disability [200] and fatigue [201].

Nonetheless, the interpretation of [18F]FDG PET is not straightforward in an inflammatory disorder such as MS, as measures of glucose metabolism may be artificially increased by local inflammation and glucose uptake by inflammatory cells [202] [203].

3.3. Flumazenil, an antagonist of the central benzodiazepine receptor

3.3.1. Properties

Flumazenil (FMZ) is an antagonist of the central benzodiazepine (BZD) receptor, a component of the ubiquitous $GABA_A$ receptor complex. $GABA_A$ receptors are pentameric channel receptors permeable to chloride ions and belong to the family of Cys-loop ligand-gated ion channels along with glycine receptors, serotonin type 3 receptors and nicotinic acetylcholine receptors. $GABA_A$ receptors are present on axo-somatic and axo-dendritic synapses on neurons throughout the cortical and subcortical GM [204]. BZD receptors are allosteric modulatory sites on $GABA_A$ receptors. Flumazenil binds with high affinity to BZD receptors containing the α1, α2, α3, or α5 subunits and less so to those containing α4 or α6 subunits.

Initially [^{3}H]FMZ for in vitro and ex vivo autoradiography, subsequently radiolabeled FMZ conjugates were developed for in vivo clinical studies with PET. In vivo [^{11}C]FMZ PET was found to strongly correlate with [^{3}H]FMZ autoradiography in hippocampal sclerosis [205]. [^{11}C]FMZ is rapidly metabolized in vivo and exhibits high uptake in GM with retention of radioactivity in BZD receptor-rich regions, such as the cerebral cortex [206]. [^{11}C]FMZ has several properties making it a useful PET tracer, including no metabolism in the brain, metabolites that do not cross the BBB, appropriate kinetics, and low nonspecific binding [207].

3.3.2. PET with [^{11}C]FMZ in neurological disorders

$GABA_A$ receptor density measured in vivo by PET with [^{11}C]FMZ has been reported as a specific marker of neuronal integrity and has allowed, over the past 15 years, to estimate neuronal damage in several neurological and psychiatric disorders.

Heiss et al. demonstrated that PET with [^{11}C]FMZ combined with measures of cerebral blood flow could distinguish between irreversibly damaged and viable penumbra tissue [208] [209]. Pascual et al. reported decreased [^{11}C]FMZ binding in the hippocampi and posterior cingulate gyri of patients with Alzheimer's disease [210]. [^{11}C]FMZ binding was decreased precisely in the regions showing the greatest degree of neuronal loss in post-mortem studies of early Alzheimer's disease. In addition, [^{11}C]FMZ hippocampal binding correlated with memory performance. In major depression, decreased binding was found in the limbic parahippocampal and right temporal cortical areas. In the temporal area, [^{11}C]FMZ binding showed a strong inverse correlation with hypothalamic-pituitary-adrenal axis activity [211]. A study using a related tracer [^{123}I]iomazenil in Huntington's disease found a 31% decrease in volume of distribution in the striatum of patients compared to age-matched controls [212]. This change was attributed to loss of binding sites and consequently synapses in these areas. No significant changes in cortical binding were found in these mildly to moderately affected patients. The authors also found strong correlations between [^{123}I]iomazenil binding and clinical functional scores. In epilepsy, PET with [^{11}C]FMZ can be acquired during the interictal period. Several studies have evaluated the clinical utility of [^{11}C]FMZ PET in patients with MRI-negative focal epilepsy. [^{11}C]FMZ PET helped identify surgically relevant abnormalities in about 50% of subjects [207]. The added value of FMZ PET compared to FDG in the context of epilepsy remains however unproven [213].

3.3.3. The Partial Saturation Method, a non invasive quantification technique

Despite promising findings, the more widespread application of [^{11}C]FMZ PET in the research or clinical setting has been limited by highly invasive modeling methods. Standard modeling protocols require serial arterial blood sampling for plasma input function to fit compartmental models. Arterial lines can cause complications such as hematoma, bleeding, and thrombosis and require local anesthetic administration. Other

modeling techniques have been proposed to analyze PET data without arterial input function. The simplified reference tissue model [214] model is applicable if a "true" reference tissue exists in which no specific binding of the radioligand occurs. It allows only measurements of the binding potential (BP) which is a combined measure of density of available neuroreceptors (Bmax) and affinity of the ligand to that receptor (K_d). Though proper quantification of changes in receptor density (Bmax) might be important to understand the pathophysiology of neurological disorders.
Some investigators have proposed using Scatchard analysis, a common in vitro method based on the equilibrium relation:

$B/F = (Bmax-B)/K_dV_R$

With: B= bound ligand concentration
F= free ligand concentration
Bmax= BZD receptor density
K_d= receptor-ligand affinity
V_R= reaction volume

The plot of B/F vs B gives a straight line whose slope is equal to the inverse of the apparent equilibrium dissociation constant (K_dV_R) and whose intercept with the B axis gives the receptor density Bmax (figure 21, red line).
Using Scatchard analyses eliminates the need for arterial blood sampling but requires separate estimation of bound and free ligand concentrations, as PET data will provide only a sum of these two components. Delforge et al. showed that bound ligand concentration decreases significantly over the usual duration of an experiment after FMZ injection with an average dose between tracer dose and saturation dose [215]. The partial saturation protocol [216] is based on this observation and allows estimation of BZD receptor density and receptor-ligand affinity from a single-injection experiment, without arterial blood sampling.

The protocol consists of a coinjection of a [^{11}C]FMZ tracer dose (about 20 mCi) and of a unlabeled FMZ partial-saturation dose (between a tracer dose and a saturation dose)

[216]. The choice of the unlabeled FMZ amount is important because it must be sufficiently large to occupy a significant percentage of receptor sites (at least 50% but preferably 70%) but not too large to observe a significant decrease of this percentage during the limited duration of the experiment (1 h at most). Data are analyzed using the usual Scatchard plot (figure 21-blue line). The free-ligand concentration F, assumed to be identical in all regions, is estimated from the pons. The pons was initially thought to devoid of BZD receptor sites but was later found to have small but not negligible BZD receptor concentrations (~4.7 pmol/mL) [216]. The percentage of PET-measured ligand concentration in the pons, which corresponds to the ligand bound to the pons receptor sites, can however be estimated as a function of time and of the injected FMZ dose. This curve may then be used in experiments to estimate the free ligand concentration F from the PET-measured pons concentration. The bound ligand concentration B in any region is then obtained by subtracting the free ligand concentration F from the PET-measured concentration. Assuming constant FMZ affinity, parametric images of the Bmax can be obtained [217], which map BZD concentration at each voxel (figure 22).

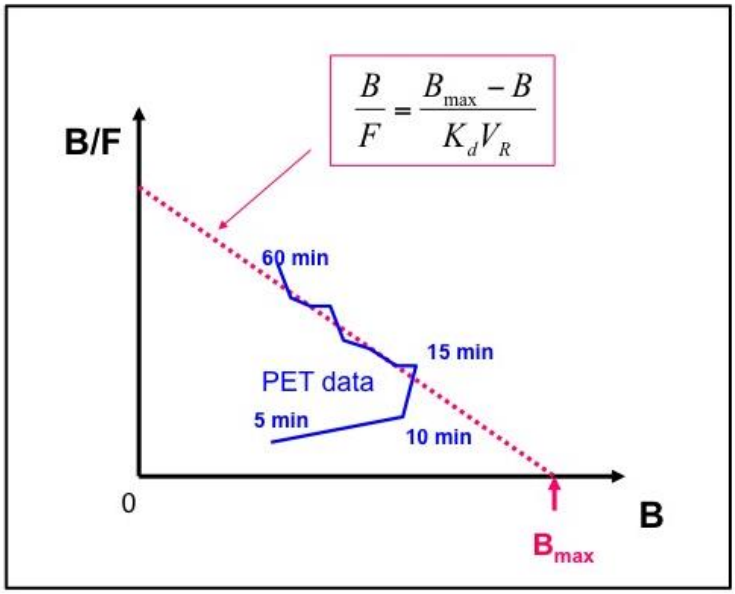

Figure 21: Scatchard curve (red) and estimation from PET examination using the partial saturation method (blue)

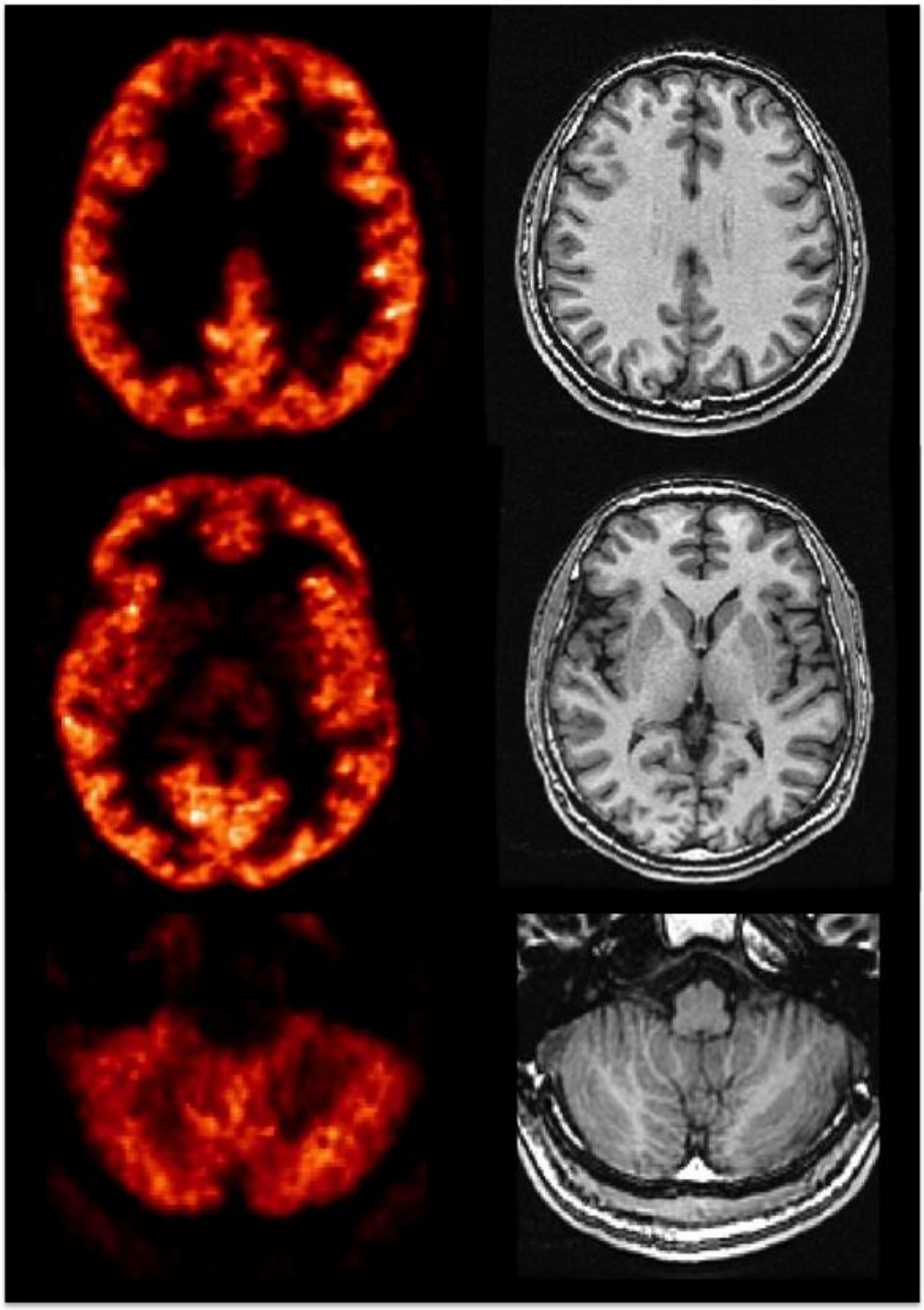

Figure 22: Parametric images of the [^{11}C]FMZ Bmax from a single experiment on a High Resolution Research Tomograph (HRRT, left) with corresponding MRI (right) at subtentorial level (top and middle) and infratentorial level (bottom).

Imaging neuronal damage in the MS grey matter using PET with [^{11}C]FMZ

1. SPECIFIC AIMS OF THE STUDY

MS has long been regarded as an inflammatory demyelinating disorder of the WM. But post-mortem studies have recently shed light on the extensive involvement of the GM and its role in disability progression in MS. Neuronal damage, characterized by synaptic and dendritic loss as well as neuronal apoptosis, is thought to be a major substrate of clinical and in particular cognitive deterioration. Measurement of GM atrophy by MRI represents an interesting prognosis marker for long-term progression. While it appears to be driven by late neuronal loss, it may not capture the entire spectrum of neurodegenerative changes occurring in the GM especially at the early stages of MS. Therefore there is a crucial need for the development of imaging techniques, aimed at visualizing and quantifying neuronal damage in MS.

$GABA_A$ receptor density measured in vivo by PET with [^{11}C]FMZ has been reported as a specific marker of neuronal integrity and has allowed to estimate neuronal damage in several neurological and psychiatric disorders. We hypothesized that this technique could provide insights into the extent of neuronal pathology in MS patients.

The aims of this pilot study are as follow:

- To quantify neuronal damage with [^{11}C]FMZ PET at different stages of the disease using a non-invasive quantification method.
- To investigate the relationship between neuronal injury and macroscopic WM damage.
- To assess the clinical significance of this technique by determining the correlation between [^{11}C]FMZ PET metrics and measures of physical and cognitive performance.

2. MATERIAL AND METHODS

This study was approved by the local Ethics committee. All subjects gave written consent for participation.

2.1. Subjects

A total of 10 healthy volunteers and 20 MS patients were initially included in the study.

Inclusion criteria for MS patients were as follow:

- Patients had a diagnosis of MS according to McDonald et al. [14]
- Either a relapsing-remitting course and EDSS < 4.0 (n=10) or a secondary progressive course and EDSS ≥ 4.0 (n=10)
- Able to understand the objectives of the study
- Able to give written consent

All subjects were free from steroids, cyclophosphamide or mitoxantrone treatment for at least 1 month, and from benzodiazepines or medications known to interact with the BZD receptor for at least 15 days before inclusion in the study.

Inclusion criteria for healthy volunteers were:

- No history of neurological illness
- Able to understand the objectives of the study
- Able to give written consent
- No abnormalities on brain MRI suggestive of on-going neurological disorder

Women that were childbearing or breastfeeding were excluded. All females were advised to use an efficient contraceptive method and a plasmatic pregnancy test was performed before each PET examination.

One healthy volunteer showed incidental abnormalities on MRI suggestive of small vessel disease, one volunteer and one SPMS patient withdrew their consent before the end of the study and one RRMS subject failed to complete the MRI exam. Therefore the final population analyzed comprised 8 healthy volunteers and 18 subjects with MS (9 RRMS and 9 SPMS).

2.2. Clinical Evaluation

Neurological and neuropsychological assessments were performed at time of MR imaging.

Physical disability was evaluated using:

- The Expanded Disability Status Scale (EDSS, Annex A)
- The 25ft timed walk (25-FW) and 9-hole peg test (9-HPT), as part of the Multiple Sclerosis Functional Composite score (MSFC).

Each subject also underwent short neuropsychological evaluation, which included:

- Paced Auditory Serial Addition Test 3 seconds (PASAT-3), also part of the MSFC, to assess attention, working memory and speed of information processing,
- Mini Mental State Examination (MMSE) a general scale sensitive to cortical degeneration
- Rey-Osterrieth Complex Figure Test to evaluate visuospatial processing [218] [219]
- Stroop Test to evaluate executive functioning [220]

2.3. Magnetic Resonance Imaging Data Acquisition

MRI was acquired on the same day as the clinical visit.

MRI was obtained for all participants on the same 1.5T Signa scanner (General Electrics Medical Systems) including:

1) 3D- Fast Spoiled Gradient Recalled Echo (FSPGR) T1-weighted: TE= 2.2, TI=600, TR= 3000 ms, FOV= 240x260 mm, matrix 192x256, slice thickness:1.3 mm 124 slices;
2) 2D- T2 weighted (FSE): TR=2920, TE=103, FOV=240x260 mm, slice thickness=4.0 mm, matrix 256x160;
3) 2D- Fast fluid attenuated inversion recovery (FLAIR) TR=8002, TE=152, FOV=240 mm, slice thickness=4.0 mm, matrix 256x256.

2.4. PET acquisition and quantification

PET imaging was acquired within 15 days of clinical and MRI examination. All subjects underwent PET with [^{11}C]FMZ on a High Resolution Research Positron Tomograph (HRRT, Siemens Medical Solution, spatial resolution= 2.5 mm), providing 110 slices of 1.1 mm thickness covering the whole brain (Annex B).

Ready-to-inject, >99% radiochemically pure [^{11}C]FMZ (ethyl 8-fluoro-5-[^{11}C]methyl-6-oxo-5,6-dihydro-4H-benzo[f]imidazo[1,5-a][1,4]diazepine-3-carboxylate or [^{11}C]Ro151788) was prepared from cyclotron-produced [^{11}C]carbon dioxide (Cyclone-18/9 cyclotron, IBA) using a commercially available TRACERLab™ FX-C synthesizer (General Electrics Medical Systems), and based on a process which was formerly performed on a home-made modular system [221].

Participants were positioned in the tomograph with their head maintained using an individually molded headholder. A 6 min brain transmission scan was performed before injection of the radioligand with a 137-Cs point source to correct the emission scan for tissue attenuations. Protocol consisted of a co-injection of carbon-11-labeled FMZ (285 ± 59 MBq) and unlabeled FMZ (10 µg/kg, Anexate ®) in order to partially saturate the BZD receptors. Twelve 3D frames of the entire brain of 5 min each were reconstructed

with an accelerated list-mode ordinary Poisson ordered-subset expectation maximization (OP-OSEM) algorithm to lower statistical noise at the voxel level without degrading spatial resolution [222]. The partial saturation protocol [215-217] was used to estimate the BZD receptor concentration (Bmax) for each voxel and voxel-based parametric images of the [^{11}C]FMZ Bmax were computed using an in-house software.

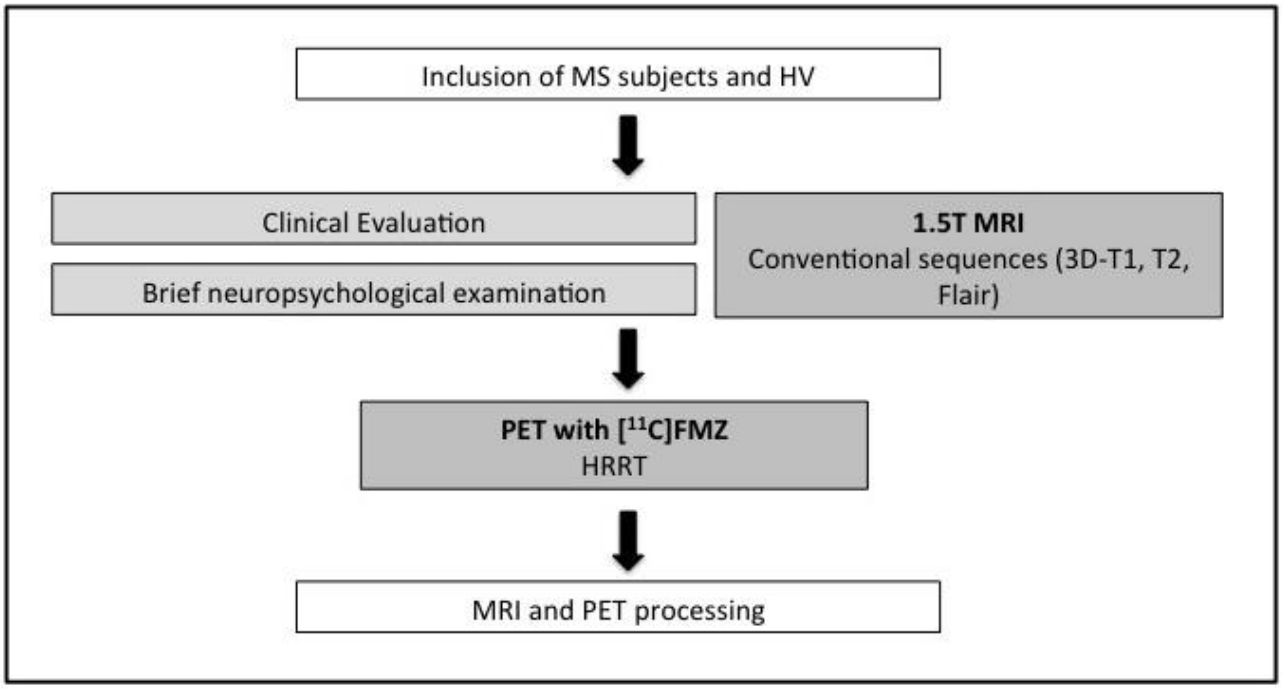

Figure 23: Study visits and steps from inclusion to image processing.

2.5. Processing

Processing steps are summarized in figure 24.

2.5.1. WM lesion segmentation and inpainting

Using a semi-automated segmentation technique based on local thresholding (Jim version 3, Xinapse Systems, UK, http://www.xinapse.com), MS lesions were delineated by a single experienced observer on the 2D-T2 images using the coregistered information from FLAIR images. WM T2 lesion volume was calculated based on the T2 lesion masks provided by Jim Software, then normalized for headsize of each subject.

Prior to the inpainting process, lesions were also segmented on 3D-FSPGR images in the native space using the coregistered information from T2-weighted and FLAIR images. We then applied an automated inpainting technique that replaces lesional voxels with values derived from the intensity distribution of the white matter outside of lesions [141].

2.5.2. Grey matter segmentation and parcellation

Cortical surface reconstruction and volumetric segmentation were performed using the "inpainted" 3D-FSPGR volumes with the Freesurfer v5.1.0 image analysis suite, (http://surfer.nmr.mgh.harvard.edu/). The technical details of these procedures are described in prior publications [223-226]. The segmentation of GM volumes and of the GM/WM interface for each subject was inspected and reprocessed after manual or automatic adjustments if errors were found.

2.5.3. *Registration*

The parametric images of [^{11}C]FMZ Bmax were registered to 3D-FSPGR images using a boundary-based registration method [227]. We visually checked all subjects to assess proper registration.

2.5.4. *Volume of interest (VOI) analyses*

Freesurfer segmentation and cortical parcellation with the Desikan-Killiani atlas label over 50 separate brain structures (Annex C).

Results for total GM (TGM), cortical GM (CGM), lobar GM (frontal, cingulate, parietal, temporal, occipital and insula) and subcortical GM (thalamus proper, caudate, pallidum, putamen, hippocampus and amygdala) are presented here.

In the cortical GM, we calculated the mean thickness of each lobe as well as the mean global cortical thickness.

The volume of each subcortical GM structure was calculated from the 3D-FSPGR images and normalized for head size.

For each volume of interest, we calculated the mean Bmax, or density of BZD receptors, as well as the total amount of [^{11}C]FMZ binding sites defined as the product of the Bmax by the total volume of the structure, then normalized by head size.

2.5.5. *Surface based analyses*

As the cortical thickness can vary substantially throughout the cortex, PET signal was registered on each individual surface and mapped along the midline of the cortical ribbon. Signal was then smoothed along the surface using a 2D 10 mm full width at half maximum (FWHM) Gaussian kernel. Data were then registered for all subjects to a surface template using FreeSurfer.

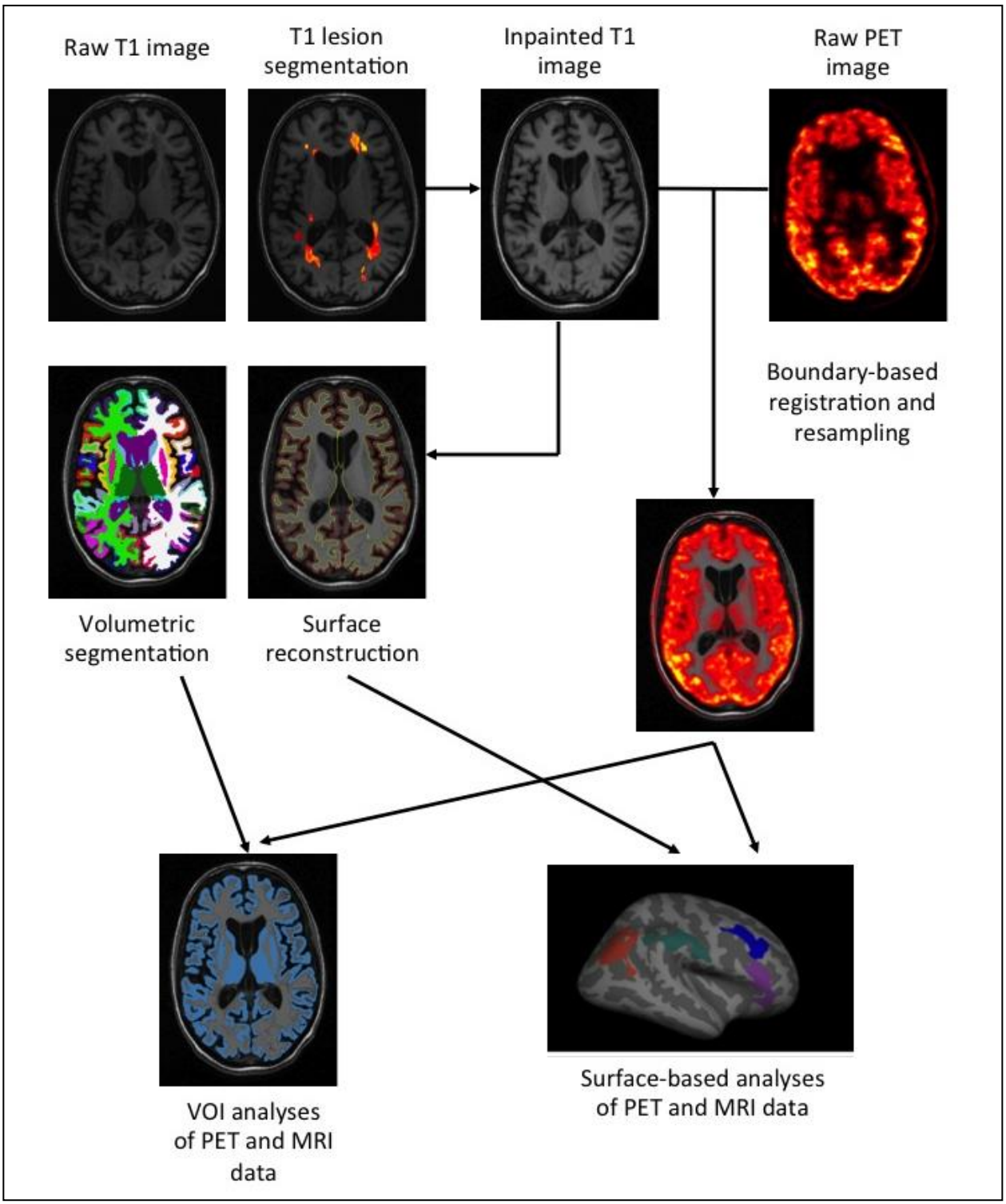

Figure 24: Processing pipeline of PET and MRI data.

2.6. Statistical analyses

Statistical analyses were performed using the R Statistics software version 2.15.2 (http://www.r-project.org/) and Matlab version R2014b (www.mathworks.com). Comparisons of demographic and clinical variables were done using the Mann-Whitney U test for quantitative data.

For volume of interest analysis, the following metrics were analyzed:

- Volume normalized by head size (volume fraction)
- Regional and global cortical thickness
- [^{11}C]FMZ Bmax
- Total amount of [^{11}C]-FMZ binding sites normalized by head size.

Comparisons between MS patients and healthy controls were performed using linear regression analyses adjusting for the effect of age and sex with a significance threshold of $p<0.05$. Exploratory subgroup comparisons of imaging data between RRMS, SPMS and control subjects were performed using the Mann-Whitney U test.

Surface based comparisons were performed using a general linear model (GLM) to test Bmax signal differences between control and MS patients on a vertex-by-vertex basis, adjusting for age and sex. A statistical threshold of $p<0.05$ was used, corrected for multiple comparisons using a Z Monte-Carlo Simulation, with 5000 iterations and a vertex-wise threshold of 0.05. A similar method was used to compare the cortical thickness between controls and patients across the whole cortex.

Partial correlation analyses were employed to assess the relationship between [^{11}C]FMZ binding sites and clinical measures (EDSS, 25FW, 9HPT, PASAT, MMSE, Stroop test and Rey Complex Figure) adjusting for the effect of age and sex in the patient population only (n=18).

The relationship between cortical thickness and Bmax across subjects both in the patient group and the control group, and between cortical [^{11}C]FMZ binding sites and WM T2 lesion load were evaluated using Spearman's rank correlation.

Correlation between cortical Bmax and PASAT scores was also computed on a vertex-by-vertex basis for all patients using a GLM (n=18).

3. RESULTS

3.1. Characteristics of MS patients and healthy controls

Demographic and clinical characteristics of MS patients and controls are presented in table 3.

A total of 8 healthy controls and 18 MS patients were included in the study. The patients were divided in 2 groups: RRMS (n=9) and SPMS (n=9). The control and MS groups did not significantly differ with regard to age (p=0.85), but RRMS subjects were younger than SPMS subjects. The groups were not matched for sex. We thus took into account both age and sex in our statistical analyses.

The SPMS group had a longer disease duration compared to the RRMS group (24.3 years vs 7.0 years). They also had higher EDSS scores (6.2 vs 2.2).

	Healthy controls (n=8)	*MS patients (n=18)*	*RRMS patients (n=9)*	*SPMS patients (n=9)*
Age, yr	45.4	42.6	33.4	51.8
	[35.8-55.3]	[25.1-56.0]	[25.1-45.8]	[45.8-56.0]
Sex (M/F)	6/2	7/11	1/8	3/6
Disease		15.7	7.0	24.3
Duration, yr		[1.8-35]	[1.8-20.2]	[12.5-35.0]
EDSS		4.2 [1.0-7.5]	2.2 [1.0-3.0]	6.2 [5.0-7.5]

Table 3: Demographic and clinical characteristics of healthy controls and MS patients included in the study (mean, range)

Comparisons of physical and cognitive performance between groups were performed using linear regression analyses adjusting for the effect of age and sex (Table 4). The 25-FW could only be assessed in 14 of the MS patients. 4 patients could not complete the task, as they were wheelchair bound. All subjects performed the rest of the clinical evaluation. We found no difference between patients and controls for the 25-FW (n=14 patients), 9HPT with nondominant hand (NDH) and cognitive tests PASAT, MMSE, or Rey Complex figure. Significant differences between patients and controls were found for the 9HPT with dominant hand (DH) and Stroop Test.

	Controls	*MS Patients*
EDSS		4.2 (2.2)
25 FW	7.4 (3.0)	10.7 (11.1)
9HPT- DH	20.6 (2.4)	28.4 (11.2)*
9HPT-NDH	21.7 (3.0)	35.1 (26.8)
PASAT	42.9 (10.4)	36.3 (11.4)
MMSE	27.6 (2.1)	27.2 (3.3)
Stroop test	51.6 (6.9)	45.4 (6.7)*
Rey Complex Figure		
Copy	34.4 (1.8)	32.7 (4.4)
Recall	19.6 (7.4)	17.7 (8.3)

Table 4: Clinical measures of physical and cognitive performance for healthy controls and MS patients. * indicates a significant difference between the 2 groups.

3.2. [^{11}C]FMZ binding in the grey matter

Reconstructed PET images yielded high resolution whole brain parametric maps of BZD receptor concentration (Bmax) that clearly localized within GM areas. The quality of the output can be assessed on figure 25, which presents parametric maps in a healthy control and in a MS patient.

[^{11}C]FMZ Bmax was 2.5 fold higher in cortical regions compared to subcortical GM: in the healthy control group, median cortical Bmax was 111.7 pmol/ml (88.3-124.8) and median subcortical GM Bmax was 43.5 pmol/ml, (37.4-51.9).

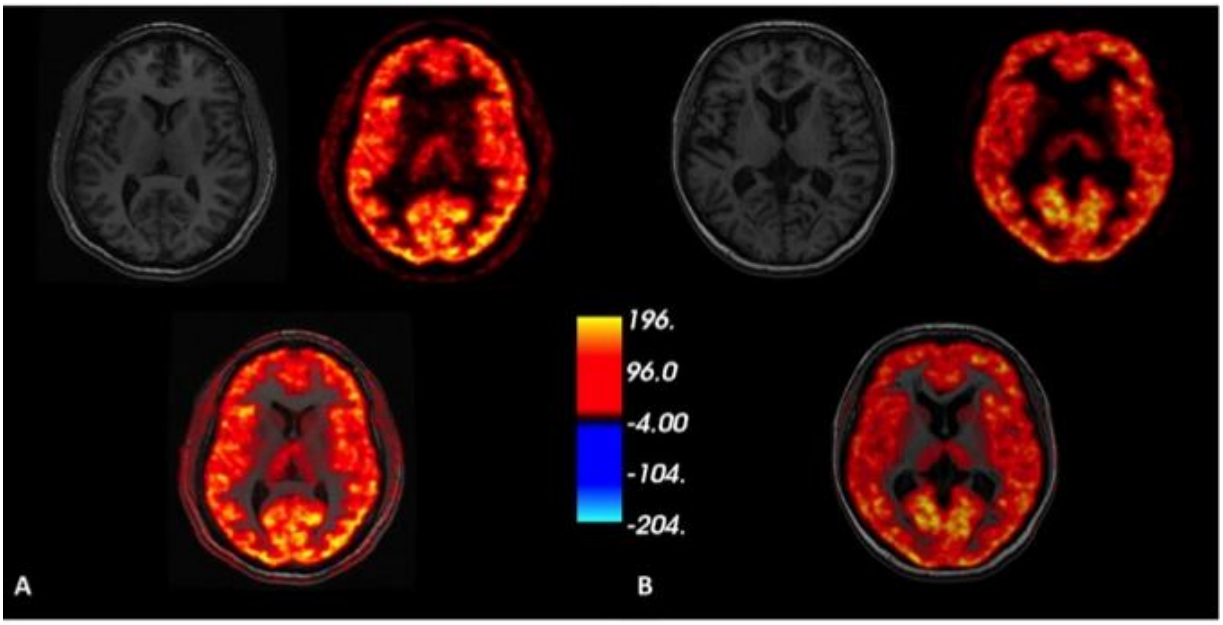

Figure 25: Parametric maps of the BZD receptor concentration (Bmax) in a healthy control (A) and MS patient (B)

Using Spearman's rank correlation test we found no correlation between total GM [^{11}C]FMZ Bmax and age either in the entire cohort of subjects (r=-0.01, p=0.96), in the MS group alone (r=-0.01, p=0.96) or in healthy controls alone (r=0.36, p=-0.38), suggesting that age did not interfere as a major confounding factor in [^{11}C]FMZ binding estimation (figure 26). However the correlation between age and volumetric measurements was significant both in the cortical and subcortical GM and justified correction for the effect of age in our statistical analyses.

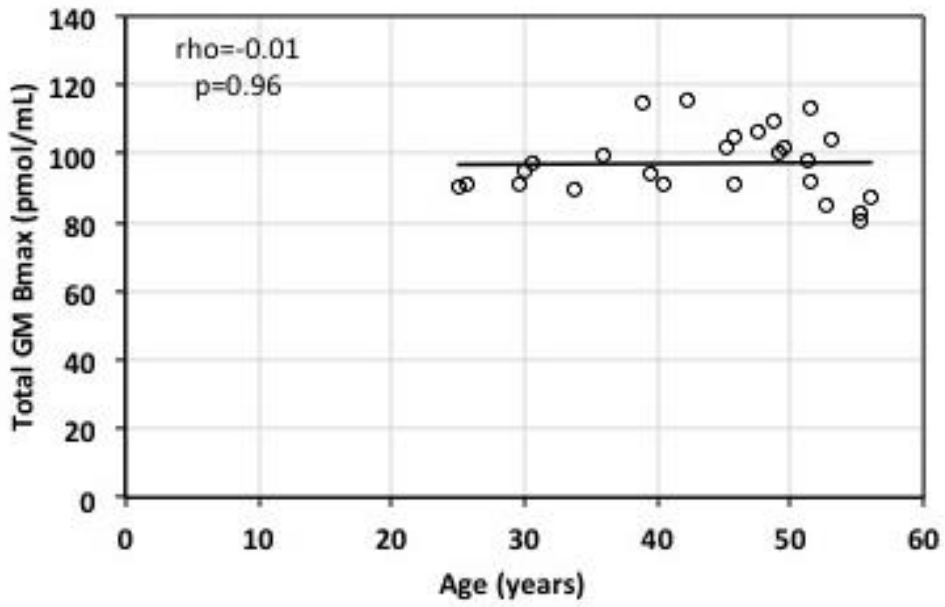

Figure 26: Spearman rank correlation between [^{11}C]FMZ Bmax and age across subjects. No correlation was found between age and [^{11}C]FMZ Bmax in either healthy controls or MS patients.

3.3. GM atrophy in MS patients

GM atrophy was assessed by means of GM volume estimation in the total GM, cortical GM and in subcortical GM structures. GM volumes were normalized for headsize prior to comparison between groups. The mean cortical thickness was also estimated for the whole cortex and for the different lobes (frontal, parietal, temporal, occipital, insula and cingulate). Cortical thinning was assessed using ROI analyses and surface-based analyses.

When total grey matter and total cortical volumes normalized for headsize were compared between the control group and the MS group, the difference did not reach significance after adjustment for age and sex (figure 27 A, B). The total volume of deep GM structures normalized for headsize was reduced in MS patients compared to HC (figure 27, C), the difference being significant after adjustment for age and sex in the

total subcortical GM (p=0.003), the thalami (p=0.0003) and the left caudate nucleus (p=0.02) (figure 27, D).

The mean cortical thickness for the whole cerebral cortex was 2.44 ± 0.08 mm in healthy controls and 2.39 ± 0.11 mm in the whole MS group, with variations depending on cortical location. On ROI analyses, cortical thickness was significantly decreased in MS patients compared to controls in the temporal and occipital lobes bilaterally (figure 27, E). Vertex-by-vertex GLM analyses adjusted for age and sex failed to detect significant cortical thinning.

Figure 27: A-C: Box and whisker diagrams of the volume fractions of the total GM (A), cortex (B) and deep GM (C) in healthy controls (HC) and MS patients. D: Volume fraction of subcortical GM structures in HC and MS patients. E: Cortical thickness in the total cortex and cortical lobes (mm) in HC and MS patients. Statistical comparisons were performed using linear regression adjusting for age and sex with a significance threshold of $p<0.05$.

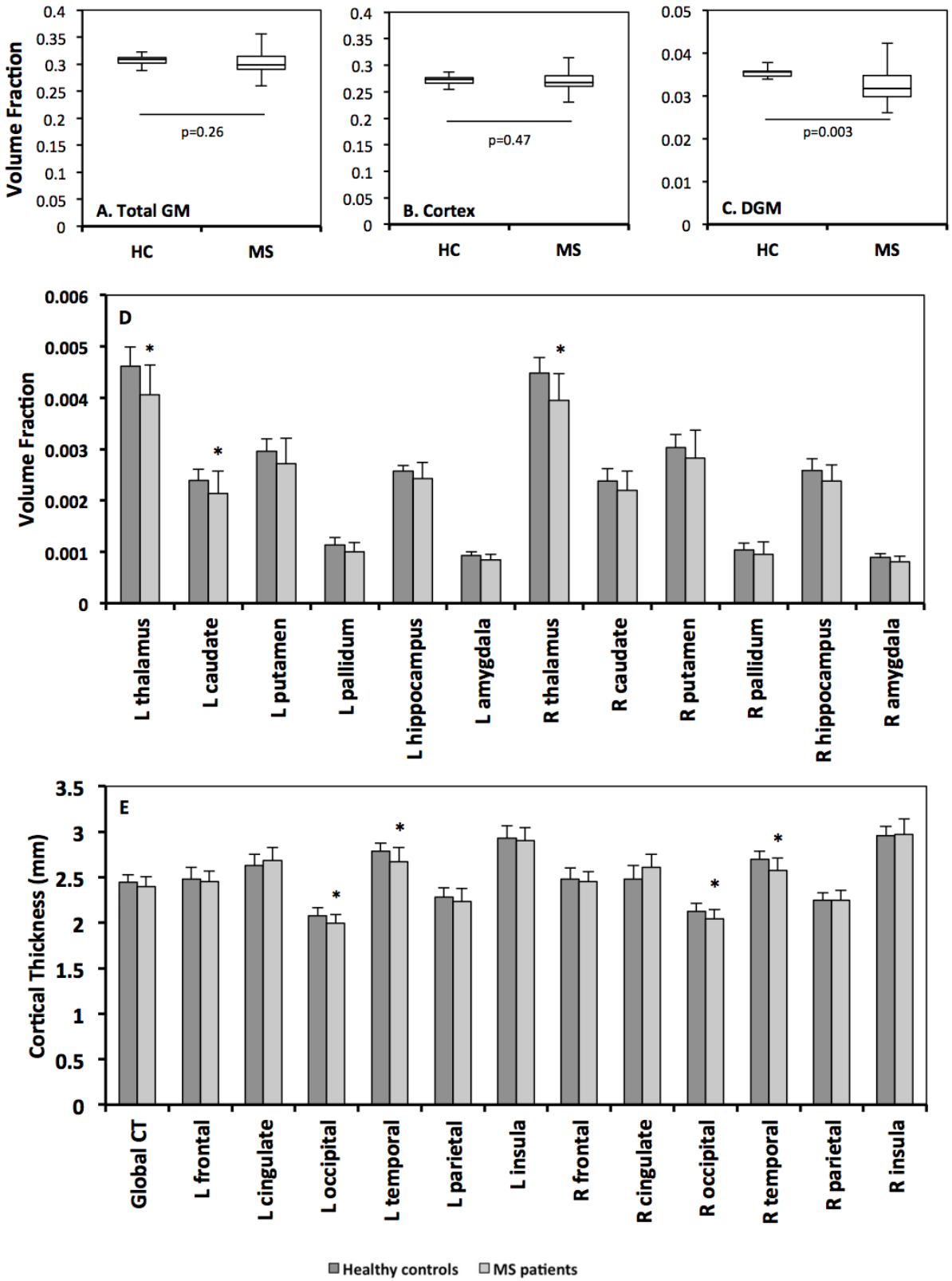
Volume Fraction
A. Total GM
p=0.26
HC
MS
B. Cortex
p=0.47
C. DGM
p=0.003
D
L thalamus
L caudate
L putamen
L pallidum
L hippocampus
L amygdala
R thalamus
R caudate
R putamen
R pallidum
R hippocampus
R amygdala
E
Cortical Thickness (mm)
Global CT
L frontal
L cingulate
L occipital
L temporal
L parietal
L insula
R frontal
R cingulate
R occipital
R temporal
R parietal
R insula
Healthy controls
MS patients

3.4. Reduced [^{11}C]FMZ binding in the MS GM

3.4.1. In cortical structures

Mean [^{11}C]FMZ Bmax was reduced in MS patients compared to controls with a 9.4% decrease in the total GM and a 10% decrease in cortical GM, the difference remaining significant when adjusted for age and sex in the cortical GM (p=0.037, fig 28 A, B).

The cortical parcellation obtained with FreeSurfer allowed a regional analysis of [^{11}C]FMZ Bmax changes, showing for the MS group a significant decrease in the parietal, cingulate, and insular cortices of both hemispheres, and in the left frontal cortex (figure 28, C).The estimated total amount of [^{11}C]FMZ binding sites, defined as the product of the Bmax by the total volume of the structure, then normalized by head size showed a decrease in similar proportion that reached significance in both the total GM (-10.3%, p=0.03) and the cortical GM (-10%, p=0.03) (figure 29 A, B).

Significant negative correlations were found between cortical thickness and cortical Bmax across cortical regions both in HC (r=-0.86, p= 0.0006) and in MS patients (r=-0.98, $p<2.2x10^{-16}$) (figure 30, A). But no correlation between cortical thickness and cortical Bmax across subjects was found either in healthy controls (r=0, p=1) or in MS patients (r=0.12, p=0.64) (figure 30, B).

3.4.2. In subcortical structures:

Bmax showed a non-significant trend in the subcortical GM of MS subjects (-8.8%, p=0.32). The difference on ROI analyses only reached statistical significance in the left amygdala (figure 31).

But the total estimated number of [^{11}C]FMZ binding sites per GM structure, showed a significant decrease (figure 32) in the:

- Total subcortical GM (-17%, p=0.008)

- Left and right thalami (-23% and -25% respectively, p=0.001)
- Left and right hippocampi (-15%, p=0.003 and -19%, p=0.005 respectively)
- Left and right amygdalae (-21%, p=0.001 and -18%, p=0.02 respectively).

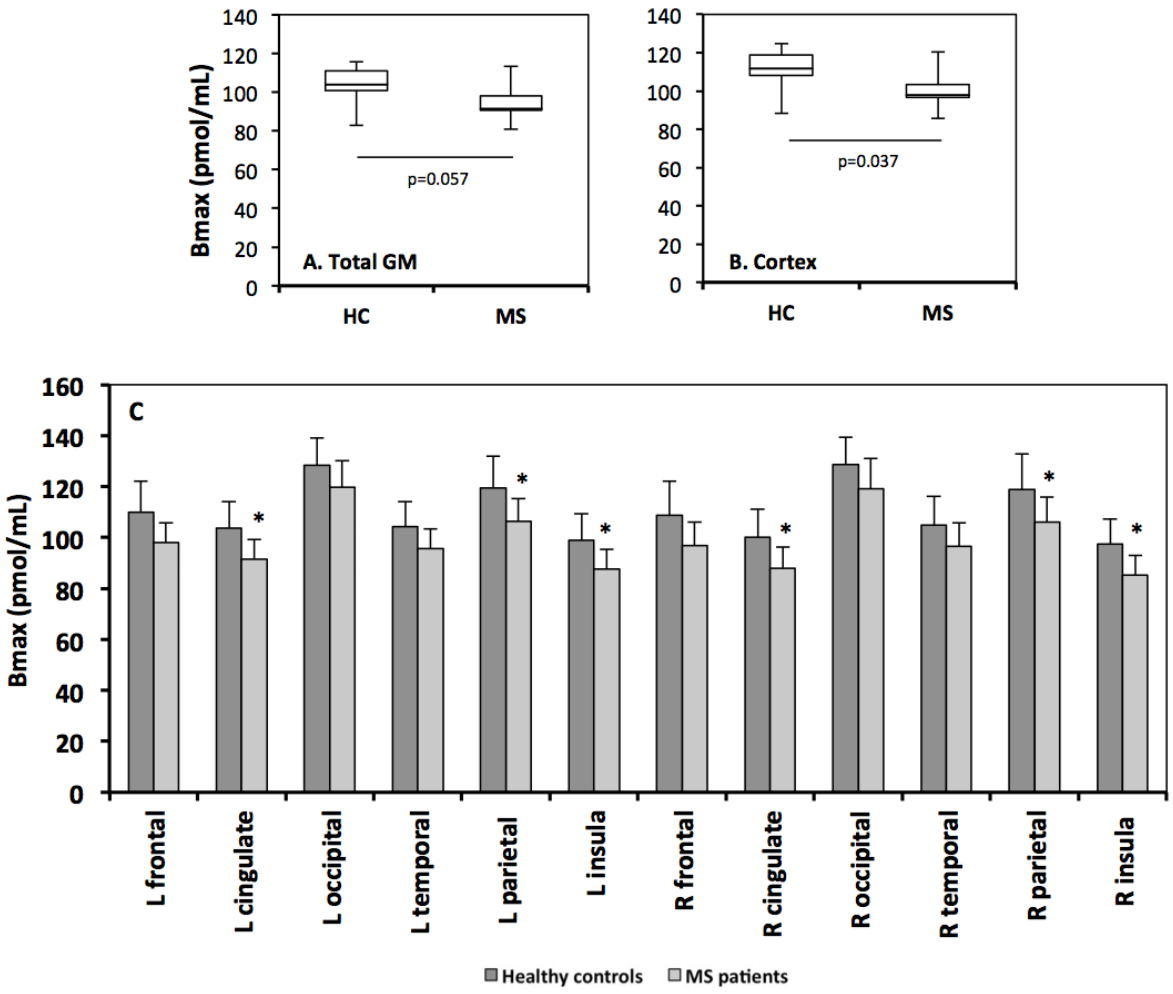

Figure 28: ROI analyses of [^{11}C]FMZ Bmax in cortical structures. A-B: Box and whisker diagrams of [^{11}C]FMZ Bmax in healthy controls (HC) and MS patients in the total GM (A) and cortex (B). C: [^{11}C]FMZ Bmax in HC and MS patients in cortical lobes. Statistical comparison was performed using linear regression adjusting for age and sex with a significance threshold of p<0.05.

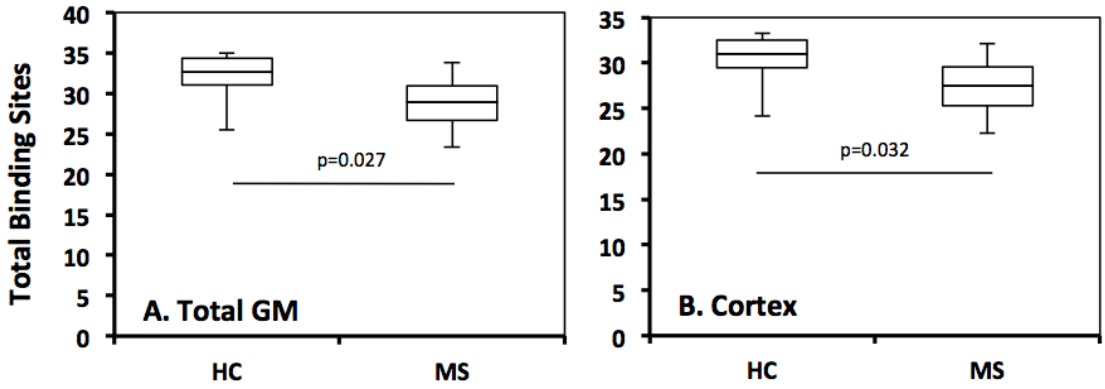

Figure 29: ROI analyses of the estimated number of [^{11}C]FMZ binding sites. Total FMZ binding sites in the total GM (A), cortex (B) of healthy controls (HC) and total MS patients.

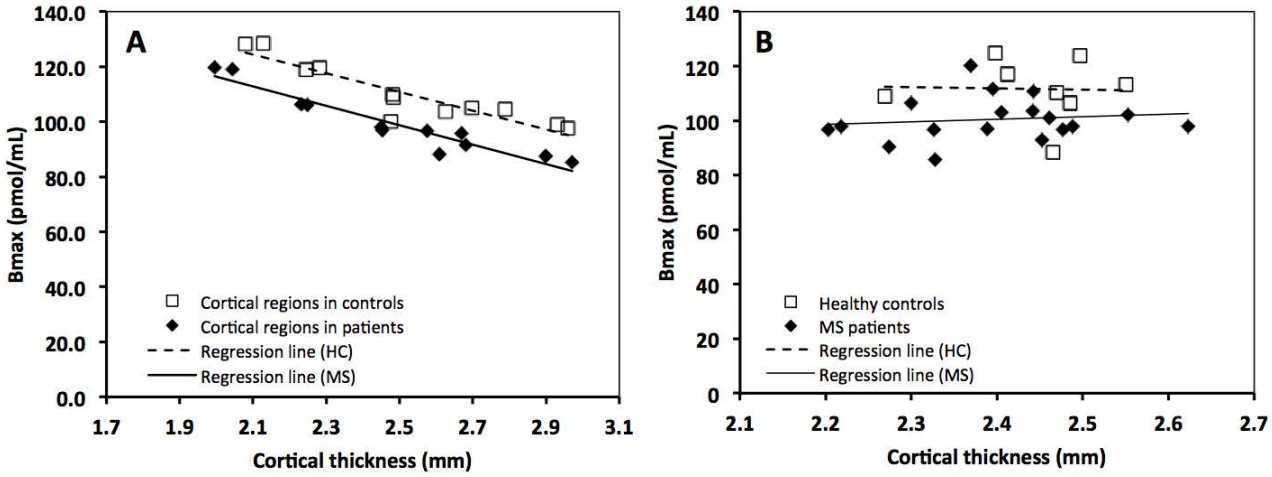

Figure 30: Spearman rank correlation between [^{11}C]-FMZ Bmax and cortical thickness across cortical regions (A) and across subjects (B). A: significant negative correlation between mean cortical thickness and [^{11}C]-FMZ Bmax across cortical regions in healthy controls (square marker, dashed regression line) and MS patients (diamond markers, solid regression line). B: no correlation between global cortical thickness and [^{11}C]-FMZ Bmax across subjects in either healthy controls or MS patients.

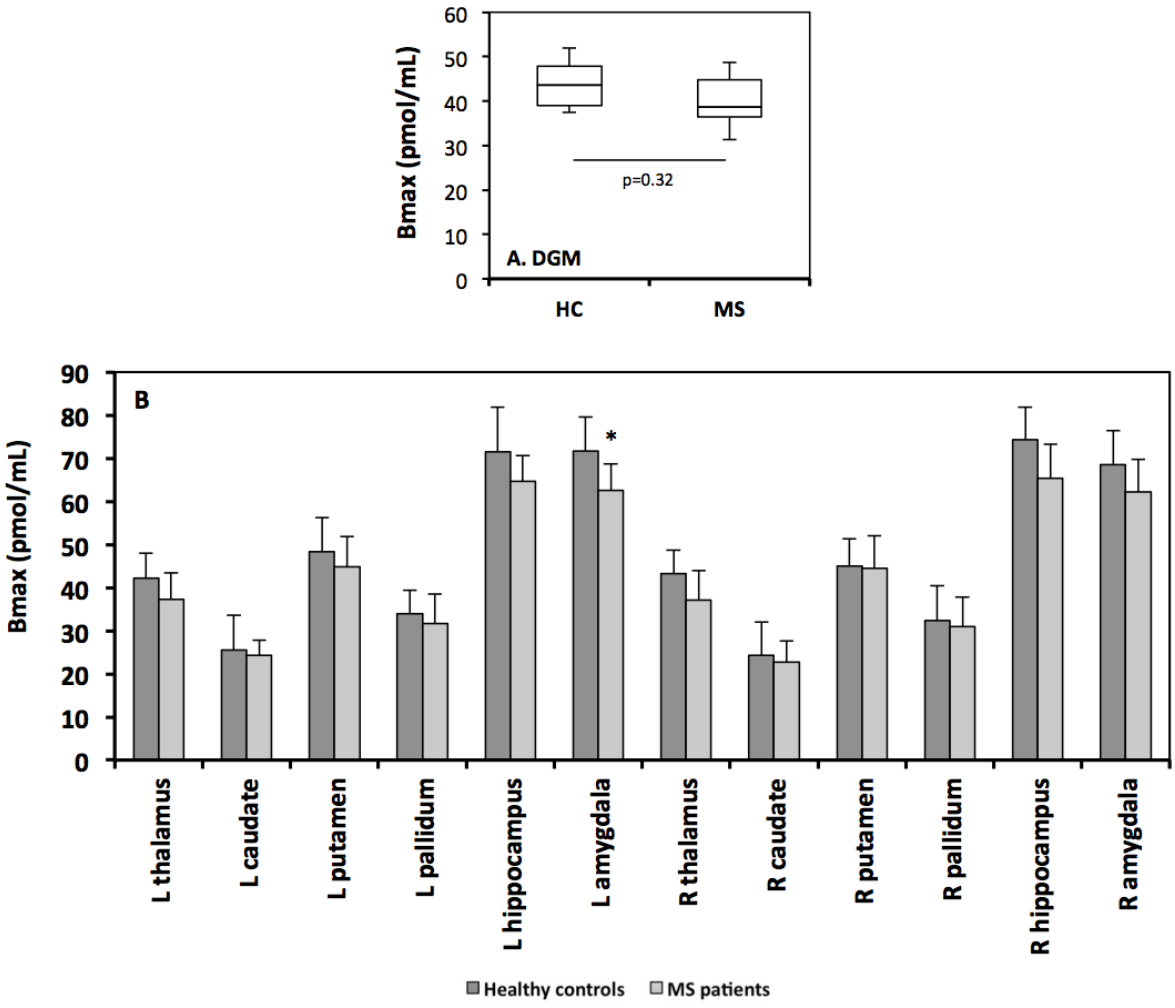

Figure 31: ROI analyses of [^{11}C]FMZ Bmax in deep GM structures A: Box and whisker diagrams of [^{11}C]FMZ Bmax in healthy controls (HC) and MS patients in the deep GM. B: [^{11}C]FMZ Bmax in HC and MS patients in individual deep GM structures. Statistical comparison was performed using linear regression adjusting for age and sex with a significance threshold of $p<0.05$.

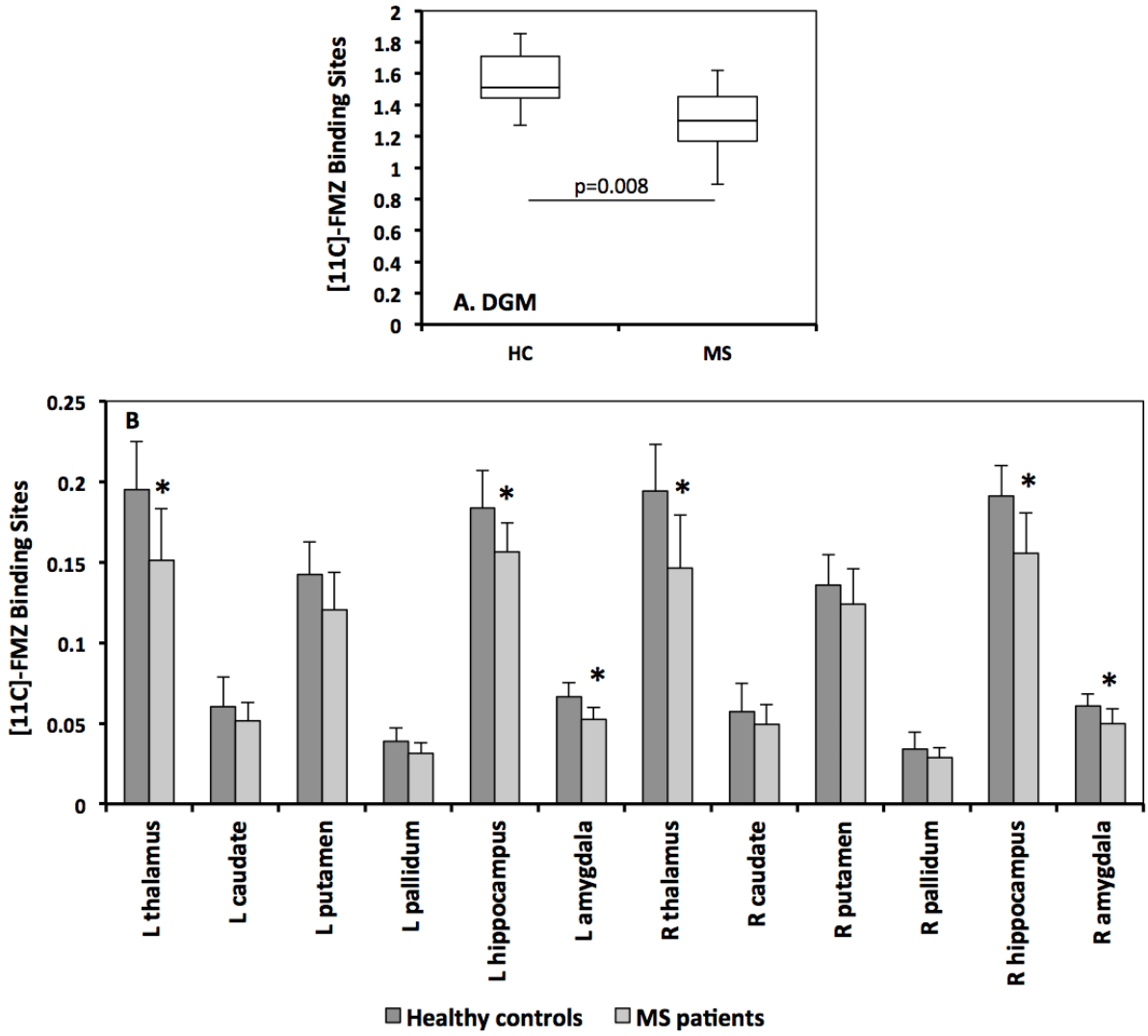

Figure 32: ROI analyses of [^{11}C]FMZ binding sites in deep GM structures. A: Box and whisker diagrams of [^{11}C]FMZ total binding sites in healthy controls (HC) and MS patients in the deep GM. B: [^{11}C]FMZ binding sites in HC and MS patients in individual deep GM structures. Statistical comparison was performed using linear regression adjusting for age and sex with a significance threshold of $p<0.05$.

3.5. Subgroup analyses of [^{11}C]FMZ binding

Two groups of patients were included in our study: RRMS (n=9) and SPMS (n=9). Considering the small sample size of these groups, such analyses are only exploratory but can provide some interesting information regarding the chronology of [^{11}C]FMZ binding over the course of the disease. The results of the subgroup analyses are presented in figure 33.

Exploratory analyses of the [^{11}C]FMZ Bmax changes in the RRMS subgroups, compared to controls showed a significant decrease in RRMS patients of:

- 11.2% (p=0.008) in total GM
- 11.3% (p=0.008) in cortical GM
- 13.7% (p=0.046) subcortical GM

The total estimated number of [^{11}C]FMZ binding sites (normalized by headsize) was found to be decreased by:

- 8.4 % (p=0.046) in total GM
- 8.1 % (p=0.046) in cortical GM
- 14% (p=0.027) in subcortical GM

When the [^{11}C]FMZ Bmax was considered in SPMS patients, there was a moderate decrease that did not reach significance in either the total GM (-7.5%, p=0.14), cortical GM (-8.6%, p=0.14) or subcortical GM (-4%, p=0.54).

However, the total amount of [^{11}C]FMZ binding sites was decreased by:

- 12.2 % (p=0.027) in total GM
- 11.8 % (p=0.027) in cortical GM
- 19.6 % (p=0.006) in subcortical GM

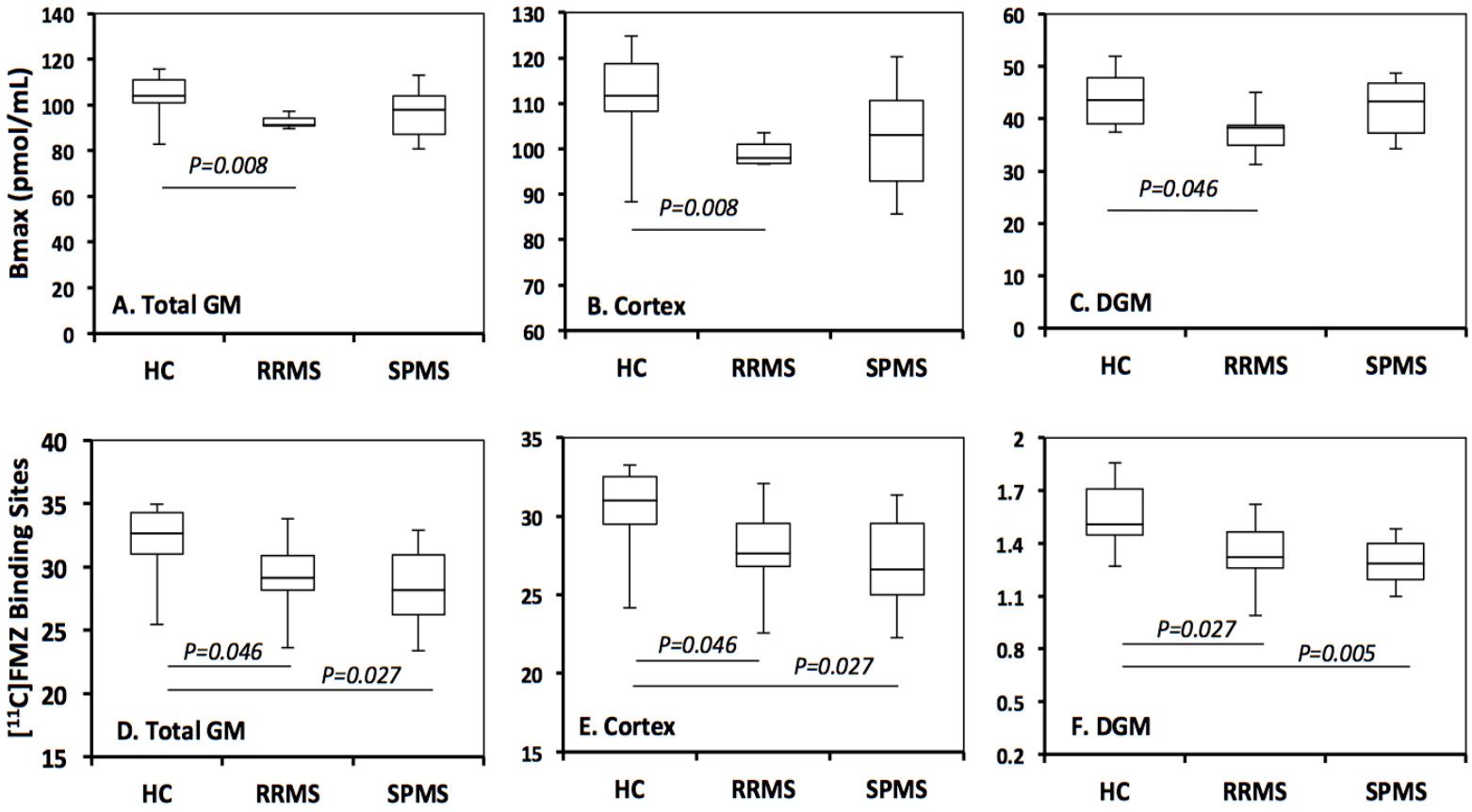

Figure 33: Subgroup comparisons Box and whisker diagrams of ^{11}C-FMZ Bmax (A, B, C) and Total FMZ Binding Sites (D, E, F) in the total GM, cortex, and DGM of healthy controls (HC), RRMS, and SPMS patients.

3.6. Cortical mapping of [^{11}C]FMZ binding changes

It was of interest to see if we could map [^{11}C]FMZ binding changes between groups to determine which cortical regions were more affected by the loss of BZD receptor sites. This was done using the vertex-by-vertex GLM procedure available in FreeSurfer. Comparisons were adjusted for the effect of age and sex and corrected for multiple comparisons.

The vertex-by-vertex GLM procedure applied to [^{11}C]FMZ PET data at the group level detected five clusters of significantly decreased [^{11}C]FMZ Bmax in MS patients compared to controls (figure 34, table 5), localized in:

- Left superior parietal gyrus (cluster-wise p-value=CWP= 0.0014)
- Right inferior parietal gyrus (CWP= 0.0002)
- Right supramarginal gyrus (CWP=0.0028)
- Right rostral middle frontal gyrus (CWP=0.0312)
- Right pars triangularis (CWP=0.0218).

Importantly, no cluster of increased [^{11}C]FMZ Bmax was detected.

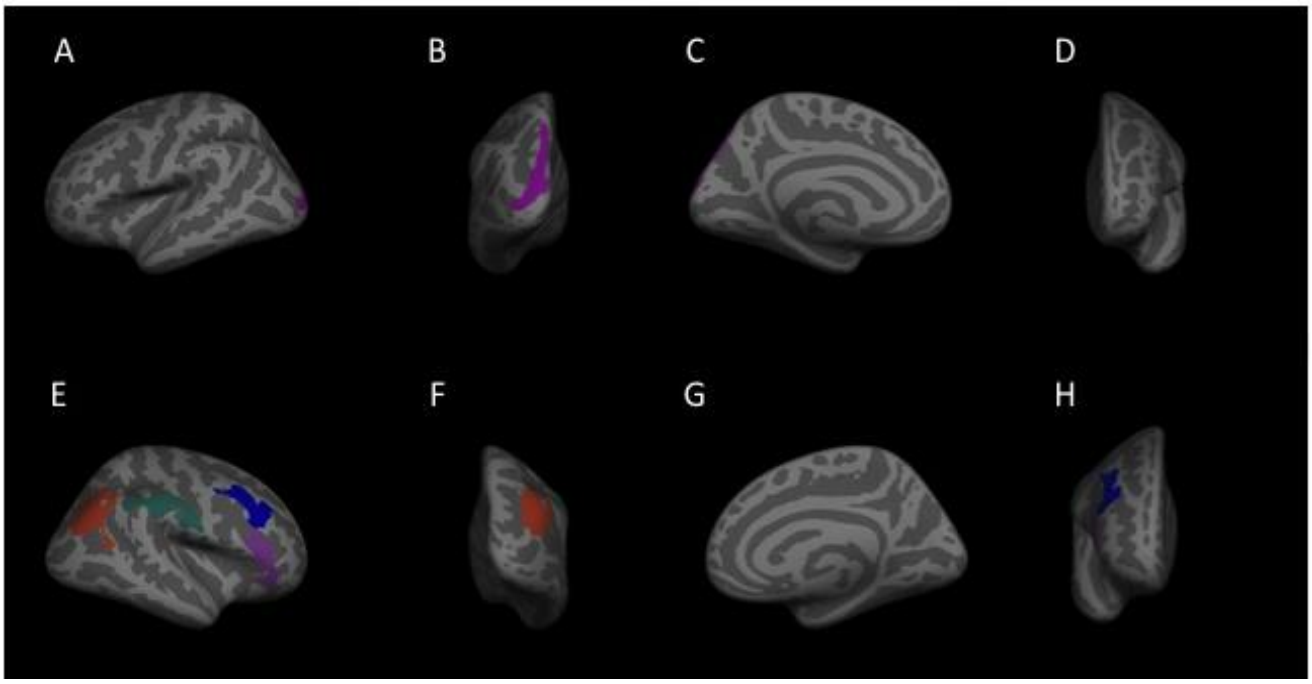

Figure 34: FreeSurfer surface-based analyses of [^{11}C]FMZ Bmax. A-H: Regions where [^{11}C]FMZ Bmax was decreased in subjects with MS compared to healthy controls, after correction for age and sex. Left hemisphere, top (A-D) and right hemisphere, bottom (E-H). No cluster of increased [^{11}C]FMZ Bmax was found.

Area of between-group difference	*Side*	*Cluster size (mm²)*	*Maxima Voxel MNI Coordinates*			*Patients mean (SD)*	*Control mean (SD)*	*CWP*
			x	**y**	**z**			
Superior Parietal	L	1711.98	-16.5	-76.7	42.3	114.3 (8.8)	126.4 (15.3)	0.0014
Inferior Parietal	R	2090.25	33.7	-69.5	37.8	127.7 (18.2)	144.4 (9.9)	0.0002
Supramarginal	R	1735.61	58.0	-25.7	35.6	110.7 (10.0)	127.1 (15.9)	0.0028
Rostral Middle Frontal	R	1214.52	44.6	26.8	31.6	107.2 (10.0)	122.3 (18.0)	0.0312
Pars Triangularis	R	1293.38	44.4	33.0	7.5	106.2 (10.9)	115.9 (18.0)	0.0218

Table 5: Clusters of decreased cortical [^{11}C]FMZ Bmax in MS patients compared to HC.

3.7. Relationship between [^{11}C]FMZ binding and white matter lesions load

To determine the impact of focal WM damage on [^{11}C]FMZ binding, we evaluated the correlations between PET measures and global T2 lesion load (figure 35).

T2 lesion load was estimated for each subject and averaged at 19,550 mm^3 in RRMS patients (2,627-37,965 mm^3) and 40,167 mm^3 in SPMS patients (5,865-66,596 mm^3).

There was a significant negative correlation between T2 lesion volume fraction and [^{11}C]FMZ binding sites in:

- Cortical GM (r=-0.51, p=0.03)
- Subcortical GM (r=-0.67, p=0.003)
- Trend only in the total GM (r=-0.46, p=0.06).

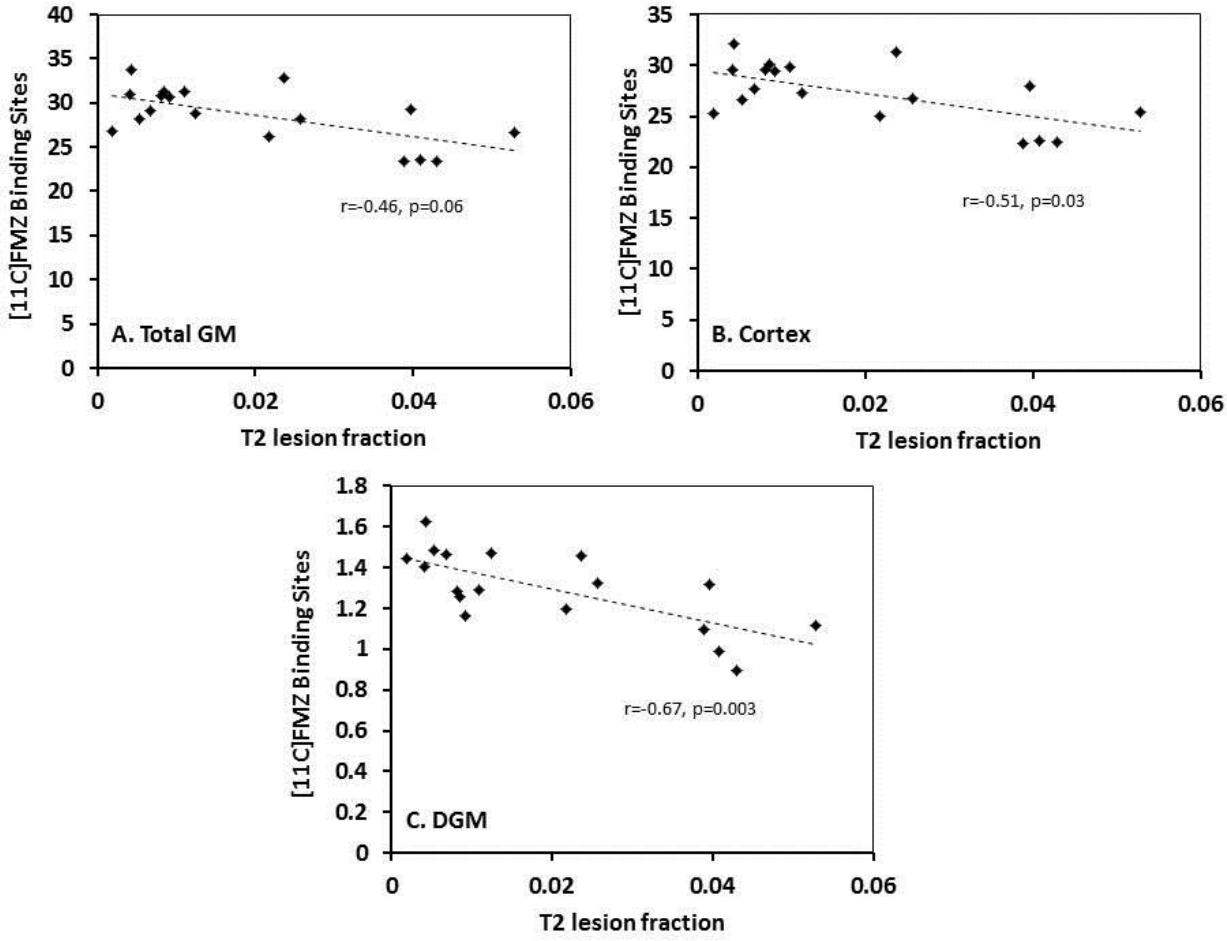

Figure 35: correlation between T2 lesion load and [^{11}C]FMZ binding sites in the cortical GM, subcortical GM and total GM of MS patients.

3.8. Relationship between [^{11}C]FMZ binding and clinical metrics

It was of interest to evaluate the clinical relevance of our PET metrics by assessing their relationship with physical and cognitive performance as part of an exploratory analysis.

Relationship between clinical scores and cortical [^{11}C]FMZ binding sites was assessed using the entire patient cohort (table 6). Significant partial correlations were found between cortical [^{11}C]FMZ binding sites and performance on:

- PASAT (r=0.52,p=0.04)
- MMSE (r=0.77, p=0.0004)
- Rey complex figure task (copy r=0.60, p=0.01; recall r=0.81, p=0.0001).

	Controls	*MS Patients*	*Correlation with cortical GM [^{11}C]FMZ binding, rho(p-value)*
EDSS		4.2 (2.2)	0.17 (0.53)
25 FW	7.4 (3.0)	10.7 (11.1)	0.04 (0.90)
9HPT- DH	20.6 (2.4)	28.4 (11.2)	0.38 (0.15)
9HPT-NDH	21.7 (3.0)	35.1 (26.8)	0.21 (0.43)
PASAT	42.9 (10.4)	36.3 (11.4)	0.52 (0.04)
MMSE	27.6 (2.1)	27.2 (3.3)	0.77 (0.0004)
Stroop test	51.6 (6.9)	45.4 (6.7)	0.39 (0.15)
Rey Complex Figure			
Copy	34.4 (1.8)	32.7 (4.4)	0.60 (0.01)
Recall	19.6 (7.4)	17.7 (8.3)	0.81 (0.0001)

Table 6: Clinical correlations. Clinical performances of HC and MS patients and correlation with cortical [^{11}C]FMZ binding (partial correlation coefficient and p-value) adjusting for the effect of age and sex in the patient population (n=18).

Correlations between cortical Bmax and PASAT performances were also tested at the surface-based level to determine the cortical regions associated with PASAT performance (figure 36, table 7). Significant positive correlations were detected in:

- Right posterior cingulate
- Right precentral
- Left postcentral gyri

No cluster with negative correlation was detected.

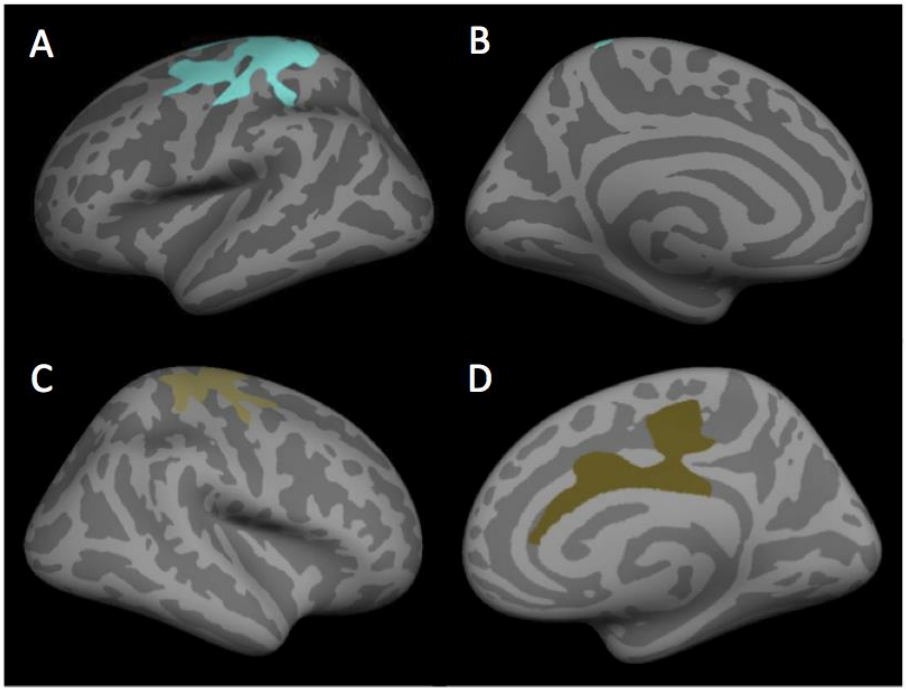

Figure 36: FreeSurfer surface-based correlations between [^{11}C]FMZ Bmax and PASAT performance. Visual representation of regions where [^{11}C]FMZ Bmax correlates positively with PASAT scores. Left hemisphere, top (A-B) and right hemisphere, bottom (C-D).

Area of between-group difference	*Side*	*Cluster size (mm²)*	*Maxima Voxel MNI Coordinates*			*CWP*
			x	**y**	**z**	
Postcentral	L	3894.97	-18.1	-33.5	61.1	0.0002
Posterior Cingulate	R	1586.47	6.4	-26.8	27.6	0.009
Precentral	R	1894.19	27.3	-21.4	63.5	0.003

Table 7: GLM clusters. Regions where cortical [^{11}C]FMZ Bmax in patients with multiple sclerosis (n=18) correlated positively with PASAT scores on surface based analyses. No negative correlation was found.

Discussion & Perspectives

1. IN VIVO QUANTIFICATION OF NEURONAL DAMAGE IN MS

This work aimed to quantify the neuronal contribution to GM damage in MS using high resolution PET and the neuronal marker [^{11}C]FMZ. It is, to our knowledge, the first controlled *in vivo* study demonstrating changes in $GABA_A$ receptor density in MS patients. We found, using both a ROI and a surface-based approach, that cortical [^{11}C]FMZ binding was reduced in MS subjects, and that surface-based analyses allowed mapping of cortical damage at the group level. In the subcortical GM, a significant decrease in $GABA_A$ receptor sites but not density was detected in the thalami, hippocampi and amygdalae. Subgroup analyses suggested that [^{11}C]FMZ binding reduction was already present in RRMS subjects, whereas GM atrophy was barely detected at this stage. Finally, cortical $GABA_A$ receptor content was found to correlate positively with cognitive performance, suggesting the clinical relevance of this quantitative measure.

MS is a diffuse chronic demyelinating disease of the CNS affecting not exclusively neurons, but also macroglial, microglial and inflammatory cells. In order to detect neuronal damage that could occur randomly in the GM of MS subjects, we took advantage of recent methodological optimizations. First, all PET images were acquired on a high-resolution research tomograph (HRRT, Annex B) which has one of the highest sensitivity and spatial resolution among currently available PET scanners (2.5 mm) and allows accurate localization of alterations in $GABA_A$ receptor density within the cortical ribbon. Secondly, we used the partial saturation method [216] to estimate receptor concentration from a single FMZ injection and without arterial blood sampling. This previously validated method exploits the natural decrease of bound ligand concentration over the duration of the experiment after labeled/unlabeled FMZ co-injection and provides an absolute quantification of BZD receptors concentration (Bmax). Thirdly, we supplemented ROI-based analyses with a surface-based approach to regionally map the differences in cortical [^{11}C]FMZ binding between MS patients and controls. While ROI analyses are constrained to predetermined GM regions either manually or automatically

delineated, surface-based analyses allow a vertex-by-vertex comparison of [^{11}C]FMZ Bmax differences between subjects. This technique has been shown to improve the reliability and detectability of PET signal changes [228] as a result of processing steps that minimize partial volume effect (PVE) from the white matter and CSF such as surface-based smoothing and sampling of PET measures halfway between the white and pial surfaces.

[^{11}C]FMZ Bmax, which estimates the density of $GABA_A$ receptors, showed more significant changes in the mildly atrophic RRMS subgroup compared to the most atrophic SPMS subjects. This was all the more unexpected as the influence of any partial volume effect should have resulted in more significant signal decrease in the grey matter of patients with marked atrophy. Therefore the impact of PVE on our results is probably minor, and this apparent discrepancy suggests that atrophy could induce an artificial increase in $GABA_A$ receptor density estimated by [^{11}C]FMZ Bmax. Such an artificial increase in density becomes easy to understand if we consider that the underlying substrate for grey matter atrophy is independent from the synaptic component [107]. Therefore atrophy partly masks the decrease in $GABA_A$ receptors number, as far as it is measured by their density in a reduced volume. Interestingly, quantifying the total number of $GABA_A$ receptors sites per region re-established the expected result by showing greater loss in the SPMS subgroup, which corroborated this hypothesis. Overall these two metrics, Bmax, and total amount of $GABA_A$ receptors, may each be useful in a clinical setting: the Bmax analysis provides a sensitive tool to detect and regionally map the neuronal component of grey matter pathology, especially in cortical regions, as soon as the earliest stages of the disease, when atrophy is only minor; the total amount of $GABA_A$ receptors estimates the overall neuronal and synaptic pathology in regions of interest, and may provide measures suitable for longitudinal follow up that will not be biased by progressive atrophy. Further work investigating how we can minimize the influence of any PVE on this second metric may be needed.

The pathological correlates of [^{11}C]FMZ binding changes detected in MS remain to be elucidated and may not be univocal. $GABA_A$ receptors are widely expressed by CNS neurons, both inhibitory and excitatory, and are enriched at axo-synaptic contacts

[229]. Therefore quantification of [^{11}C]FMZ binding, while assessing mainly inhibitory neurotransmission, is not an intrinsic measure of GABAergic neurons themselves. Moreover, variations of $GABA_A$ receptor content is not expected to exclusively reflect neuronal death or loss, and may also indicate dendritic or synaptic changes. In the rodent EAE model, impaired GABA transmission has been reported in the striatum and hippocampus [230] [231], along with drastic dendritic and synaptic alterations from the earliest inflammatory phase of the disease [155]. Reduction in flunitrazepam-sensitive $GABA_A$ receptor density without changes in affinity was also found in cortical synaptosomes of EAE rats [232]. In post-mortem samples from MS subjects, significant synaptic loss along with less pronounced evidence of neuronal death were described in the neocortex [83] [105], as well as in deep GM structures, notably the thalamus and hippocampus [110] [109]. Post mortem studies have confirmed a reduction in $GABA_A$-related gene transcripts and loss of inhibitory interneurons in MS, supporting the notion that cortical neurons of chronic MS patients have significantly decreased inhibitory innervation [123]. Cawley et al [233] provided evidence of reduced $GABA_A$ levels in the hippocampus and sensorimotor cortex of SPMS patients using MR spectroscopy and suggested that lower $GABA_A$ concentrations correlated with reduced motor function. Injury of GABAergic inhibitory systems is an early event thought to trigger excitotoxicity via up-regulation of glutamate-mediated neurotransmission resulting in extensive neuronal and synaptic damage [234] [235]. Impaired GABAergic transmission might also lead to neurodegeneration by increasing the energy expenditure of neurons that have a reduced capacity to produce ATP due to mitochondrial dysfunction [123]. Depending on the disease stage, [^{11}C]FMZ binding changes described in MS subjects could therefore reflect a combination of synapse/dendrite damage and neuronal loss.

Generalized GM atrophy in MS has been widely reported by histopathological [105] [112] and MRI studies [115] [147] [236] [237] [238] [239]. In this small cohort, grey matter atrophy was easily identified in the deep grey matter of patients, and was detectable but not significant at the relapsing stage, especially in cortical regions. Recent studies have shed light on the relationship between MRI-measured cortical atrophy and neuronal damage in MS [107] [154]. The authors have shown that neurodegenerative processes drive GM atrophy in the cortex, as they found significant correlations between

cortical volume and neuronal density or neuronal numbers, but no correlations with myelin density. In the present study, cortical thinning was significant in the temporal and occipital lobes bilaterally, reaching about 4-5% in ROI analyses. We related cortical thickness to [^{11}C]-FMZ binding, as a potential marker for neuronal integrity in vivo. Correlations were assessed both across cortical regions and across subjects. First, we found a linear decrease in mean [^{11}C]-FMZ Bmax with increasing global thickness across cortical lobar areas, both in healthy controls and MS patients separately. Lafougere et al. [240] described a similar relationship in heterotypical and temporo-occipital homotypical cortices. However, when we assessed the relationship between cortical thickness and [^{11}C]-FMZ binding across subjects in the MS group and the healthy control group, no correlation was found. These results do not antagonize the recent findings cited above. It can be postulated that [^{11}C]FMZ PET metrics reflect not only neuronal loss, but also subtle neurodegenerative changes such as synaptic loss or dendritic transections which may precede neuronal loss and are not fully captured by measures of GM volume. Therefore measuring neuronal damage by PET and GM volume by MRI does not provide redundant information and the combined use of [^{11}C]FMZ PET and MRI could synergistically contribute to a better evaluation and understanding of neurodegeneration in MS.

2. CLINICAL RELEVANCE OF PET WITH [^{11}C]FMZ

Despite uncertainties regarding the interpretation of [^{11}C]FMZ PET data at the sub-cellular level, the clinical relevance of this imaging biomarker was suggested by our exploratory analyses as it was found to correlate with several clinical measures. The lack of significant cross-sectional correlation between [^{11}C]FMZ binding and the main metrics of physical disability (EDSS, 25-foot walk test) in this small population was not surprising as these metrics are drastically influenced by spinal cord pathology, a condition that could not be taken into account in a study focusing on the brain. However, we found significant correlations between cortical [^{11}C]FMZ binding and performance on several cognitive tests. Correlations were found with MMSE, a general cognitive scale, PASAT, a widely used test evaluating attention, working memory and information processing speed, and Rey Complex Figure Test which captures visuo-spatial processing. All these cognitive domains are amongst the most affected in MS [241]. This reinforces the view that cortical neuronal damage may be a key pathological substrate leading to cognitive deficits in MS, a hypothesis previously suggested by structural MRI studies [242] [243] [244], or MR spectroscopy [245] [246]. Surface-based analyses enabled us to map several relevant cortical areas for PASAT performance, which were located in the right posterior cingulate cortex (PCC), the left postcentral gyrus and the right precentral gyrus, with a trend in the left PCC (significant correlation before correction for multiple comparisons, data not shown). These areas are consistent with current knowledge as postcentral and precentral gyri have been described as belonging to the PASAT network [247] [248] and PCC has been identified as a key structure involved in adaptative cerebral plasticity in MS [247]. PCC is a highly connected structure acting within the default mode network (DMN), and controlling the focus of attention through its interaction with the prefrontal cortex [249]. PCC dysfunction together with DMN disconnection may be possible triggering events for the onset of cognitive symptoms in MS [243] [250] [251].

3. UNDERLYING MECHANISMS OF NEURONAL DAMAGE IN MS

3.1. Relationship between WM and GM damage

The mechanisms underlying structural and functional neuronal damage within the MS grey matter haven't yet been elucidated, especially its relation to demyelination and inflammation. Of particular interest is the association between neurodegeneration and focal white matter damage, the most striking feature of the disease. Our group of patients presented a wide range of T2 lesion burden. Our results showed a significant yet moderate relationship between WM T2-weighted lesion load and the cortical $GABA_A$ receptors. The relationship was stronger in the subcortical GM. Our results support the notion that focal damage to WM tracts contribute at least partly to the on-going damage to neuronal and synaptic structures in the MS GM. This might be explained by underlying mechanisms of anterograde or retrograde degeneration [85]. Consistent with this notion that WM and GM are inter-related processes, several MRI studies have reported significant correlation between WM damage and GM atrophy, in deep GM structures [252] or cortical structures [253]. Longitudinal studies analyzing GM atrophy using VBM or similar techniques [254] [255] showed an association between global WM lesion volumes and increasing GM volume loss especially in fronto-temporal areas. Bernfeldt et al. demonstrated more widespread cortical GM atrophy in patients with longitudinal changes in T2 lesion volumes compared to patients with stable lesion loads [255] [256]. Location of WM damage was shown to contribute to clinical disability [238]. Similarly, the spatial distribution of WM T2 lesions is relevant to GM volume loss. Mulhau et al recently unveiled a significant spatial relationship between WM lesions and thalamus pathology [257]. This might be further explained by the fact that the thalamus is a relay organ, receiving input from multiple connected WM fibers. In the MS cortex, highly connected structures such as the cingulate gyrus or the insula appear more prone to volume loss, reinforcing the role of WM disconnection in the development of GM atrophy. WM lesions, however only seem to account for less than

half of the variance in GM atrophy in the early stages of the disease [258] and histopathological studies of late MS patients have outlined a dissocation between plaque load and pathological markers of neurodegeneration [259] [112]. These findings suggest the impact of other processes in the progression of GM and specifically neuronal damage.

More subtle and diffuse changes occurring within the NAWM may also contribute to the cortical abnormalities observed using [^{11}C]FMZ PET. Such relationship was not evaluated in our pilot study. Quantitative MRI metrics have been shown to be sensitive to microstructural changes in post-mortem tissue [260] [112] and have been used to quantify white matter integrity in MS. In a recent paper, Kolasinski et al. also suggested that functional anatomical connectivity might be relevant to the spread of MS pathology in a "tract-specific pattern" [112]. Focal changes in MRI cortical thickness showed a clear intra-tract correlation with changes in WM microstructure. The correlation was reproduced using traditional histological metrics or DTI-derived measures of WM integrity. Tract-specific measures of WM integrity were not only found to better correlate with corresponding cortical thickness but also related better to measures of disability [179] than measures of global WM changes. Longitudinal study design could help understand the temporality of these events and determine whether tract-specific WM damage predicts GM as suggested by prior MRI work [253]

In a new prospective project (clinicaltrial.gov ID: NCT01651520), we are planning to assess the chronology of occurrence and the prognostic value of neuronal damage measured by [^{11}C]FMZ PET in early RRMS and PPMS patients. Acquisition of multimodal MRI data at each timepoint will also help address the relationship between GM and WM pathology. Four groups of subjects will be included: i) patients with RRMS with less than 5 years disease duration (revised Mc Donald criteria, n=20); ii) patients with RRMS with over 5 years but less than 10 years disease duration (n=20); iii) patients with a primary progressive MS (PPMS) with less than 10 years disease duration (n=20); iv) healthy volunteers matched for age and sex (2/3 matched with RRMS patients; 1/3 matched with PPMS patients). Preliminary data of a subgroup of early

RRMS patients (n=9, age= 35.1 years, mean disease duration=23 months) and controls (n=7, age=32.3 years) is available. In a preliminary work (unpublished data), we related T2 lesion load and NAWM FA within 3 WM tracts (thalamo-prefrontal, cingulate and cortico-spinal) to [^{11}C]FMZ Bmax in anatomically related cortical areas (rostral middle frontal, posterior cingulate, precentral) in patients only. The cross-sectional correlations between these metrics failed to show significant relationship between focal or diffuse intra-tract WM damage and GM neuronal injury (figure 37). A trend was found between FA within cingulate white matter tracts and posterior cingulate Bmax (rho=-0.40, p=0.097). Considering the short disease duration, follow-up of these subjects will be very informative to determine the nature and chronology of a relationship between these two phenomena.

Cortico-spinal tract	Bmax (pmol/mL)	T2 lesion fraction	FA in NAWM
Mean	97,41	1,23 %	0,33
SD	11,98	1,05	0,024
Rho		0,035	-0,52
P-value		0.89	0.27

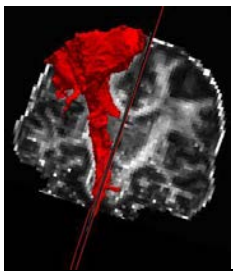

Thalamo-prefrontal	Bmax (pmol/mL)	T2 lesion fraction	FA in NAWM
Mean	112,5	3,26 %	0,34
SD	9,87	2,23	0,057
Rho		0,17	-0,26
P-value		0,49	0,29

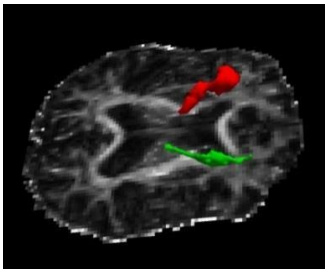

Cingulate	Bmax (pmol/mL)	T2 lesion fraction	FA in NAWM
Mean	107,0	1,58 %	0,30
SD	10,83	1,95	0,055
Rho		0,096	-0,40
P-value		0,71	0,097

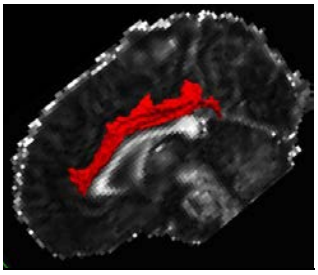

Figure 37: Correlations between T2 lesion load and NAWM FA within 3 white matter tracts (thalamo-prefrontal, cingulate and cortico-spinal) and [^{11}C]FMZ Bmax in anatomically related cortical areas (rostral middle frontal, posterior cingulate, precentral) in early RRMS patients (unpublished data).

3.2. Relationship between GM demyelination and neurodegeneration

The in vivo relationship between cortical neuronal damage and cortical demyelination also needs to be investigated. Studies of autopsy material have determined that demyelination is extensive in the GM of patients with MS, especially in the secondary progressive phase of the disease [84]. The seminal work by Peterson et al. [83] identified axonal transections, dendritic transections and neuronal deaths by apoptosis within areas of cortical demyelination in MS brains. Wegner et al. [105] later suggested that neuronal degenerative changes and synaptic loss occur within neocortical lesions, whereas non-lesional neocortex does not show significant changes in neuronal or synaptic density. Furthermore, reduction in synaptic density and decreased expression of neuronal proteins involved in neuronal survival were also reported in demyelinated hippocampi from post-mortem MS brains [109]. However, other studies have been challenging these findings and described extensive neuronal and dendritic loss as well as evidence of mitochondrial dysfunction in myelinated cortical areas [261] [124]. The methodological and sampling differences between these studies limit their comparability. Thus more work is needed, as it remains important to determine to what extent GM demyelination and neurodegeneration are inter-related. This relationship might be explored in vivo in a multimodal approach by combining [^{11}C]-FMZ high resolution PET with MR imaging sequences able to visualize GM lesions such as Double Inversion Recovery (DIR).

In a presentation by Theodore Soulier, MSc, highlighted at the ECTRIMS meeting in Copenhagen in October 2013, we addressed this specific question [262]. In our new cohort of 9 early RRMS patients, 8 presented DIR-visible cortical lesions and were selected for preliminary analyses (figure 38). We compared [^{11}C]FMZ Bmax within DIR lesions and cortical normal-appearing GM (NAGM). A significant 16.4% decrease in Bmax ($p=0.023$) was found in cortical lesions (86,35 pmol/mL ± 4,64 pmol/mL) compared to NAGM (103,31 pmol/mL ± 2,93 pmol/mL) (figure 39). No significant difference was found between NAGM Bmax in MS patients compared to healthy

controls. These findings suggest that a significant level of neuronal injury might occur in conjunction with demyelination at the early stages of the disease, and be limited to areas of GM demyelination. Neuronal injury in demyelinated GM may relate to acute damage to axo-dendritic processes secondary to inflammation [81]. Indeed, Lucchinetti et al. reported significant inflammation within early cortical lesions, which differed from chronic GM lesions in that respect. The authors also described neuronal damage occurring on a background of inflammation at this stage supporting the notion of a secondary neurodegenerative process, in the context of local inflammation in early MS [86]. The inflammatory milieu may alter expression and phosphorylation of AMPA receptors or downregulate genes involved in glutamatergic neurotransmission, thus promoting neuronal and synaptic damage via glutamate accumulation and excitotoxicity [263]. As the disease evolves, inflammation becomes much less pronounced within cortical lesions and the relationship between GM demyelination and neuronal/synaptic injury may not be as exclusive. Longitudinal follow-up of our subjects as well as assessment of patients at different stages of the disease may provide greater insights on the evolving interplay between these two processes.

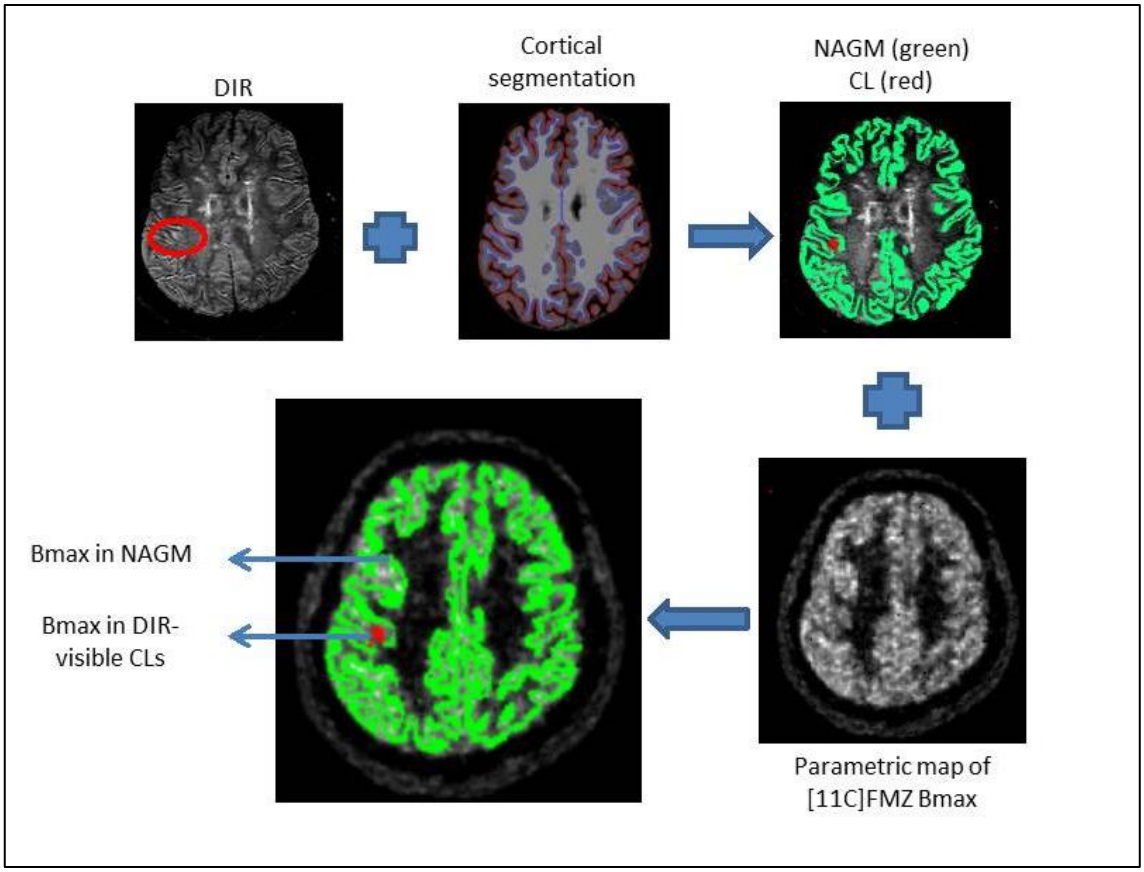

Figure 38: Processing steps undertaken to analyze and compare Bmax within DIR-visible cortical lesions (CLs) and normal appearing cortical GM (NAGM).

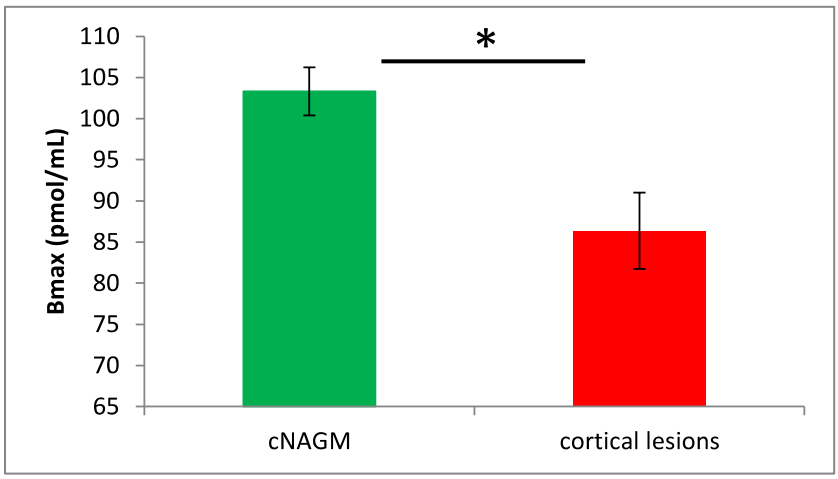

Figure 39: Comparison of mean [11C]FMZ Bmax in cortical NAGM (cNAGM) and within DIR-visible cortical lesions (-16.4%, p=0.023).

3.3. Other aspects

Other mechanisms at play in the MS grey matter have been proposed. Evidence of cerebral hypoperfusion in MS is currently gaining some attention as it may negatively impact an already precarious energy balance in neuronal cells [130]. From a clinical standpoint, reduction in cerebral blood flow (CBF) has been associated with cognitive deficits and fatigue in MS patients [264] [134].

In a recent work led with the team of Dr Wolinsky at the University of Texas at Houston and recently presented at ECTRIMS, I was able to show that hypoperfusion is a widespread phenomenon in the MS GM, which can be assessed using non-invasive MRI techniques. We performed pseudo-continuous arterial spin labeling (pCASL) MRI in 34 MS patients (5 CIS, 24 RRMS, 5 SPMS) and 19 healthy controls and used a region-of-interest and a surface-based approach to evaluate cortical and subcortical GM blood flow differences between groups. ROI analyses showed diffuse decrease of CBF in MS neocortex and DGM structures compared to controls, in proportions that surpassed that of atrophy measures (figure 40). Thalami and Pallidi showed the most significant decrease in CBF among DGM structures (-29% and -25% respectively, $p<0.005$ adjusting for age and sex). Fronto-temporal cortices were among the most affected in surface-based analyses (figure 41, table 8). We also found a moderate yet significant positive relationship between cortical hypoperfusion and cortical volume at the cross-sectional level ($rho=0.36$, $p=0.03$).

Manipulation of 2D pCASL data can be challenging and care must be taken to apply partial volume effect correction algorithms to limit cross-tissue contamination. Surface-based analyses present a definite advantage in this regard as we have discussed earlier. The interpretation of our results also requires caution. We will need to establish that cerebral hyperperfusion in MS does not simply reflect contemporaneous loss of neurons and atrophy but is rather an early and integral feature of MS pathophysiology. Debernard et al. [131] provided evidence of cerebral hypoperfusion at the very early

stages of MS before atrophy was even detectable. In our cohort, the decrease in CBF was of greater amplitude than corresponding atrophy measures. Other objective findings support the notion of primary hypoperfusion in MS. Elevated levels of Endothelin-1 (ET-1), a vasoconstrictive agent, have been found in serum and CSF of MS patients [265] [266] and were associated with reduced blood flow velocities [267]. ET-1 was also detected in reactive astrocytes in post-mortem MS brains [268]. Ultimately, interrogation of longitudinal data will be of great importance, as it will allow us to determine whether hypoperfusion heralds or follows irreversible tissue loss. Combination of perfusion MRI techniques, such as pCASL, with [^{11}C]FMZ PET could help more specifically define the role of cerebral hypoperfusion in neuronal pathology. pCASL data was acquired in a group of early RRMS patients and healthy controls that will be used to evaluate the relationship between GM blood flow and [^{11}C]FMZ bmax both cross-sectionally and longitudinally. This could potentially unveil novel pathways of tissue destruction in MS and contribute to the development of therapies targeting the neuronal compartment.

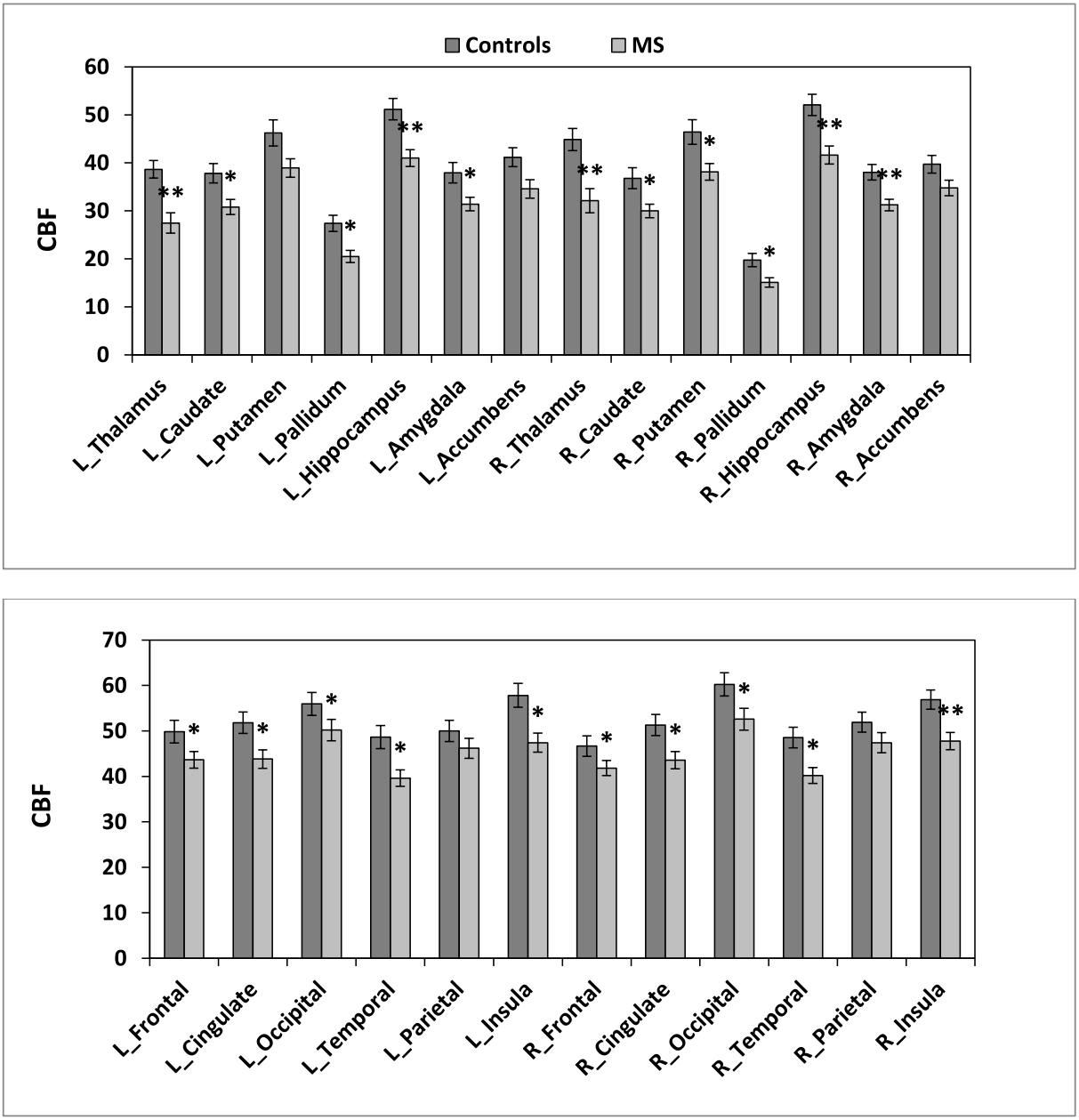

Figure 40: ROI analyses of cerebral blood flow (CBF, mL/100g/min) in deep GM structures (top) and cortical lobes (bottom). In DGM structures, maximum decrease of CBF was found in the Thalami (-29%, p=0.00005 and -28%, p=0.0002) and Pallidi (-25%, p=0.003 and -24%, p=0.003). Global cortical CBF was 44.0 mL/100g/min (±10.6) in MS patients vs 50.4 mL/100g/min (±9.8) in controls (-13%, p=0.01). Most cortical structures were hypo-perfused in MS patients.

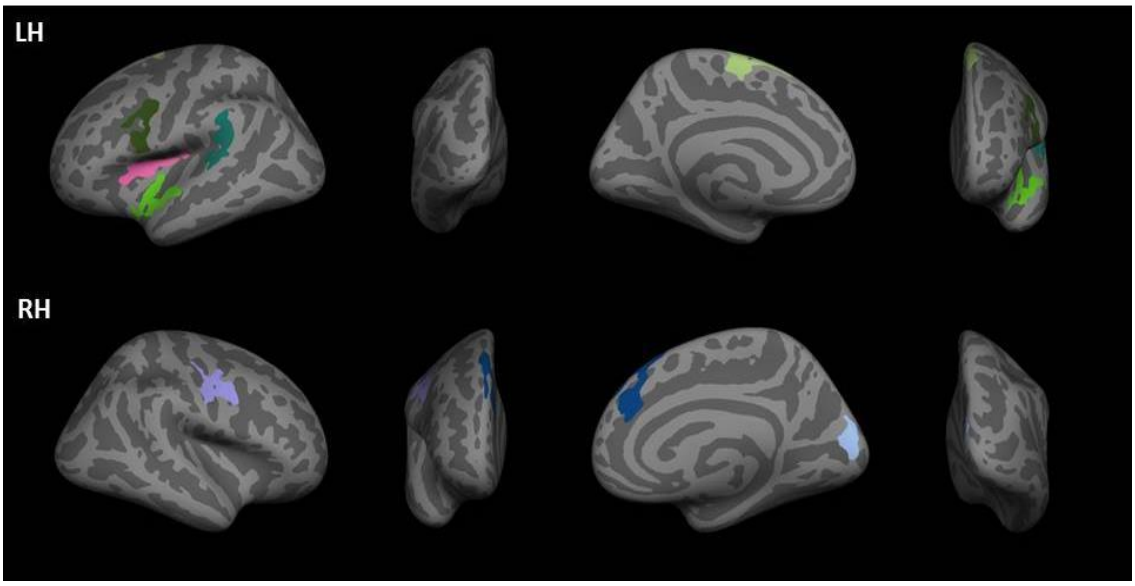

Figure 41: Surface-based comparisons CBF between MS patients and healthy controls. The vertex-by-vertex GLM procedure applied to CBF data at the group level (after adjustment for the effect of age and sex and correction for multiple comparisons) detected eight clusters of significantly decreased blood flow in MS patients compared to controls. No cluster of increased CBF was detected.

Area of between-group difference	Side	Cluster size (mm2)	Maxima Voxel MNI Coordinates			CWP
			x	y	z	
Superior Frontal	L	920.37	-10.6	-8.9	67.4	0.0018
Precentral	L	755.72	-43.5	-2.3	-32.6	0.0098
Superior Temportal	L	748.67	-51.5	-8.1	-4.1	0.0114
Insula	L	627.14	-35.8	1.9	14.7	0.033
Supramarginal	L	881.05	-47.6	-43.6	21.4	0.0034
Precentral	R	870.36	41.4	-11.3	37.9	0.0024
Superior Frontal	R	868.85	10	30.4	54.2	0.0024
Pericalcarine	R	601.36	14	-87.4	6.6	0.035

Table 8: Clusters of decreased CBF in MS patients compared to controls detected by surface based analyses.

4. FUTURE ROLE OF [^{11}C]FMZ PET IN MS

With this pilot work, we have shown that PET with [^{11}C]FMZ could be performed and adequately quantified in a non-invasive manner in MS patients to detect early neuronal injury to the GM. PET has also been used to investigate underlying pathophysiology of neuroinflammation, demyelination and remyelination in MS. In the particular case of [^{11}C]-labeled tracers, the need and high cost of on-site cyclotron production of isotopes has limited the availability and widespread application of PET. Fluorinated analogs [269] have been proposed and should enable the integration of FMZ PET in clinical practice or for evaluation of novel therapies targeting the neuronal compartment.

Meanwhile, [^{11}C]FMZ PET has the potential to inform our understanding of non-conventional MRI techniques in the assessment of neuronal pathology. As a specific marker of the neuronal compartment, [^{11}C]FMZ may be used to evaluate the validity and specificity of neuroimaging techniques in vivo. It may also be used to test mechanistic hypotheses by combining imaging approaches, in which the strengths of MRI may add to those of PET.

In our pilot cohort of MS patients, we had set out to compare [^{11}C]FMZ binding, glucose metabolism evaluated using PET with [^{18}F]FDG and multimodal MRI metrics in the thalamus of MS patients and controls (figure 42). In agreement with prior findings, we found higher FA values in MS patients compared to healthy controls. This increase, even though not significant, was more pronounced in progressive patients. MTR modifications were minor in the thalamus. This is not a surprising finding since MTR has been shown to be mainly affected by myelin content rather than neuronal damage. Spectra analysis showed a slight decrease in NAA/Cr ratio in progressive patients, due in equal proportions to a decrease in NAA (neuronal injury) and increase in Creatine (gliosis). There was a moderate decrease in neuronal metabolism in RR patients that could reflect early disruption between thalamus nuclei and the cortex as suggested by Derrache et al. (2006). However this difference did not reach statistical significance. No

change in metabolism was observed in progressive patients. This might be explained by the significant volume reduction observed in this structure, which could induce an artificial increase in FDG uptake. Please note that no arterial blood sampling for PET quantification was performed. Overall, changes measured with [^{11}C]FMZ were of much greater amplitude than those noted with multimodal MRI or PET using FDG, suggesting that [^{11}C]FMZ PET may provide a more sensitive quantitative marker of thalamic injury. This approach and correlations between the different metrics need to be validated in a larger group of MS patients.

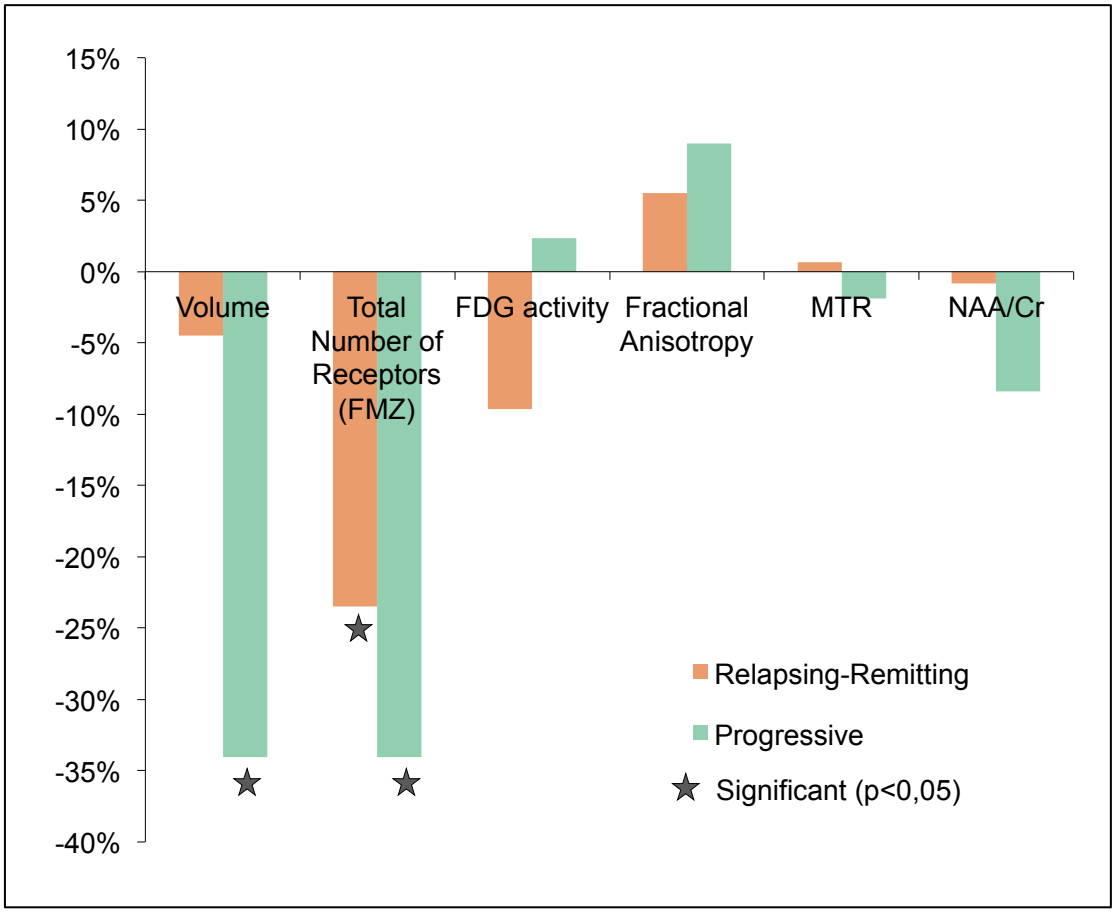

Figure 42: Patients vs controls comparisons of [^{11}C]FMZ, [^{18}F]FDG and multimodal MRI metrics in the thalamus. Unpublished data from our pilot cohort.

A novel multishell DTI imaging and modeling technique has been introduced to measure neurite density and orientation dispersion (NODDI) in vivo [270]. This technique provides neurite orientation dispersion indices (ODI) thought to quantify the

pattern of sprawling dendritic processes. Grussu et al. at a recent ECTRIMS meeting presented a meaningful comparison of NODDI and histopathological measures in the lumbar spine of MS patients and demonstrated that ODI correlated with the circular variance or spread of neuritis [271]. ODI in the DGM of RRMS patients has been shown to correlate with physical disability scores [272]. In a future study, we plan investigate the relationship between FMZ binding and dendritic arborization changes assessed with NODDI at 7T from the early phases of RRMS and PPMS. This will contribute to further our understanding of the early neurodegenerative processes occurring in the MS GM.

Furthermore, functional neuroimaging (fMRI) studies have highlighted the role of brain plasticity and cortical reorganization in disability progression in MS, suggesting that increased cortical recruitment might attenuate the consequences of MS-related tissue damage on physical and cognitive performance. Several groups have shown that MS patients with normal cognitive performance exhibit greater brain activation compared to controls during a cognitive task [248] [273] [247]. Moreover, subjects with MS recruit additional brain areas, usually not involved in the execution of the task. With the progression of the disease and the appearance of clinical symptoms, this compensatory mechanism tends to fail, and decreased activation is usually observed in late-stage MS in task-related fMRI studies [274]. A more recent approach, resting state fMRI, allows investigation of functional connectivity and cortical reorganization without the challenges of task-active fMRI investigation [275]. Louapre et al. showed that functional connectivity in the default-mode network and the fronto-parietal attention networks was selectively impaired in MS patients with severe early cognitive deficits [243]. In a recent paper, Roosendaal et al. demonstrated that early functional changes at rest could be detected in CIS patients, and that these changes were lost at later stages of the disease [276]. The authors suggested that cortical reorganization of brain networks is an early and finite phenomenon in MS, which may be hindered by increasing structural injury. A question thus remains: what drives the extinction of brain plasticity mechanisms as the disease progresses? To answer this question, the dynamic relation between underlying structural abnormalities such as GM neuronal pathology and functional connectivity needs to be investigated further, and may be addressed by combining resting-state fMRI and [^{11}C]FMZ PET.

5. LIMITS OF PRESENT STUDY

The work presented here has some limitations. The sample of MS patients and controls is small and rather heterogeneous. The sex ratio between patients and controls was not matched. Similarly, while the control and MS groups did not differ with regard to age, the RRMS subjects were significantly younger than their SPMS counterparts. Consequently, the results of this pilot study will need to be replicated in a larger and homogeneous cohort of MS patients, with adequate matching to a control population. The study of early MS patients (<5 years) is attractive as GM atrophy at this stage is not prominent and may not confound measurements of the density of BZD receptors using [^{11}C]FMZ PET. This will also help us elucidate the early phenomena at play in the MS GM.

The cross-sectional design of this work can help us appreciate the correlations between neuronal damage and clinical metrics at one point in time. In order to fully understand the temporal relationship between early neuronal damage and disability in MS, longitudinal follow up of MS patients will be necessary. This is also true to understand the interplay between neuronal damage and other aspect of MS pathophysiology such as WM focal lesions, WM diffuse pathology or GM demyelination. With these objectives in mind, we have continued to enroll in new longitudinal studies of early RRMS and PPMS patients aiming to assess the prognostic value of [^{11}C]-FMZ PET and the relationship between neuronal damage and other important processes as the disease evolves.

Finally, some technical limitations need to be brought to attention. While we have taken steps to limit the influence of partial volume effect in the study of cortical [^{11}C]-FMZ binding, by means of surface-based smoothing and sampling of PET measures halfway between the white and the pial surface in our surface based analyses, new processing techniques should allow us to further limit its unavoidable impact on PET data. Steps will be taken to investigate this issue.

Conclusion

Overall this work highlights the potential of [^{11}C]FMZ PET as a new biomarker of neuronal pathology in MS, which might lead to greater insights into the neurodegenerative mechanisms involved in MS. Further longitudinal studies will determine the chronology of [^{11}C]FMZ binding in MS, the prognostic value of this technique and the interplay between neuronal damage and other aspects of MS pathophysiology.

[^{11}C]FMZ PET-derived metrics may also be of great interest for trials evaluating neuroprotective drugs. The high cost of PET examination together with the restricted availability of [^{11}C]FMZ could impede a large application of this technology in a very near future. The production of a fluorinated analog of this tracer should facilitate such clinical applications, and allow innovative pathophysiological studies.

Combining [^{11}C]FMZ PET with advanced MRI sequences will help clarify the relative contribution of white matter or cortical demyelination to neuronal damage and help evaluate the impact of neuronal damage on structural and functional brain connectivity. FMZ PET studies may improve our understanding of the neuronal substrate of cognitive deficits in MS. By investigating predominantly inhibitory neurotransmission through $GABA_A$ receptors, [^{11}C]FMZ PET could provide insights on functional mechanisms underlying MS-related cognitive dysfunction: cortical neuronal synchrony, which is regulated by GABAergic neurotransmission, is considered mandatory for cognitive processing [277], and could emerge as a key substrate for the pathophysiology of MS cognitive deficits, as previously suggested in schizophrenia or Alzheimer's disease [278] [279].

Annex

1. ANNEX A: EDSS (from nationalmssociety.org)

Kurtzke Expanded Disability Status Scale (EDSS)

- ❑ 0.0 - Normal neurological exam (all grade 0 in all Functional System (FS) scores*).
- ❑ 1.0 - No disability, minimal signs in one FS* (i.e., grade 1).
- ❑ 1.5 - No disability, minimal signs in more than one FS* (more than 1 FS grade 1).
- ❑ 2.0 - Minimal disability in one FS (one FS grade 2, others 0 or 1).
- ❑ 2.5 - Minimal disability in two FS (two FS grade 2, others 0 or 1).
- ❑ 3.0 - Moderate disability in one FS (one FS grade 3, others 0 or 1) or mild disability in three or four FS (three or four FS grade 2, others 0 or 1) though fully ambulatory.
- ❑ 3.5 - Fully ambulatory but with moderate disability in one FS (one grade 3) and one or two FS grade 2; or two FS grade 3 (others 0 or 1) or five grade 2 (others 0 or 1).
- ❑ 4.0 - Fully ambulatory without aid, self-sufficient, up and about some 12 hours a day despite relatively severe disability consisting of one FS grade 4 (others 0 or 1), or combination of lesser grades exceeding limits of previous steps; able to walk without aid or rest some 500 meters.
- ❑ 4.5 - Fully ambulatory without aid, up and about much of the day, able to work a full day, may otherwise have some limitation of full activity or require minimal assistance; characterized by relatively severe disability usually consisting of one FS grade 4 (others or 1) or combinations of lesser grades exceeding limits of previous steps; able to walk without aid or rest some 300 meters.
- ❑ 5.0 - Ambulatory without aid or rest for about 200 meters; disability severe enough to impair full daily activities (e.g., to work a full day without special provisions); (Usual FS equivalents are one grade 5 alone, others 0 or 1; or combinations of lesser grades usually exceeding specifications for step 4.0).
- ❑ 5.5 - Ambulatory without aid for about 100 meters; disability severe enough to preclude full daily activities; (Usual FS equivalents are one grade 5 alone, others 0 or 1; or combination of lesser grades usually exceeding those for step 4.0).
- ❑ 6.0 - Intermittent or unilateral constant assistance (cane, crutch, brace) required to walk about 100 meters with or without resting; (Usual FS equivalents are combinations with more than two FS grade 3+).

❑ 6.5 - Constant bilateral assistance (canes, crutches, braces) required to walk about 20 meters without resting; (Usual FS equivalents are combinations with more than two FS grade 3+).

❑ 7.0 - Unable to walk beyond approximately 5 meters even with aid, essentially restricted to wheelchair; wheels self in standard wheelchair and transfers alone; up and about in wheelchair some 12 hours a day; (Usual FS equivalents are combinations with more than one FS grade 4+; very rarely pyramidal grade 5 alone).

❑ 7.5 - Unable to take more than a few steps; restricted to wheelchair; may need aid in transfer; wheels self but cannot carry on in standard wheelchair a full day; May require motorized wheelchair; (Usual FS equivalents are combinations with more than one FS grade 4+).

❑ 8.0 - Essentially restricted to bed or chair or perambulated in wheelchair, but may be out of bed itself much of the day; retains many self-care functions; generally has effective use of arms; (Usual FS equivalents are combinations, generally grade 4+ in several systems).

❑ 8.5 - Essentially restricted to bed much of day; has some effective use of arm(s); retains some self-care functions; (Usual FS equivalents are combinations, generally 4+ in several systems).

❑ 9.0 - Helpless bed patient; can communicate and eat; (Usual FS equivalents are combinations, mostly grade 4+).

❑ 9.5 - Totally helpless bed patient; unable to communicate effectively or eat/swallow; (Usual FS equivalents are combinations, almost all grade 4+).

❑ 10.0 - Death due to MS.

---

*Excludes cerebral function grade 1.

Note 1: EDSS steps 1.0 to 4.5 refer to patients who are fully ambulatory and the precise step number is defined by the Functional System score(s). EDSS steps 5.0 to 9.5 are defined by the impairment to ambulation and usual equivalents in Functional Systems scores are provided.

Note 2: EDSS should not change by 1.0 step unless there is a change in the same direction of at least one step in at least one FS.

Sources: Kurtzke JF. Rating neurologic impairment in multiple sclerosis: an expanded disability status scale (EDSS). Neurology. 1983 Nov;33(11):1444-52.

Haber A, LaRocca NG. eds. Minimal Record of Disability for multiple sclerosis. New York: National Multiple Sclerosis Society; 1985.

2. ANNEX B: PET scanners

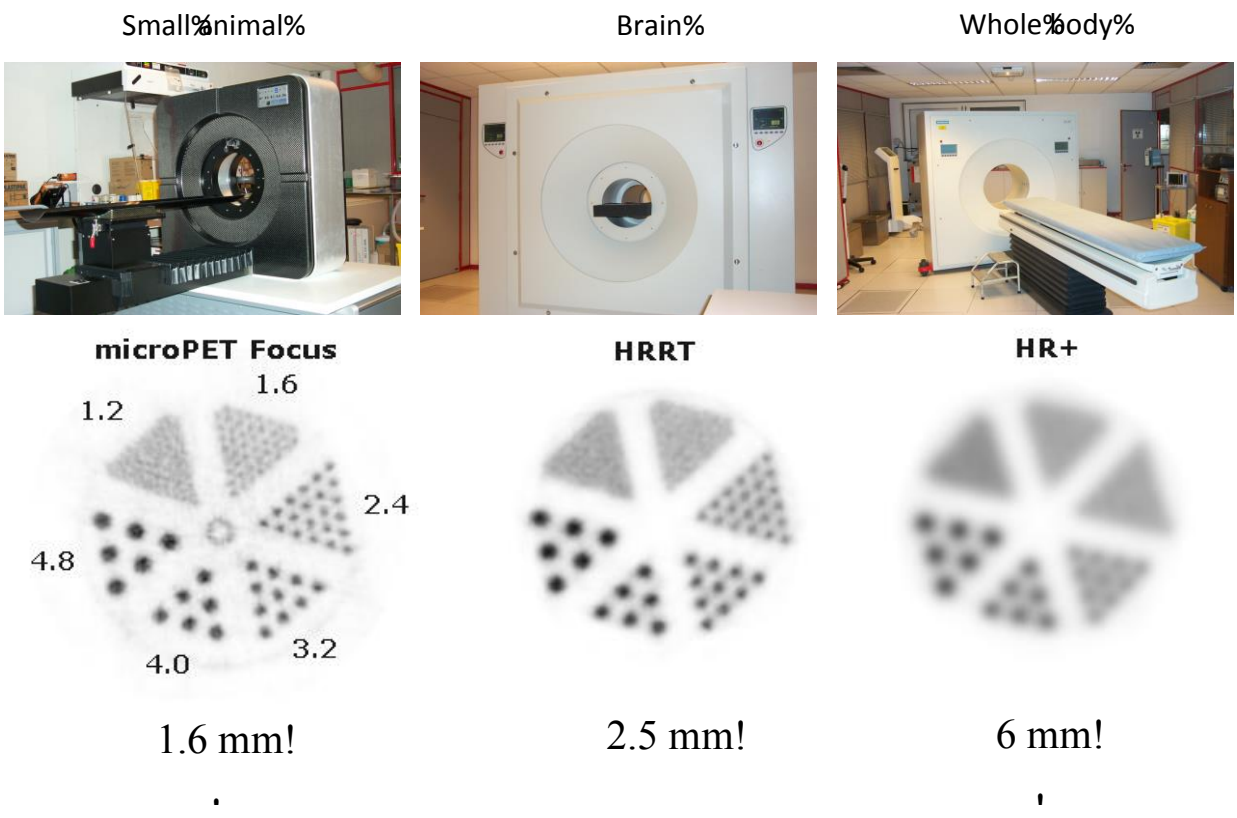

Different types of available PET scanners with corresponding spatial resolution.

3. ANNEX C: DESIKAN-KILLIANI ATLAS

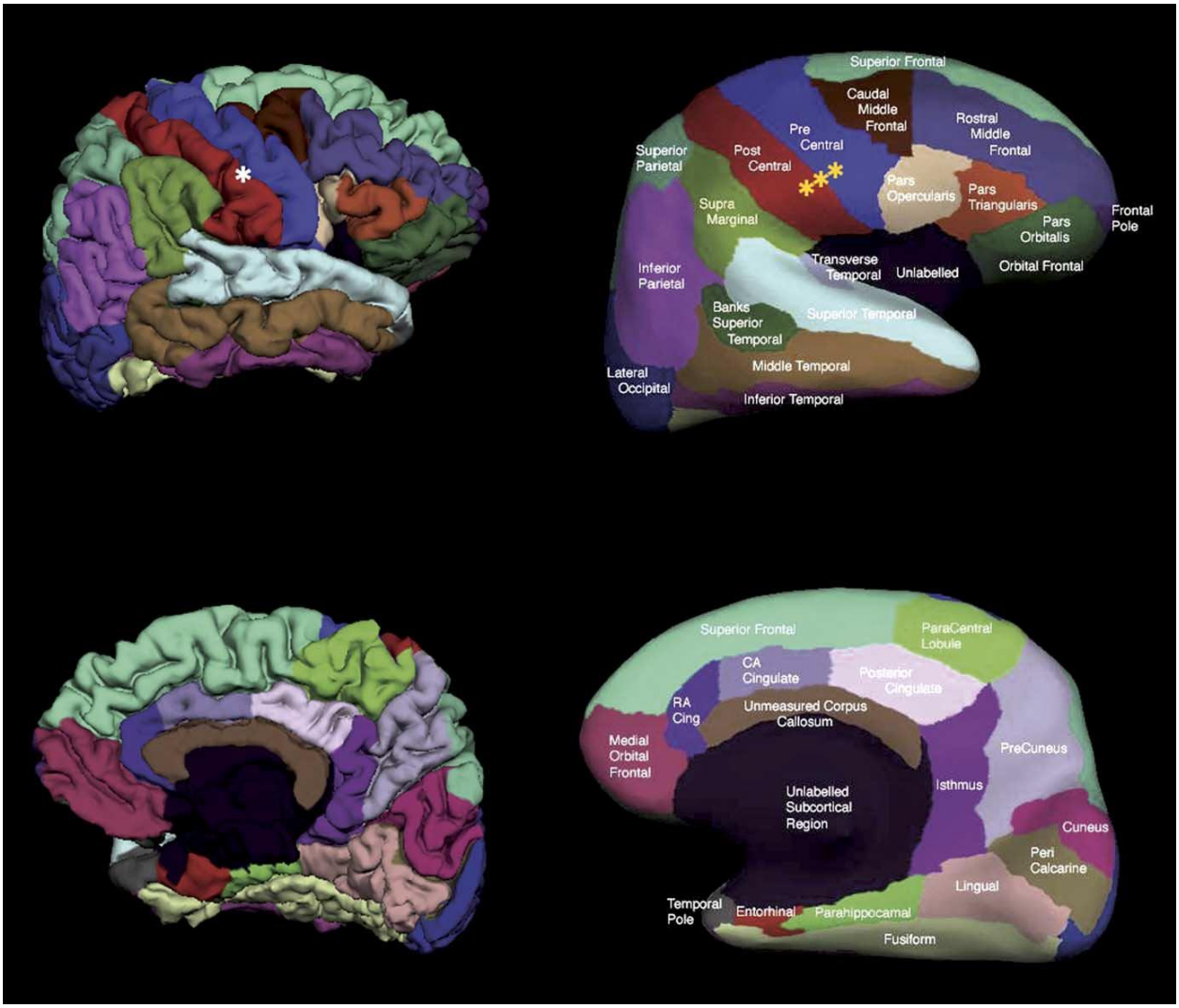

The Desikan-Killiani atlas is an automated labeling system that was developed for subdividing the human cerebral cortex on MRI into gyral based regions of interest (ROIs). It was created using a dataset of 40 MRI scans with 34 manually identified cortical ROIs in each in each individual hemispheres.

Source: An automated labeling system for subdividing the human cerebral cortex on MRI scans into gyral based regions of interest. Rahul S. Desikan, Florent Segonne, Bruce Fischl, Brian T. Quinn, Bradford C. Dickerson, Deborah Blacker, Randy L. Buckner, Anders M. Dale, R. Paul Maguire, Bradley T. Hyman, Marilyn S. Albert, and Ronald J. Killiany. NeuroImage 31 (2006) 968 – 980 [280].

Bibliography

1. Cruveilhier, J., *Anatomie pathologique du corps humain : ou Descriptions, avec figures lithographiâees et coloriâees, des diverses altâerations morbides dont le corps humain est susceptible*. 1829, Paris: Bailliáere.
2. Caswell, R., *Pathological Anatomy: Illustrations of the Elementary Forms of Disease*. 1838.
3. Melcon, M.O., J. Correale, and C.M. Melcon, *Is it time for a new global classification of multiple sclerosis?* J Neurol Sci, 2014. **344**(1-2): p. 171-81.
4. Confavreux, C. and S. Vukusic, *Natural history of multiple sclerosis: a unifying concept*. Brain, 2006. **129**(Pt 3): p. 606-16.
5. Noonan, C.W., et al., *The prevalence of multiple sclerosis in 3 US communities*. Prev Chronic Dis, 2010. **7**(1): p. A12.
6. Koch-Henriksen, N. and P.S. Sorensen, *The changing demographic pattern of multiple sclerosis epidemiology*. Lancet Neurol, 2010. **9**(5): p. 520-32.
7. Munger, K.L., et al., *Serum 25-hydroxyvitamin D levels and risk of multiple sclerosis*. JAMA, 2006. **296**(23): p. 2832-8.
8. Martinelli, V., et al., *Vitamin D levels and risk of multiple sclerosis in patients with clinically isolated syndromes*. Mult Scler, 2014. **20**(2): p. 147-55.
9. Mowry, E.M., et al., *Vitamin D status predicts new brain magnetic resonance imaging activity in multiple sclerosis*. Ann Neurol, 2012. **72**(2): p. 234-40.
10. Riise, T., M.W. Nortvedt, and A. Ascherio, *Smoking is a risk factor for multiple sclerosis*. Neurology, 2003. **61**(8): p. 1122-4.
11. Levin, L.I., et al., *Temporal relationship between elevation of epstein-barr virus antibody titers and initial onset of neurological symptoms in multiple sclerosis*. JAMA, 2005. **293**(20): p. 2496-500.
12. Confavreux, C., et al., *Relapses and progression of disability in multiple sclerosis*. N Engl J Med, 2000. **343**(20): p. 1430-8.
13. Polman, C.H., et al., *Diagnostic criteria for multiple sclerosis: 2010 revisions to the McDonald criteria*. Ann Neurol, 2011. **69**(2): p. 292-302.
14. McDonald, W.I., et al., *Recommended diagnostic criteria for multiple sclerosis: guidelines from the International Panel on the diagnosis of multiple sclerosis*. Ann Neurol, 2001. **50**(1): p. 121-7.
15. Polman, C.H., et al., *Diagnostic criteria for multiple sclerosis: 2005 revisions to the "McDonald Criteria"*. Ann Neurol, 2005. **58**(6): p. 840-6.
16. Bot, J.C., et al., *Spinal cord abnormalities in recently diagnosed MS patients: added value of spinal MRI examination*. Neurology, 2004. **62**(2): p. 226-33.
17. Rovira, A., et al., *Evidence-based guidelines: MAGNIMS consensus guidelines on the use of MRI in multiple sclerosis-clinical implementation in the diagnostic process*. Nat Rev Neurol, 2015. **11**(8): p. 471-82.
18. Kearney, H., D.H. Miller, and O. Ciccarelli, *Spinal cord MRI in multiple sclerosis--diagnostic, prognostic and clinical value*. Nat Rev Neurol, 2015. **11**(6): p. 327-38.

19. Barkhof, F., et al., *Comparison of MRI criteria at first presentation to predict conversion to clinically definite multiple sclerosis.* Brain, 1997. **120 (Pt 11)**: p. 2059-69.
20. Swanton, J.K., et al., *Modification of MRI criteria for multiple sclerosis in patients with clinically isolated syndromes.* J Neurol Neurosurg Psychiatry, 2006. **77**(7): p. 830-3.
21. Lublin, F.D., et al., *Defining the clinical course of multiple sclerosis: the 2013 revisions.* Neurology, 2014. **83**(3): p. 278-86.
22. Granberg, T., et al., *Radiologically isolated syndrome--incidental magnetic resonance imaging findings suggestive of multiple sclerosis, a systematic review.* Mult Scler, 2013. **19**(3): p. 271-80.
23. Okuda, D.T., et al., *Incidental MRI anomalies suggestive of multiple sclerosis: the radiologically isolated syndrome.* Neurology, 2009. **72**(9): p. 800-5.
24. Okuda, D.T., et al., *Radiologically isolated syndrome: 5-year risk for an initial clinical event.* PLoS One, 2014. **9**(3): p. e90509.
25. Brownlee, W.J., et al., *Earlier and more frequent diagnosis of multiple sclerosis using the McDonald criteria.* J Neurol Neurosurg Psychiatry, 2015. **86**(5): p. 584-5.
26. Mowry, E.M., et al., *Clinical predictors of early second event in patients with clinically isolated syndrome.* J Neurol, 2009. **256**(7): p. 1061-6.
27. Feuillet, L., et al., *Early cognitive impairment in patients with clinically isolated syndrome suggestive of multiple sclerosis.* Multiple Sclerosis, 2007. **13**(1): p. 124-127.
28. Zhang, Q., et al., *Relationship between HLA-DRB1 polymorphism and susceptibility or resistance to multiple sclerosis in Caucasians: a meta-analysis of non-family-based studies.* Autoimmun Rev, 2011. **10**(8): p. 474-81.
29. Tintore, M., et al., *Baseline MRI predicts future attacks and disability in clinically isolated syndromes.* Neurology, 2006. **67**(6): p. 968-72.
30. Scalfari, A., et al., *Onset of secondary progressive phase and long-term evolution of multiple sclerosis.* J Neurol Neurosurg Psychiatry, 2014. **85**(1): p. 67-75.
31. Vukusic, S. and C. Confavreux, *Prognostic factors for progression of disability in the secondary progressive phase of multiple sclerosis.* J Neurol Sci, 2003. **206**(2): p. 135-7.
32. Stankoff, B., et al., *Age at onset determines the occurrence of the progressive phase of multiple sclerosis.* Neurology, 2007. **68**(10): p. 779-81.
33. Sormani, M.P., et al., *Surrogate endpoints for EDSS worsening in multiple sclerosis. A meta-analytic approach.* Neurology, 2010. **75**(4): p. 302-9.
34. Kremenchutzky, M., et al., *The natural history of multiple sclerosis: a geographically based study 9: observations on the progressive phase of the disease.* Brain, 2006. **129**(Pt 3): p. 584-94.
35. Scalfari, A., et al., *The natural history of multiple sclerosis: a geographically based study 10: relapses and long-term disability.* Brain, 2010. **133**(Pt 7): p. 1914-29.
36. Tintore, M., et al., *Defining high, medium and low impact prognostic factors for developing multiple sclerosis.* Brain, 2015. **138**(Pt 7): p. 1863-74.

37. Confavreux, C., S. Vukusic, and P. Adeleine, *Early clinical predictors and progression of irreversible disability in multiple sclerosis: an amnesic process.* Brain, 2003. **126**(Pt 4): p. 770-82.
38. Leray, E., et al., *Evidence for a two-stage disability progression in multiple sclerosis.* Brain, 2010. **133**(Pt 7): p. 1900-13.
39. Calabrese, M., et al., *The changing clinical course of multiple sclerosis: a matter of gray matter.* Ann Neurol, 2013. **74**(1): p. 76-83.
40. Castro-Borrero, W., et al., *Current and emerging therapies in multiple sclerosis: a systematic review.* Ther Adv Neurol Disord, 2012. **5**(4): p. 205-20.
41. Kalincik, T., et al., *Defining reliable disability outcomes in multiple sclerosis.* Brain, 2015. **138**(Pt 11): p. 3287-98.
42. Broadley, S.A., et al., *Therapeutic approaches to disease modifying therapy for multiple sclerosis in adults: an Australian and New Zealand perspective: part 1 historical and established therapies. MS Neurology Group of the Australian and New Zealand Association of Neurologists.* J Clin Neurosci, 2014. **21**(11): p. 1835-46.
43. Babbe, H., et al., *Clonal expansions of CD8(+) T cells dominate the T cell infiltrate in active multiple sclerosis lesions as shown by micromanipulation and single cell polymerase chain reaction.* J Exp Med, 2000. **192**(3): p. 393-404.
44. Patani, R., et al., *Remyelination can be extensive in multiple sclerosis despite a long disease course.* Neuropathol Appl Neurobiol, 2007. **33**(3): p. 277-87.
45. Trapp, B.D., et al., *Axonal transection in the lesions of multiple sclerosis.* N Engl J Med, 1998. **338**(5): p. 278-85.
46. Kuhlmann, T., et al., *Acute axonal damage in multiple sclerosis is most extensive in early disease stages and decreases over time.* Brain, 2002. **125**(Pt 10): p. 2202-12.
47. Su, K.G., et al., *Axonal degeneration in multiple sclerosis: the mitochondrial hypothesis.* Curr Neurol Neurosci Rep, 2009. **9**(5): p. 411-7.
48. Barkhof, F., *MRI in multiple sclerosis: correlation with expanded disability status scale (EDSS).* Mult Scler, 1999. **5**(4): p. 283-6.
49. Bar-Zohar, D., et al., *Magnetic resonance imaging metrics and their correlation with clinical outcomes in multiple sclerosis: a review of the literature and future perspectives.* Mult Scler, 2008. **14**(6): p. 719-27.
50. Franklin, R.J., et al., *Neuroprotection and repair in multiple sclerosis.* Nat Rev Neurol, 2012. **8**(11): p. 624-34.
51. Patrikios, P., et al., *Remyelination is extensive in a subset of multiple sclerosis patients.* Brain, 2006. **129**(Pt 12): p. 3165-72.
52. Stankoff, B., et al., *Imaging central nervous system myelin by positron emission tomography in multiple sclerosis using [methyl-(1)(1)C]-2-(4'-methylaminophenyl)- 6-hydroxybenzothiazole.* Ann Neurol, 2011. **69**(4): p. 673-80.
53. Frischer, J.M., et al., *Clinical and pathological insights into the dynamic nature of the white matter multiple sclerosis plaque.* Ann Neurol, 2015. **78**(5): p. 710-21.
54. Frischer, J.M., et al., *The relation between inflammation and neurodegeneration in multiple sclerosis brains.* Brain, 2009. **132**(Pt 5): p. 1175-89.
55. Mahad, D.H., B.D. Trapp, and H. Lassmann, *Pathological mechanisms in progressive multiple sclerosis.* The Lancet Neurology, 2015. **14**(2): p. 183-193.

56. Allen, I.V. and S.R. McKeown, *A histological, histochemical and biochemical study of the macroscopically normal white matter in multiple sclerosis.* J Neurol Sci, 1979. **41**(1): p. 81-91.
57. Seewann, A., et al., *Diffusely abnormal white matter in chronic multiple sclerosis: imaging and histopathologic analysis.* Arch Neurol, 2009. **66**(5): p. 601-9.
58. Kutzelnigg, A., et al., *Cortical demyelination and diffuse white matter injury in multiple sclerosis.* Brain, 2005. **128**(Pt 11): p. 2705-12.
59. Ciccarelli, O., et al., *Pathogenesis of multiple sclerosis: insights from molecular and metabolic imaging.* Lancet Neurol, 2014. **13**(8): p. 807-22.
60. Ajami, B., et al., *Infiltrating monocytes trigger EAE progression, but do not contribute to the resident microglia pool.* Nat Neurosci, 2011. **14**(9): p. 1142-9.
61. Moore, G.R., et al., *Dirty-appearing white matter in multiple sclerosis: preliminary observations of myelin phospholipid and axonal loss.* J Neurol, 2008. **255**(11): p. 1802-11, discussion 1812.
62. Lee, Y., et al., *Oligodendroglia metabolically support axons and contribute to neurodegeneration.* Nature, 2012. **487**(7408): p. 443-8.
63. Funfschilling, U., et al., *Glycolytic oligodendrocytes maintain myelin and long-term axonal integrity.* Nature, 2012. **485**(7399): p. 517-21.
64. Asaf, A., S. Evan, and A. Anat, *Injury to white matter tracts in relapsing-remitting multiple sclerosis: A possible therapeutic window within the first 5 years from onset using diffusion-tensor imaging tract-based spatial statistics.* Neuroimage Clin, 2015. **8**: p. 261-6.
65. Gallo, A., et al., *Diffusion-tensor magnetic resonance imaging detects normal-appearing white matter damage unrelated to short-term disease activity in patients at the earliest clinical stage of multiple sclerosis.* Arch Neurol, 2005. **62**(5): p. 803-8.
66. Vrenken, H., et al., *Diffusely abnormal white matter in progressive multiple sclerosis: in vivo quantitative MR imaging characterization and comparison between disease types.* AJNR Am J Neuroradiol, 2010. **31**(3): p. 541-8.
67. Schmierer, K., et al., *Magnetization transfer ratio and myelin in postmortem multiple sclerosis brain.* Ann Neurol, 2004. **56**(3): p. 407-15.
68. Liu, Z., et al., *Magnetization transfer ratio measures in normal-appearing white matter show periventricular gradient abnormalities in multiple sclerosis.* Brain, 2015. **138**(Pt 5): p. 1239-46.
69. Narayanan, S., et al., *Imaging of axonal damage in multiple sclerosis: spatial distribution of magnetic resonance imaging lesions.* Ann Neurol, 1997. **41**(3): p. 385-91.
70. Haines, J.D., et al., *Multiple sclerosis patient-derived CSF induces transcriptional changes in proliferating oligodendrocyte progenitors.* Mult Scler, 2015.
71. Vidaurre, O.G., et al., *Cerebrospinal fluid ceramides from patients with multiple sclerosis impair neuronal bioenergetics.* Brain, 2014. **137**(Pt 8): p. 2271-86.
72. Narayana, P.A., et al., *Hypoperfusion and T1-hypointense lesions in white matter in multiple sclerosis.* Mult Scler, 2014. **20**(3): p. 365-73.

73. Zaaraoui, W., et al., *Occurrence of neuronal dysfunction during the first 5 years of multiple sclerosis is associated with cognitive deterioration.* J Neurol, 2011. **258**(5): p. 811-9.
74. Deloire, M.S., et al., *Cognitive impairment as marker of diffuse brain abnormalities in early relapsing remitting multiple sclerosis.* J Neurol Neurosurg Psychiatry, 2005. **76**(4): p. 519-26.
75. Park, E., et al., *(11)C-PBR28 imaging in multiple sclerosis patients and healthy controls: test-retest reproducibility and focal visualization of active white matter areas.* Eur J Nucl Med Mol Imaging, 2015. **42**(7): p. 1081-92.
76. Abourbeh, G., et al., *Imaging microglial/macrophage activation in spinal cords of experimental autoimmune encephalomyelitis rats by positron emission tomography using the mitochondrial 18 kDa translocator protein radioligand [(1)(8)F]DPA-714.* J Neurosci, 2012. **32**(17): p. 5728-36.
77. Rissanen, E., et al., *In Vivo Detection of Diffuse Inflammation in Secondary Progressive Multiple Sclerosis Using PET Imaging and the Radioligand (1)(1)C-PK11195.* J Nucl Med, 2014. **55**(6): p. 939-44.
78. Giannetti, P., et al., *Increased PK11195-PET binding in normal-appearing white matter in clinically isolated syndrome.* Brain, 2015. **138**(Pt 1): p. 110-9.
79. Brownell, B. and J.T. Hughes, *The distribution of plaques in the cerebrum in multiple sclerosis.* J Neurol Neurosurg Psychiatry, 1962. **25**: p. 315-20.
80. Gilmore, C.P., et al., *Regional variations in the extent and pattern of grey matter demyelination in multiple sclerosis: a comparison between the cerebral cortex, cerebellar cortex, deep grey matter nuclei and the spinal cord.* J Neurol Neurosurg Psychiatry, 2009. **80**(2): p. 182-7.
81. Vercellino, M., et al., *Demyelination, inflammation, and neurodegeneration in multiple sclerosis deep gray matter.* J Neuropathol Exp Neurol, 2009. **68**(5): p. 489-502.
82. Dutta, R., et al., *Hippocampal demyelination and memory dysfunction are associated with increased levels of the neuronal microRNA miR-124 and reduced AMPA receptors.* Ann Neurol, 2013. **73**(5): p. 637-45.
83. Peterson, J.W., et al., *Transected neurites, apoptotic neurons, and reduced inflammation in cortical multiple sclerosis lesions.* Annals of Neurology, 2001. **50**(3): p. 389-400.
84. Bo, L., et al., *Intracortical multiple sclerosis lesions are not associated with increased lymphocyte infiltration.* Mult Scler, 2003. **9**(4): p. 323-31.
85. Calabrese, M., et al., *Exploring the origins of grey matter damage in multiple sclerosis.* Nat Rev Neurosci, 2015. **16**(3): p. 147-58.
86. Lucchinetti, C.F., et al., *Inflammatory cortical demyelination in early multiple sclerosis.* N Engl J Med, 2011. **365**(23): p. 2188-97.
87. Magliozzi, R., et al., *Meningeal B-cell follicles in secondary progressive multiple sclerosis associate with early onset of disease and severe cortical pathology.* Brain, 2007. **130**(Pt 4): p. 1089-104.
88. Seewann, A., et al., *Postmortem verification of MS cortical lesion detection with 3D DIR.* Neurology, 2012. **78**(5): p. 302-8.
89. Nelson, F., et al., *Improved identification of intracortical lesions in multiple sclerosis with phase-sensitive inversion recovery in combination with fast*

double inversion recovery MR imaging. AJNR Am J Neuroradiol, 2007. **28**(9): p. 1645-9.
90. Nielsen, A.S., et al., *Focal cortical lesion detection in multiple sclerosis: 3 Tesla DIR versus 7 Tesla FLASH-T2*. J Magn Reson Imaging, 2012. **35**(3): p. 537-42.
91. Pitt, D., et al., *Imaging cortical lesions in multiple sclerosis with ultra-high-field magnetic resonance imaging*. Arch Neurol, 2010. **67**(7): p. 812-8.
92. Favaretto, A., et al., *The Parallel Analysis of Phase Sensitive Inversion Recovery (PSIR) and Double Inversion Recovery (DIR) Images Significantly Improves the Detection of Cortical Lesions in Multiple Sclerosis (MS) since Clinical Onset*. PLoS One, 2015. **10**(5): p. e0127805.
93. Jonkman, L.E., et al., *Ultra-High-Field MRI Visualization of Cortical Multiple Sclerosis Lesions with T2 and T2*: A Postmortem MRI and Histopathology Study*. AJNR Am J Neuroradiol, 2015.
94. Yao, B., et al., *7 Tesla magnetic resonance imaging to detect cortical pathology in multiple sclerosis*. PLoS One, 2014. **9**(10): p. e108863.
95. Seewann, A., et al., *Imaging the tip of the iceberg: visualization of cortical lesions in multiple sclerosis*. Mult Scler, 2011. **17**(10): p. 1202-10.
96. Filippi, M., et al., *Intracortical lesions: relevance for new MRI diagnostic criteria for multiple sclerosis*. Neurology, 2010. **75**(22): p. 1988-94.
97. Geurts, J.J., et al., *Consensus recommendations for MS cortical lesion scoring using double inversion recovery MRI*. Neurology, 2011. **76**(5): p. 418-24.
98. Harrison, D.M., et al., *Association of Cortical Lesion Burden on 7-T Magnetic Resonance Imaging With Cognition and Disability in Multiple Sclerosis*. JAMA Neurol, 2015. **72**(9): p. 1004-12.
99. Favaretto, A., et al., *MRI-detectable cortical lesions in the cerebellum and their clinical relevance in multiple sclerosis*. Mult Scler, 2015.
100. Harrison, D.M., et al., *Thalamic lesions in multiple sclerosis by 7T MRI: Clinical implications and relationship to cortical pathology*. Mult Scler, 2015. **21**(9): p. 1139-50.
101. Papadopoulou, A., et al., *Contribution of cortical and white matter lesions to cognitive impairment in multiple sclerosis*. Mult Scler, 2013. **19**(10): p. 1290-6.
102. Calabrese, M., et al., *Low degree of cortical pathology is associated with benign course of multiple sclerosis*. Mult Scler, 2013. **19**(7): p. 904-11.
103. Nelson, F., et al., *Intracortical lesions by 3T magnetic resonance imaging and correlation with cognitive impairment in multiple sclerosis*. Mult Scler, 2011. **17**(9): p. 1122-9.
104. Mike, A., et al., *Identification and clinical impact of multiple sclerosis cortical lesions as assessed by routine 3T MR imaging*. AJNR Am J Neuroradiol, 2011. **32**(3): p. 515-21.
105. Wegner, C., et al., *Neocortical neuronal, synaptic, and glial loss in multiple sclerosis*. Neurology, 2006. **67**(6): p. 960-7.
106. Vercellino, M., et al., *Grey matter pathology in multiple sclerosis*. J Neuropathol Exp Neurol, 2005. **64**(12): p. 1101-7.
107. Popescu, V., et al., *What drives MRI-measured cortical atrophy in multiple sclerosis?* Mult Scler, 2015. **21**(10): p. 1280-90.

108. Klaver, R., et al., *Neuronal and axonal loss in normal-appearing gray matter and subpial lesions in multiple sclerosis.* J Neuropathol Exp Neurol, 2015. **74**(5): p. 453-8.
109. Dutta, R., et al., *Demyelination causes synaptic alterations in hippocampi from multiple sclerosis patients.* Ann Neurol, 2011. **69**(3): p. 445-54.
110. Cifelli, A., et al., *Thalamic neurodegeneration in multiple sclerosis.* Ann Neurol, 2002. **52**(5): p. 650-3.
111. Papadopoulos, D., et al., *Substantial archaeocortical atrophy and neuronal loss in multiple sclerosis.* Brain Pathol, 2009. **19**(2): p. 238-53.
112. Kolasinski, J., et al., *A combined post-mortem magnetic resonance imaging and quantitative histological study of multiple sclerosis pathology.* Brain, 2012. **135**(Pt 10): p. 2938-51.
113. Magliozzi, R., et al., *A Gradient of neuronal loss and meningeal inflammation in multiple sclerosis.* Ann Neurol, 2010. **68**(4): p. 477-93.
114. De Stefano, N., et al., *Evidence of early cortical atrophy in MS: relevance to white matter changes and disability.* Neurology, 2003. **60**(7): p. 1157-62.
115. Sailer, M., et al., *Focal thinning of the cerebral cortex in multiple sclerosis.* Brain, 2003. **126**(Pt 8): p. 1734-44.
116. Jehna, M., et al., *Periventricular lesions correlate with cortical thinning in multiple sclerosis.* Ann Neurol, 2015. **78**(4): p. 530-9.
117. Bergsland, N., et al., *Corticospinal tract integrity is related to primary motor cortex thinning in relapsing-remitting multiple sclerosis.* Mult Scler, 2015.
118. Howell, O.W., et al., *Meningeal inflammation is widespread and linked to cortical pathology in multiple sclerosis.* Brain, 2011. **134**(Pt 9): p. 2755-71.
119. Androdias, G., et al., *Meningeal T cells associate with diffuse axonal loss in multiple sclerosis spinal cords.* Ann Neurol, 2010. **68**(4): p. 465-76.
120. Fischer, M.T., et al., *Disease-specific molecular events in cortical multiple sclerosis lesions.* Brain, 2013. **136**(Pt 6): p. 1799-815.
121. Lassmann, H., *Multiple sclerosis: Lessons from molecular neuropathology.* Exp Neurol, 2013.
122. Witte, M.E., et al., *Mitochondrial dysfunction contributes to neurodegeneration in multiple sclerosis.* Trends Mol Med, 2014. **20**(3): p. 179-87.
123. Dutta, R., et al., *Mitochondrial dysfunction as a cause of axonal degeneration in multiple sclerosis patients.* Ann Neurol, 2006. **59**(3): p. 478-89.
124. Campbell, G.R., et al., *Mitochondrial DNA deletions and neurodegeneration in multiple sclerosis.* Ann Neurol, 2011. **69**(3): p. 481-92.
125. Trapp, B.D. and P.K. Stys, *Virtual hypoxia and chronic necrosis of demyelinated axons in multiple sclerosis.* Lancet Neurol, 2009. **8**(3): p. 280-91.
126. Stys, P.K., *Axonal degeneration in multiple sclerosis: is it time for neuroprotective strategies?* Ann Neurol, 2004. **55**(5): p. 601-3.
127. Waxman, S.G., *Mechanisms of disease: sodium channels and neuroprotection in multiple sclerosis-current status.* Nat Clin Pract Neurol, 2008. **4**(3): p. 159-69.
128. Haider, L., *Inflammation, Iron, Energy Failure, and Oxidative Stress in the Pathogenesis of Multiple Sclerosis.* Oxid Med Cell Longev, 2015. **2015**: p. 725370.
129. Hametner, S., et al., *Iron and neurodegeneration in the multiple sclerosis brain.* Ann Neurol, 2013. **74**(6): p. 848-61.

130. D'Haeseleer, M., et al., *Cerebral hypoperfusion: a new pathophysiologic concept in multiple sclerosis?* J Cereb Blood Flow Metab, 2015. **35**(9): p. 1406-10.
131. Debernard, L., et al., *Reduced grey matter perfusion without volume loss in early relapsing-remitting multiple sclerosis.* J Neurol Neurosurg Psychiatry, 2014. **85**(5): p. 544-51.
132. Steen, C., et al., *Cerebral white matter blood flow and energy metabolism in multiple sclerosis.* Mult Scler, 2013. **19**(10): p. 1282-9.
133. Lucchinetti, C., et al., *Heterogeneity of multiple sclerosis lesions: implications for the pathogenesis of demyelination.* Ann Neurol, 2000. **47**(6): p. 707-17.
134. Aviv, R.I., et al., *Decreased frontal lobe gray matter perfusion in cognitively impaired patients with secondary-progressive multiple sclerosis detected by the bookend technique.* AJNR Am J Neuroradiol, 2012. **33**(9): p. 1779-85.
135. Francis, P.L., et al., *Robust perfusion deficits in cognitively impaired patients with secondary-progressive multiple sclerosis.* AJNR Am J Neuroradiol, 2013. **34**(1): p. 62-7.
136. Zambonin, J., et al., *Identification and investigation of mitochondria lacking cytochrome c oxidase activity in axons.* J Neurosci Methods, 2010. **192**(1): p. 115-20.
137. Muhlert, N., et al., *Memory in multiple sclerosis is linked to glutamate concentration in grey matter regions.* J Neurol Neurosurg Psychiatry, 2014. **85**(8): p. 833-9.
138. Azevedo, C.J., et al., *In vivo evidence of glutamate toxicity in multiple sclerosis.* Ann Neurol, 2014. **76**(2): p. 269-78.
139. Inglese, M., *MRI measures of neuroprotection and repair in multiple sclerosis.* Journal of the Neurological Sciences, 2011. **311**: p. S16-S23.
140. Vigeveno, R.M., et al., *Shifting imaging targets in multiple sclerosis: from inflammation to neurodegeneration.* J Magn Reson Imaging, 2012. **36**(1): p. 1-19.
141. Chard, D.T., et al., *Reducing the impact of white matter lesions on automated measures of brain gray and white matter volumes.* J Magn Reson Imaging, 2010. **32**(1): p. 223-8.
142. Chard, D. and D. Miller, *Grey matter pathology in clinically early multiple sclerosis: evidence from magnetic resonance imaging.* J Neurol Sci, 2009. **282**(1-2): p. 5-11.
143. Rocca, M.A., et al., *Clinically Isolated Syndrome Suggestive of Multiple Sclerosis: Dynamic Patterns of Gray and White Matter Changes-A 2-year MR Imaging Study.* Radiology, 2015: p. 150532.
144. Perez-Miralles, F., et al., *Clinical impact of early brain atrophy in clinically isolated syndromes.* Mult Scler, 2013. **19**(14): p. 1878-86.
145. Audoin, B., et al., *Atrophy mainly affects the limbic system and the deep grey matter at the first stage of multiple sclerosis.* J Neurol Neurosurg Psychiatry, 2010. **81**(6): p. 690-5.
146. Calabrese, M., et al., *Regional Distribution and Evolution of Gray Matter Damage in Different Populations of Multiple Sclerosis Patients.* PLoS One, 2015. **10**(8): p. e0135428.
147. Fisher, E., et al., *Gray matter atrophy in multiple sclerosis: a longitudinal study.* Ann Neurol, 2008. **64**(3): p. 255-65.

148. Calabrese, M., et al., *The predictive value of gray matter atrophy in clinically isolated syndromes.* Neurology, 2011. **77**(3): p. 257-63.
149. Roosendaal, S.D., et al., *Grey matter volume in a large cohort of MS patients: relation to MRI parameters and disability.* Mult Scler, 2011. **17**(9): p. 1098-106.
150. Jacobsen, C., et al., *Brain atrophy and disability progression in multiple sclerosis patients: a 10-year follow-up study.* J Neurol Neurosurg Psychiatry, 2014. **85**(10): p. 1109-15.
151. Lavorgna, L., et al., *Clinical and magnetic resonance imaging predictors of disease progression in multiple sclerosis: a nine-year follow-up study.* Mult Scler, 2014. **20**(2): p. 220-6.
152. Hofstetter, L., et al., *Progression in disability and regional grey matter atrophy in relapsing-remitting multiple sclerosis.* Mult Scler, 2014. **20**(2): p. 202-13.
153. Ontaneda, D., R.J. Fox, and J. Chataway, *Clinical trials in progressive multiple sclerosis: lessons learned and future perspectives.* The Lancet Neurology, 2015. **14**(2): p. 208-223.
154. Carassiti, D., et al., *Cortical atrophy predicts neuronal loss in MS: a post-mortem study using unbiased sampling*. 2015: ECTRIMS, Barcelona.
155. Centonze, D., et al., *Inflammation triggers synaptic alteration and degeneration in experimental autoimmune encephalomyelitis.* J Neurosci, 2009. **29**(11): p. 3442-52.
156. Neves, G., S.F. Cooke, and T.V. Bliss, *Synaptic plasticity, memory and the hippocampus: a neural network approach to causality.* Nat Rev Neurosci, 2008. **9**(1): p. 65-75.
157. Michailidou, I., et al., *Complement C1q-C3-associated synaptic changes in multiple sclerosis hippocampus.* Ann Neurol, 2015. **77**(6): p. 1007-26.
158. Novkovic, T., et al., *Hippocampal function is compromised in an animal model of multiple sclerosis.* Neuroscience, 2015.
159. Nakamura, K., et al., *Correlation between brain volume change and T2 relaxation time induced by dehydration and rehydration: implications for monitoring atrophy in clinical studies.* Neuroimage Clin, 2014. **6**: p. 166-70.
160. Duning, T., et al., *Dehydration confounds the assessment of brain atrophy.* Neurology, 2005. **64**(3): p. 548-50.
161. De Stefano, N., et al., *Establishing pathological cut-offs of brain atrophy rates in multiple sclerosis.* J Neurol Neurosurg Psychiatry, 2015.
162. De Stefano, N. and D.L. Arnold, *Towards a better understanding of pseudoatrophy in the brain of multiple sclerosis patients.* Mult Scler, 2015. **21**(6): p. 675-6.
163. Alexander, A.L., et al., *Diffusion tensor imaging of the brain.* Neurotherapeutics, 2007. **4**(3): p. 316-29.
164. Sbardella, E., et al., *DTI Measurements in Multiple Sclerosis: Evaluation of Brain Damage and Clinical Implications.* Mult Scler Int, 2013. **2013**: p. 671730.
165. Hasan, K.M., et al., *Caudate nuclei volume, diffusion tensor metrics, and T(2) relaxation in healthy adults and relapsing-remitting multiple sclerosis patients: implications for understanding gray matter degeneration.* J Magn Reson Imaging, 2009. **29**(1): p. 70-7.
166. Calabrese, M., et al., *Cortical diffusion-tensor imaging abnormalities in multiple sclerosis: a 3-year longitudinal study.* Radiology, 2011. **261**(3): p. 891-8.

167. Yaldizli, O., et al., *Characteristics of lesional and extra-lesional cortical grey matter in relapsing-remitting and secondary progressive multiple sclerosis: A magnetisation transfer and diffusion tensor imaging study*. Mult Scler, 2015.
168. Vrenken, H., et al., *Altered diffusion tensor in multiple sclerosis normal-appearing brain tissue: cortical diffusion changes seem related to clinical deterioration*. J Magn Reson Imaging, 2006. **23**(5): p. 628-36.
169. Cappellani, R., et al., *Diffusion tensor MRI alterations of subcortical deep gray matter in clinically isolated syndrome*. J Neurol Sci, 2014. **338**(1-2): p. 128-34.
170. Bozzali, M., et al., *Quantification of brain gray matter damage in different MS phenotypes by use of diffusion tensor MR imaging*. AJNR Am J Neuroradiol, 2002. **23**(6): p. 985-8.
171. Rovaris, M., et al., *Grey matter damage predicts the evolution of primary progressive multiple sclerosis at 5 years*. Brain, 2006. **129**(Pt 10): p. 2628-34.
172. Mottershead, J.P., et al., *High field MRI correlates of myelin content and axonal density in multiple sclerosis--a post-mortem study of the spinal cord*. J Neurol, 2003. **250**(11): p. 1293-301.
173. Song, S.K., et al., *Dysmyelination revealed through MRI as increased radial (but unchanged axial) diffusion of water*. Neuroimage, 2002. **17**(3): p. 1429-36.
174. Wheeler-Kingshott, C.A. and M. Cercignani, *About "axial" and "radial" diffusivities*. Magn Reson Med, 2009. **61**(5): p. 1255-60.
175. Wang, Y., et al., *Differentiation and quantification of inflammation, demyelination and axon injury or loss in multiple sclerosis*. Brain, 2015. **138**(Pt 5): p. 1223-38.
176. Nazeri, A., et al., *Functional consequences of neurite orientation dispersion and density in humans across the adult lifespan*. J Neurosci, 2015. **35**(4): p. 1753-62.
177. Bodini, B., et al., *A novel approach with "skeletonised MTR" measures tract-specific microstructural changes in early primary-progressive MS*. Hum Brain Mapp, 2014. **35**(2): p. 723-33.
178. Moll, N.M., et al., *Multiple sclerosis normal-appearing white matter: pathology-imaging correlations*. Ann Neurol, 2011. **70**(5): p. 764-73.
179. Harrison, D.M., et al., *Tract-specific quantitative MRI better correlates with disability than conventional MRI in multiple sclerosis*. J Neurol, 2013. **260**(2): p. 397-406.
180. Crespy, L., et al., *Prevalence of grey matter pathology in early multiple sclerosis assessed by magnetization transfer ratio imaging*. PLoS One, 2011. **6**(9): p. e24969.
181. Filippi, M., et al., *Gray matter damage predicts the accumulation of disability 13 years later in MS*. Neurology, 2013. **81**(20): p. 1759-67.
182. Mallik, S., et al., *Regional patterns of grey matter atrophy and magnetisation transfer ratio abnormalities in multiple sclerosis clinical subgroups: a voxel-based analysis study*. Mult Scler, 2015. **21**(4): p. 423-32.
183. Khaleeli, Z., et al., *Localized grey matter damage in early primary progressive multiple sclerosis contributes to disability*. Neuroimage, 2007. **37**(1): p. 253-61.
184. Fjaer, S., et al., *Deep gray matter demyelination detected by magnetization transfer ratio in the cuprizone model*. PLoS One, 2013. **8**(12): p. e84162.
185. Chen, J.T., et al., *Clinically feasible MTR is sensitive to cortical demyelination in MS*. Neurology, 2013. **80**(3): p. 246-52.

186. Derakhshan, M., et al., *Surface-based analysis reveals regions of reduced cortical magnetization transfer ratio in patients with multiple sclerosis: A proposed method for imaging subpial demyelination.* Hum Brain Mapp, 2014. **35**(7): p. 3402-13.
187. Moffett, J.R., et al., *N-Acetylaspartate in the CNS: from neurodiagnostics to neurobiology.* Prog Neurobiol, 2007. **81**(2): p. 89-131.
188. Patel, T.B. and J.B. Clark, *Synthesis of N-acetyl-L-aspartate by rat brain mitochondria and its involvement in mitochondrial/cytosolic carbon transport.* Biochem J, 1979. **184**(3): p. 539-46.
189. Pokryszko-Dragan, A., et al., *Magnetic resonance spectroscopy findings as related to fatigue and cognitive performance in multiple sclerosis patients with mild disability.* J Neurol Sci, 2014. **339**(1-2): p. 35-40.
190. Wylezinska, M., et al., *Thalamic neurodegeneration in relapsing-remitting multiple sclerosis.* Neurology, 2003. **60**(12): p. 1949-54.
191. Geurts, J.J., et al., *MR spectroscopic evidence for thalamic and hippocampal, but not cortical, damage in multiple sclerosis.* Magn Reson Med, 2006. **55**(3): p. 478-83.
192. Chard, D.T., et al., *Brain metabolite changes in cortical grey and normal-appearing white matter in clinically early relapsing-remitting multiple sclerosis.* Brain, 2002. **125**(Pt 10): p. 2342-52.
193. Sharma, R., P.A. Narayana, and J.S. Wolinsky, *Grey matter abnormalities in multiple sclerosis: proton magnetic resonance spectroscopic imaging.* Mult Scler, 2001. **7**(4): p. 221-6.
194. Bjartmar, C., et al., *Neurological disability correlates with spinal cord axonal loss and reduced N-acetyl aspartate in chronic multiple sclerosis patients.* Ann Neurol, 2000. **48**(6): p. 893-901.
195. Sokoloff, L., *Localization of functional activity in the central nervous system by measurement of glucose utilization with radioactive deoxyglucose.* J Cereb Blood Flow Metab, 1981. **1**(1): p. 7-36.
196. Sokoloff, L., *Relationships among local functional activity, energy metabolism, and blood flow in the central nervous system.* Fed Proc, 1981. **40**(8): p. 2311-6.
197. Pozzilli, C., et al., *Relationship between corpus callosum atrophy and cerebral metabolic asymmetries in multiple sclerosis.* J Neurol Sci, 1992. **112**(1-2): p. 51-7.
198. Bakshi, R., et al., *High-resolution fluorodeoxyglucose positron emission tomography shows both global and regional cerebral hypometabolism in multiple sclerosis.* J Neuroimaging, 1998. **8**(4): p. 228-34.
199. Blinkenberg, M., et al., *A longitudinal study of cerebral glucose metabolism, MRI, and disability in patients with MS.* Neurology, 1999. **53**(1): p. 149-53.
200. Sorensen, P.S., et al., *The relationship between MRI and PET changes and cognitive disturbances in MS.* J Neurol Sci, 2006. **245**(1-2): p. 99-102.
201. Derache, N., et al., *Reduced thalamic and cerebellar rest metabolism in relapsing-remitting multiple sclerosis, a positron emission tomography study: correlations to lesion load.* J Neurol Sci, 2006. **245**(1-2): p. 103-9.
202. Radu, C.G., et al., *Positron emission tomography with computed tomography imaging of neuroinflammation in experimental autoimmune encephalomyelitis.* Proc Natl Acad Sci U S A, 2007. **104**(6): p. 1937-42.

203. Buck, D., et al., *18F-FDG PET detects inflammatory infiltrates in spinal cord experimental autoimmune encephalomyelitis lesions.* J Nucl Med, 2012. **53**(8): p. 1269-76.
204. Fritschy, J.M. and P. Panzanelli, *GABAA receptors and plasticity of inhibitory neurotransmission in the central nervous system.* Eur J Neurosci, 2014. **39**(11): p. 1845-65.
205. Koepp, M.J., et al., *In vivo [11C]flumazenil-PET correlates with ex vivo [3H]flumazenil autoradiography in hippocampal sclerosis.* Ann Neurol, 1998. **43**(5): p. 618-26.
206. Andersson, J.D. and C. Halldin, *PET radioligands targeting the brain GABAA /benzodiazepine receptor complex.* J Labelled Comp Radiopharm, 2013. **56**(3-4): p. 196-206.
207. Hammers, A., *Flumazenil positron emission tomography and other ligands for functional imaging.* Neuroimaging Clin N Am, 2004. **14**(3): p. 537-51.
208. Heiss, W.D., et al., *Early [(11)C]Flumazenil/H(2)O positron emission tomography predicts irreversible ischemic cortical damage in stroke patients receiving acute thrombolytic therapy.* Stroke, 2000. **31**(2): p. 366-9.
209. Heiss, W.D., et al., *Penumbral probability thresholds of cortical flumazenil binding and blood flow predicting tissue outcome in patients with cerebral ischaemia.* Brain, 2001. **124**(Pt 1): p. 20-9.
210. Pascual, B., et al., *Decreased carbon-11-flumazenil binding in early Alzheimer's disease.* Brain, 2012. **135**(Pt 9): p. 2817-25.
211. Klumpers, U.M., et al., *Reduced parahippocampal and lateral temporal GABAA-[11C]flumazenil binding in major depression: preliminary results.* Eur J Nucl Med Mol Imaging, 2010. **37**(3): p. 565-74.
212. Pinborg, L.H., et al., *Benzodiazepine receptor quantification in Huntington's disease with [(123)I]omazenil and SPECT.* J Neurol Neurosurg Psychiatry, 2001. **70**(5): p. 657-61.
213. Rheims, S., J. Jung, and P. Ryvlin, *Combination of PET and Magnetoencephalography in the Presurgical Assessment of MRI-Negative Epilepsy.* Front Neurol, 2013. **4**: p. 188.
214. Lammertsma, A.A. and S.P. Hume, *Simplified reference tissue model for PET receptor studies.* Neuroimage, 1996. **4**(3 Pt 1): p. 153-8.
215. Delforge, J., et al., *Quantification of benzodiazepine receptors in human brain using PET, [11C]flumazenil, and a single-experiment protocol.* J Cereb Blood Flow Metab, 1995. **15**(2): p. 284-300.
216. Delforge, J., et al., *Quantitation of benzodiazepine receptors in human brain using the partial saturation method.* J Nucl Med, 1996. **37**(1): p. 5-11.
217. Delforge, J., et al., *Parametric images of benzodiazepine receptor concentration using a partial-saturation injection.* J Cereb Blood Flow Metab, 1997. **17**(3): p. 343-55.
218. Rey, A., *L'examen psychologique dans les cas d'encephalopathie traumatique.* Archives de Psychologie, 1941. **28**: p. 215-285.
219. Osterrieth, P.A., *Filetest de copie d'une figure complex: contribution a l'etude de la perception et de la memoire.* Archives de Psychologie, 1944. **30**: p. 206-56.
220. Spreen, O. and E. Strauss, *A compendium of neuropsychological tests: administration, norms, and commentary.* Oxford University Press, 1998.

221. Maziere, M., et al., *[In vivo study of benzodiazepine receptors using positron emission tomography].* Encephale, 1983. **9**(4 Suppl 2): p. 151B-160B.
222. Sureau, F.C., et al., *Impact of image-space resolution modeling for studies with the high-resolution research tomograph.* J Nucl Med, 2008. **49**(6): p. 1000-8.
223. Dale, A.M., B. Fischl, and M.I. Sereno, *Cortical surface-based analysis. I. Segmentation and surface reconstruction.* Neuroimage, 1999. **9**(2): p. 179-94.
224. Fischl, B. and A.M. Dale, *Measuring the thickness of the human cerebral cortex from magnetic resonance images.* Proc Natl Acad Sci U S A, 2000. **97**(20): p. 11050-5.
225. Fischl, B., et al., *Whole brain segmentation: automated labeling of neuroanatomical structures in the human brain.* Neuron, 2002. **33**(3): p. 341-55.
226. Fischl, B., et al., *Automatically parcellating the human cerebral cortex.* Cereb Cortex, 2004. **14**(1): p. 11-22.
227. Greve, D.N. and B. Fischl, *Accurate and robust brain image alignment using boundary-based registration.* Neuroimage, 2009. **48**(1): p. 63-72.
228. Greve, D.N., et al., *Cortical surface-based analysis reduces bias and variance in kinetic modeling of brain PET data.* Neuroimage, 2014. **92**: p. 225-36.
229. Jacob, T.C., S.J. Moss, and R. Jurd, *GABA(A) receptor trafficking and its role in the dynamic modulation of neuronal inhibition.* Nat Rev Neurosci, 2008. **9**(5): p. 331-43.
230. Rossi, S., et al., *Impaired striatal GABA transmission in experimental autoimmune encephalomyelitis.* Brain Behav Immun, 2011. **25**(5): p. 947-56.
231. Ziehn, M.O., et al., *Hippocampal CA1 atrophy and synaptic loss during experimental autoimmune encephalomyelitis, EAE.* Lab Invest, 2010. **90**(5): p. 774-86.
232. Cid, M.P., et al., *Participation of the GABAergic system on the glutamate release of frontal cortex synaptosomes from Wistar rats with experimental autoimmune encephalomyelitis.* Neuroscience, 2011. **189**: p. 337-44.
233. Cawley, N., et al., *Reduced gamma-aminobutyric acid concentration is associated with physical disability in progressive multiple sclerosis.* Brain, 2015. **138**(Pt 9): p. 2584-95.
234. Mandolesi, G., et al., *Interleukin-1beta alters glutamate transmission at purkinje cell synapses in a mouse model of multiple sclerosis.* J Neurosci, 2013. **33**(29): p. 12105-21.
235. Vercellino, M., et al., *Altered glutamate reuptake in relapsing-remitting and secondary progressive multiple sclerosis cortex: correlation with microglia infiltration, demyelination, and neuronal and synaptic damage.* J Neuropathol Exp Neurol, 2007. **66**(8): p. 732-9.
236. Fisniku, L.K., et al., *Gray matter atrophy is related to long-term disability in multiple sclerosis.* Ann Neurol, 2008. **64**(3): p. 247-54.
237. Chen, J.T., et al., *Relating neocortical pathology to disability progression in multiple sclerosis using MRI.* Neuroimage, 2004. **23**(3): p. 1168-75.
238. Charil, A., et al., *Focal cortical atrophy in multiple sclerosis: relation to lesion load and disability.* Neuroimage, 2007. **34**(2): p. 509-17.
239. Narayana, P.A., et al., *Regional cortical thickness in relapsing remitting multiple sclerosis: A multi-center study.* Neuroimage Clin, 2012. **2**: p. 120-31.

240. la Fougere, C., et al., *Where in-vivo imaging meets cytoarchitectonics: the relationship between cortical thickness and neuronal density measured with high-resolution [18F]flumazenil-PET.* Neuroimage, 2011. **56**(3): p. 951-60.
241. Chiaravalloti, N.D. and J. DeLuca, *Cognitive impairment in multiple sclerosis.* Lancet Neurol, 2008. **7**(12): p. 1139-51.
242. Amato, M.P., V. Zipoli, and E. Portaccio, *Multiple sclerosis-related cognitive changes: a review of cross-sectional and longitudinal studies.* J Neurol Sci, 2006. **245**(1-2): p. 41-6.
243. Louapre, C., et al., *Brain networks disconnection in early multiple sclerosis cognitive deficits: An anatomofunctional study.* Hum Brain Mapp, 2014.
244. Calabrese, M., et al., *Cortical pathology and cognitive impairment in multiple sclerosis.* Expert Rev Neurother, 2011. **11**(3): p. 425-32.
245. Blinkenberg, M., et al., *Cerebral metabolism, magnetic resonance spectroscopy and cognitive dysfunction in early multiple sclerosis: an exploratory study.* Neurol Res, 2012. **34**(1): p. 52-8.
246. Mathiesen, H.K., et al., *Correlation of global N-acetyl aspartate with cognitive impairment in multiple sclerosis.* Arch Neurol, 2006. **63**(4): p. 533-6.
247. Forn, C., et al., *Cortical reorganization during PASAT task in MS patients with preserved working memory functions.* Neuroimage, 2006. **31**(2): p. 686-91.
248. Audoin, B., et al., *Compensatory cortical activation observed by fMRI during a cognitive task at the earliest stage of MS.* Hum Brain Mapp, 2003. **20**(2): p. 51-8.
249. Leech, R. and D.J. Sharp, *The role of the posterior cingulate cortex in cognition and disease.* Brain, 2014. **137**(Pt 1): p. 12-32.
250. Rocca, M.A., et al., *Large-scale neuronal network dysfunction in relapsing-remitting multiple sclerosis.* Neurology, 2012. **79**(14): p. 1449-57.
251. Filippi, M., et al., *Multiple sclerosis: effects of cognitive rehabilitation on structural and functional MR imaging measures--an explorative study.* Radiology, 2012. **262**(3): p. 932-40.
252. Rocca, M.A., et al., *Thalamic damage and long-term progression of disability in multiple sclerosis.* Radiology, 2010. **257**(2): p. 463-9.
253. Bodini, B., et al., *White and Grey Matter Damage in Early Primary-Progressive MS: the Chicken or the Egg?* 2013: ECTRIMS, Copenhagen.
254. Battaglini, M., et al., *Voxel-wise assessment of progression of regional brain atrophy in relapsing-remitting multiple sclerosis.* J Neurol Sci, 2009. **282**(1-2): p. 55-60.
255. Bendfeldt, K., et al., *Association of regional gray matter volume loss and progression of white matter lesions in multiple sclerosis - A longitudinal voxel-based morphometry study.* Neuroimage, 2009. **45**(1): p. 60-7.
256. Bendfeldt, K., et al., *Spatiotemporal distribution pattern of white matter lesion volumes and their association with regional grey matter volume reductions in relapsing-remitting multiple sclerosis.* Hum Brain Mapp, 2010. **31**(10): p. 1542-55.
257. Muhlau, M., et al., *White-matter lesions drive deep gray-matter atrophy in early multiple sclerosis: support from structural MRI.* Mult Scler, 2013. **19**(11): p. 1485-92.

258. Sepulcre, J., et al., *Contribution of white matter lesions to gray matter atrophy in multiple sclerosis: evidence from voxel-based analysis of T1 lesions in the visual pathway*. Arch Neurol, 2009. **66**(2): p. 173-9.
259. DeLuca, G.C., et al., *The contribution of demyelination to axonal loss in multiple sclerosis*. Brain, 2006. **129**(Pt 6): p. 1507-16.
260. Schmierer, K., et al., *Diffusion tensor imaging of post mortem multiple sclerosis brain*. Neuroimage, 2007. **35**(2): p. 467-77.
261. Witte, M.E., et al., *Reduced expression of PGC-1alpha partly underlies mitochondrial changes and correlates with neuronal loss in multiple sclerosis cortex*. Acta Neuropathol, 2013. **125**(2): p. 231-43.
262. Soulier, T., et al., *Neuronal damage in cortical lesions: a PET study with [11C]-flumazenil in early relapsing multiple sclerosis*. 2013: ECTRIMS, Copenhagen.
263. Centonze, D., et al., *The link between inflammation, synaptic transmission and neurodegeneration in multiple sclerosis*. Cell Death Differ, 2010. **17**(7): p. 1083-91.
264. Inglese, M., et al., *Perfusion magnetic resonance imaging correlates of neuropsychological impairment in multiple sclerosis*. J Cereb Blood Flow Metab, 2008. **28**(1): p. 164-71.
265. Haufschild, T., et al., *Increased endothelin-1 plasma levels in patients with multiple sclerosis*. J Neuroophthalmol, 2001. **21**(1): p. 37-8.
266. Speciale, L., et al., *Endothelin and nitric oxide levels in cerebrospinal fluid of patients with multiple sclerosis*. J Neurovirol, 2000. **6 Suppl 2**: p. S62-6.
267. Pache, M., et al., *Extraocular blood flow and endothelin-1 plasma levels in patients with multiple sclerosis*. Eur Neurol, 2003. **49**(3): p. 164-8.
268. D'Haeseleer, M., et al., *Cerebral hypoperfusion in multiple sclerosis is reversible and mediated by endothelin-1*. Proc Natl Acad Sci U S A, 2013. **110**(14): p. 5654-8.
269. Odano, I., et al., *[18F]flumazenil binding to central benzodiazepine receptor studies by PET--quantitative analysis and comparisons with [11C]flumazenil*. Neuroimage, 2009. **45**(3): p. 891-902.
270. Zhang, H., et al., *NODDI: practical in vivo neurite orientation dispersion and density imaging of the human brain*. Neuroimage, 2012. **61**(4): p. 1000-16.
271. Grussu, F., et al., *Quantitative histological validation of NODDI MRI indices of neurite morphology in multiple sclerosis spinal cord*. 2015: ECTRIMS, Barcelona.
272. Kipp, L., et al., *Neurite orientation dispersion and density imaging (NODDI) in RRMS*. 2015: ECTRIMS, Barcelona.
273. Mainero, C., et al., *fMRI evidence of brain reorganization during attention and memory tasks in multiple sclerosis*. Neuroimage, 2004. **21**(3): p. 858-67.
274. Bonnet, M.C., et al., *Cognitive compensation failure in multiple sclerosis*. Neurology, 2010. **75**(14): p. 1241-8.
275. Rocca, M.A., et al., *Clinical and imaging assessment of cognitive dysfunction in multiple sclerosis*. Lancet Neurol, 2015. **14**(3): p. 302-17.
276. Roosendaal, S.D., et al., *Resting state networks change in clinically isolated syndrome*. Brain, 2010. **133**(Pt 6): p. 1612-21.
277. Bissonette, G.B., et al., *Prefrontal cognitive deficits in mice with altered cerebral cortical GABAergic interneurons*. Behav Brain Res, 2014. **259**: p. 143-51.

278. Lewis, D.A., *Inhibitory neurons in human cortical circuits: substrate for cognitive dysfunction in schizophrenia.* Curr Opin Neurobiol, 2014. **26C**: p. 22-26.
279. Sun, B., et al., *Imbalance between GABAergic and Glutamatergic Transmission Impairs Adult Neurogenesis in an Animal Model of Alzheimer's Disease.* Cell Stem Cell, 2009. **5**(6): p. 624-33.
280. Desikan, R.S., et al., *An automated labeling system for subdividing the human cerebral cortex on MRI scans into gyral based regions of interest.* Neuroimage, 2006. **31**(3): p. 968-80.

Publications

Related to doctoral work:

1. Freeman L., Garcia-Lorenzo D., Bottin L., Leroy C., Louapre C., Bodini B., Papeix C., Assouad R., Granger B., Tourbah A., Dollé F., Lubetzki C., Bottlaender M., Stankoff B. (2015) the neuronal component of gray matter damage in multiple sclerosis: a [^{11}C]flumazenil positron emission tomography study. Ann Neurol. 78(4):554-67, 2015.

2. Bodini B., Veronese M., Garcia-Lorenzo D., Battaglini, M., Poirion E., Chardain A., Freeman L., Louapre C., Tchikviladzé M., Papeix C., Dolle F., Zalc B., Lubetzki C., Bottlaender M., Turkheimer F., Stankoff B.Dynamic imaging of individual remyelination profiles in multiple sclerosis, in revision .

3. Govindarajan K.A., Freeman L., Cai C., Rahbar M.H., Narayana P.A.. Effect of intrinsic and extrinsic factors on global and regional cortical thickness. PLoS One. 9(5):e96429, 2014.

4. Louapre C., Perlbarg V., Garcia-Lorenzo D., Urbanski M., Benali H., Assouad R., Galanaud D., Freeman L., Papeix C., Tourbah A., Lubetzki C., Lehericy S., Stankoff B. Brain networks disconnection in early MS cognitive deficits: an anatomo-functional study. Human Brain Mapp. 35(9):4706-172014.

5. Stankoff B., Freeman L., Aigrot M.S., Chardain A., Dolle F., Williams A., Galanaud D., Armand L., Lehericy S., Lubetzki C., Zalc B., Bottlaender M. Imaging CNS myelin by PET using the thioflavin derivative 11C-PIB. Ann Neurol, 69(4):673-80, 2011.

6. Freeman L., Louapre C., Galanaud D., Stankoff B. Central Nervous System Imaging in Multiple Sclerosis. Presse Med, 2010; 39(3): 349-58.

Unrelated to doctoral work:

1. Brandel J.P., Galanaud D., Freeman L., Laplanche J.L., Haik S. Variant or Sporadic Creutzfeld Jakob disease? Lancet, 75(9718): 889, 2010.

2. Chan E., Charles P., Ribai P., Goizet C., Marelli C., Vincitorio C.M., Bayon A.L., Guyant-Maréchal L., Vandenberghe N., Anheim M., Devos D., Freeman L., Ber I.L., N'guyen K., Tchikviladzé M., Labauge P., Hannequin D., Brice A., Durr A., du Montcel S.T. Quantitative assessment of the evolution of cerebellar signs in spinocerebellar ataxias. Mov Disord. 26(3) :534-8, 2011.

Oral communications

Regional:

1. Freeman L. Quantification de la souffrance neuronale au sein de la substance grise de patients atteints de Sclérose en Plaques: une étude en tomographie a émission de positrons avec le [11C]-Flumazenil. Journée Nationale des Internes de Neurologie, Paris, France, February 2009 *(Award- Best Oral Communication)*

2. Freeman L. Validation de critères IRM afin de diagnostiquer différents types de leukoencephalopathies, Paris, France, January 2010 *(Award- Best Oral Presentation)*

International:

1. Freeman L., Sedel F., Papeix C., Galanaud D., Granger B., Tourbah A., Chabriat H., Labauge P. Validation of MR criteria to diagnose different types of leukoencephalopathies in a series of 75 consecutive patients. ECTRIMS 2009

2. Freeman L., Leroy C., Galanaud D., Assouad R., Tourbah A., Papeix C., Comtat C., Lubetzki C., Delforge J., Bottlaender M., Stankoff B. Early neuronal damage in patients with MS detected by PET using [11C]-Flumazenil. ECTRIMS 2010 *(Award- Best Oral Presentation by a Young researcher)*

3. Freeman L., Garcia-Lorenzo D., Bottin L., Bodini B., Assouad R., Tourbah A., Papeix C., Comtat C., Lubetzki C., Delforge J., Bottlaender M., Stankoff B . Evidence of widespread cortical neuronal damage in patients with multiple sclerosis: a surface-based study using PET with [11C]-flumazenil. ECTRIMS 2013.

4. Lalys F., Freeman L.*, Staewen T.D., Lincoln J., Nelson F., Datta S., Narayana P., Cofield S., Gustafson T., Cutter G., Lublin F., Wolinsky J. Early on-treatment T2 and T1 subtraction MRI predicts imaging and clinical outcomes in the CombiRx cohort. ACTRIMS/ ECTRIMS 2014 (*presenter).

Abstracts:

1. Freeman L., Leroy C., Galanaud D., Sureau F., Assouad R., Tourbah A., Papeix C., Comtat C., Trebossen R, Lubetzki C, Delforge J, Bottlaender M, Stankoff B. Neuronal pathology in deep grey matter structures: a multimodal imaging analysis combining PET and MRI. ECTRIMS 2009.

2. Freeman L., Leroy C., Galanaud D., Assouad R., Tourbah A., Papeix C., Comtat C., Lubetzki C., Delforge J., Bottlaender M., Stankoff B. Assessment of Neuronal Pathology in the Cerebral Grey Matter of Patients with MS: Added Value of PET with [11C]-Flumazenil. AAN 2010.

3. Freeman L., Tourbah A., Galanaud D., Papeix C., Granger B., Chabriat H., Labauge P, Sedel F. Differential diagnosis of Adult Leucoencephalopathies: validation of MR criteria in a series of 75 patients. AAN 2010.

4. Freeman L., Leroy C., Galanaud D., Sureau F., Assouad R., Tourbah A., Papeix C., Comtat C., Trebossen R., Lubetzki C., Delforge J., Bottlaender M., Stankoff B. Quantification de la souffrance neuronale au sein de la substance grise de patients atteints de sclérose en plaques (SEP): une étude en tomographie à émission de positons (TEP) avec le [11C]-Flumazenil. JNLF 2010.

5. Leroy C., Comtat C., Trebossen R., Freeman L., Stankoff B., Ribeiro M.J., Bottlaender M. Optimal correction of body weight for simplified quantification of PET cerebral glucose metabolism using SUV. SNM 2010.

6. Chardain C., Freeman L., Galanaud D., Louapre C., Papeix C., Zalc B., Lehericy S., Lubetzki C., Bottlaender M., Stankoff B. Quantification of myelin loss and repair in multiple sclerosis lesions by PET using [11C]-PIB: a pilot study combining PET and multimodal MRI. ECTRIMS 2010.

7. Bodini B., Bottin L., Freeman L., Chardain A., Battaglini M., Ciccarelli C., Papeix C., Galanaud D., Zalc B., García-Lorenzo D., Lehéricy S., Lubetzki C., Bottlaender M., Stankoff B. Assessment of myelin content by positron emission tomography with [methyl-^{11}C]-2-(4'-methylaminophenyl)- 6-hydroxybenzothiazole in relapsing-remitting MS. ECTRIMS 2012.

8. Soulier T., García-Lorenzo D., Bodini B., Freeman L., Tchikviladze M., Lehéricy S., Bottlaender M., Lubetzki C., Stankoff B. Neuronal damage in cortical lesions: a PET study with [11C]-flumazenil in early relapsing multiple sclerosis. ECTRIMS 2013.

9. Bodini B., Veronese M., Garcia-Lorenzo D., Freeman L., Papeix C., Zalc B., Tchikviladze M., Lubetzki C., Bottlaender M., Turkheimer F. Positron emission tomography (PET) with [^{11}C]-PIB : a clinically relevant tool for voxel-wise myelin quantification in MS. ECTRIMS 2013.

10. Lalys F., Freeman L., Lincoln J., Nelson F., Narayana P., Cofield S., Gustafson T., Cutter G., Lublin F., Wolinsky J. Predicting Confirmed Disability Progression In MS: Importance Of Early On-Treatment MRI Changes On Modeling The CombiRx Trial Database. AAN 2014.

11. Bodini B., Veronese M., Garcia-Lorenzo D., Battaglini M., Poiron E., Freeman L., Papeix C., Zalc B., Tchikviladze M., Lubetzki C., Bottlaender M., Turkheimer F., Stankoff B. Exploring extent, localization and time course of remyelination in MS with ^{11}C-PIB PET. ACTRIMS/ECTRIMS 2014.

12. Bodini B., Veronese M., Garcia-Lorenzo D., Battaglini M., Poiron E., Freeman L., Papeix C., Zalc B., Tchikviladze M., Lubetzki C., Bottlaender M., Turkheimer F., Stankoff B. Spontanous remyelination has a major impact on clinical disability in multiple sclerosis: a longitudinal PET study with 11C-PIB. AAN 2015.

13. Freeman L., Lincoln J., Narayana P., Wolinsky J. (2015) Evidence of widespread cortical hypoperfusion in MS: a surface-based MRI study with pseudo-continuous arterial spin labeling. ECTRIMS 2015.

Auteur : Léorah Freeman

Directeur : Pr Bruno Stankoff

Titre de la thèse en Français :

Imagerie de la dégénérescence neuronale dans une maladie démyélinisante: la sclérose en plaques.

Résumé :

La sclérose en plaques (SEP) a longtemps été considérée comme une affection inflammatoire démyélinisante de la substance blanche. (SB) Hors, de nombreuses études ont démontré l'implication extensive de la substance grise (SG). La souffrance neuronale joue un rôle majeur dans la détérioration physique et cognitive des patients atteints de SEP. Le développement de nouvelles techniques d'imagerie capables de quantifier cette atteinte neuronale est devenu crucial.

Grace à la tomographie par émission de positons (TEP) et au radiotraceur [^{11}C]flumazenil ([^{11}C]FMZ), antagoniste du récepteur central aux benzodiazépines, nous avons quantifié de façon non-invasive la souffrance neuronale de la SG chez des patients atteints de SEP à différents stades de la maladie.

Une cohorte de 18 patients atteints de SEP a été comparée à 8 sujets sains. Les participants ont bénéficié d'une évaluation clinique, cognitive, et radiologique par TEP au [^{11}C]FMZ et IRM. Les données TEP ont été évaluées par région d'intérêt et vertex-à-vertex.

Des réductions significatives de l'activité TEP au [^{11}C]FMZ ont été mises en évidence au sein de la SG corticale et sous-corticale des patients comparés aux contrôles. Ces changements étaient présents dès le stade rémittent de la maladie et corrélaient modérément avec la charge lésionnelle de la SB. L'activité TEP corticale était aussi associée à la performance cognitive des patients.

Cette étude pilote est la première à quantifier in vivo la souffrance neuronale chez des patients atteints de SEP. Nos résultats permettent de proposer la TEP au [^{11}C]FMZ comme marqueur spécifique et discriminant de l'atteinte neuronale de la SG dans la SEP.

Mots clés : sclérose en plaques, neurodégénérescence, TEP, IRM, Flumazenil, récepteurs $GABA_A$.

Titre de la thèse en anglais:

Imaging the neurodegenerative component of a demyelinating disorder : multiple sclerosis.

Résumé en anglais :

Multiple sclerosis (MS) has long been regarded as an inflammatory demyelinating disorder of the white matter. But post-mortem studies have recently shed light on the extensive involvement of the grey matter (GM). Neuronal damage, characterized by synaptic and dendritic loss as well as neuronal apoptosis, is thought to be a major substrate of physical and cognitive deterioration in MS patients. There is a crucial need for new imaging techniques able to specifically assess neuronal damage in MS.

Using positron emission tomography (PET) with [^{11}C]flumazenil ([^{11}C]FMZ), an antagonist of the central benzodiazepine site located within the $GABA_A$ receptor, and a non-invasive quantification method, we measured and mapped neurodegenerative changes in the GM of patients with MS at distinct disease stages.

A cohort of 18 MS patients was compared to 8 healthy controls and underwent neurological and cognitive evaluations, high-resolution dynamic [^{11}C]FMZ PET imaging and brain MRI. PET data were evaluated using a region of interest and a surface-based approach.

[^{11}C]FMZ binding was significantly decreased in the cortical and subcortical GM of MS patients compared to controls. These changes were significant in both progressive and relapsing-remitting forms of the disease and correlated moderately with white matter lesion load. [^{11}C]FMZ cortical binding was also associated with cognitive performance.

This pilot study is the first to quantify in vivo the neurodegenerative changes occurring in MS. Our results show that PET with [^{11}C]FMZ could be a promising and sensitive quantitative marker to assess and map the neuronal substrate of GM pathology in MS.

Key words: multiple sclerosis, neurodegeneration, PET, MRI, Flumazenil, $GABA_A$ receptors.